

**MODELING WETTABILITY ALTERATION DURING
IMMISCIBLE CARBON DIOXIDE FLOODING PROCESS**

BY

SAAD MENAHI AL-MUTAIRI

A Dissertation Presented to the
DEANSHIP OF GRADUATE STUDIES

KING FAHD UNIVERSITY OF PETROLEUM & MINERALS

DHAHRAN, SAUDI ARABIA

In Partial Fulfillment of the
Requirements for the Degree of

DOCTOR OF PHILOSOPHY

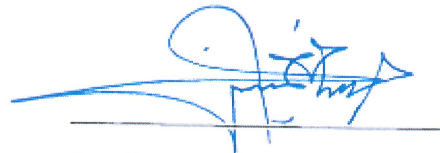
In

Petroleum Engineering

December 2013

KING FAHD UNIVERSITY OF PETROLEUM & MINERALS
DHAHRAN- 31261, SAUDI ARABIA
DEANSHIP OF GRADUATE STUDIES

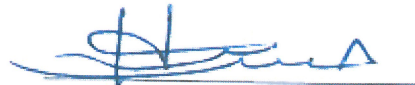
This dissertation, written by SAAD MENAHI AL-MUTAIRI under the direction his dissertation advisor and approved by his dissertation committee, has been presented and accepted by the Dean of Graduate Studies, in partial fulfillment of the requirements for the degree of **DOCTOR OF PHILOSOPHY IN PETROLEUM ENGINEERING.**



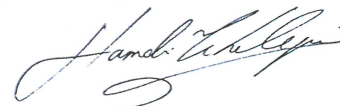
Dr. Sidqi A. Abu-Khamsin
(Advisor)



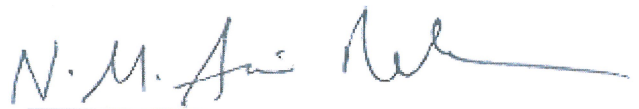
Dr. M. Enamul Hossain
(Co-Advisor)



Dr. Hasan Y. Al-Yousef
(Member)



Dr. Hamdi Tchelep
(Member)



Dr. Noor M. Anisur Rahman
(Member)



Dr. Abdullah S. Al-Sultan
Department Chairman



Dr. Salam A. Zummo
Dean of Graduate Studies

21/12/13

Date



© Saad Menahi Al-Mutairi

2013

|Dedicated to My Mother, Mizunah |

ACKNOWLEDGMENTS

All praises and adoration are due to Allah, the lord of incomparable Majesty, who in His infinite mercies has given me the grace to accomplish this work. Whatever he gives, nobody can withhold and whatever he withholds nobody can give. Without His Grace this work would have come to nothing. May His peace and blessings be on our noble Prophet Muhammad, his household, his companions and the generality of Muslims till the end of time.

My profound gratitude goes to my dissertation advisor, Dr. Sidqi Abu-Khamsin, and co-advisor Dr. M. Enamul Hossain. Their advice and constructive criticism have made this thesis a success. My thanks are extended to the dissertation committee members, Dr. Hasan Al-Yousef, Dr. Hamdi Tchelepi and Dr. Noor M. Anisur Rahman for their advice and assistance accorded me during the course of this work. Many thanks go also to the Chairman and other faculty members and staff of the Petroleum Engineering department.

Thanks to my loving mother for her continuous prayers. Also, thanks to my supportive wife and kids for their patience and goodwill to attend classes at evening times for almost four years.

Finally, I would like to acknowledge Saudi Aramco Company represented by Southern Reservoir Management Department for its continuous support and encouragement during the whole Ph.D. program.]

TABLE OF CONTENTS

ACKNOWLEDGMENTS	V
LIST OF TABLES	IX
LIST OF FIGURES	X
LIST OF ABBREVIATIONS.....	XIII
ABSTRACT.....	XIX
ملخص الرسالة	XXI
CHAPTER 1 INTRODUCTION.....	1
1.1 Rock Wettability	1
1.2 Wettability Modeling	3
1.3 Enhanced Oil Recovery (EOR).....	4
1.4 CO ₂ Properties.....	6
1.5 Background of CO ₂ Flooding	7
1.6 CO ₂ Miscible Displacement	7
1.7 CO ₂ Immiscible Displacement	9
1.8 Effects of CO ₂ on Oil Properties.....	12
CHAPTER 2 LITERATURE REVIEW.....	14
2.1 Laboratory Experiments	15
2.2 Numerical/Analytical Simulation Models	20
CHAPTER 3 STATEMENT OF THE PROBLEM.....	24
3.1 Knowledge Gap.....	24
3.2 Objectives	25

3.3	Research Approach	25
CHAPTER 4 MATHEMATICAL MODEL DEVELOPMENT		27
4.1	Background.....	27
4.2	Model Assumptions	27
4.3	Development of CO ₂ -Oil Displacement Model.....	28
4.3.1	Inspection of Displacement Model Dimensions	33
4.3.2	Investigations of the Nonlinear Term in the Displacement Model	35
4.4	Development of a Modified Corey Relative Permeability Model.....	38
4.5	Development of a Wettability Alteration Model	42
4.6	Modeling Wettability Alteration on Continuous Basis during Immiscible CO ₂ Flooding Process	45
CHAPTER 5 DEVELOPMENT OF THE NUMERICAL SIMULATION MODEL ...		46
5.1	Model Description.....	46
5.2	Boundary Conditions.....	47
5.3	Discretization of the CO ₂ Saturation Equation	48
5.4	Discretization of the Pressure Equations.....	52
CHAPTER 6 EXPERIMENTAL WORK		60
6.1	Wettability Alteration Experiment.....	60
6.1.1	Experimental Setup.....	61
6.1.2	Experimental Procedure	63
6.2	Core Flooding Experiment	67
6.2.1	Experimental Setup.....	67
6.2.2	Experimental Procedure	70
CHAPTER 7 RESULTS AND DISCUSSION.....		77

7.1 Wettability Alteration Model Calibration.....	77
7.2 Displacement Models Comparison	83
7.3 Limitations of the Proposed Model	93
7.4 Incorporation of Wettability Alteration Phenomenon	93
7.5 Effect of Residual Oil Saturation on Oil Recovery	99
7.6 CO₂-Oil Displacement Model Verification.....	100
 CHAPTER 8 CONCLUSIONS & RECOMMENDATIONS FOR FUTURE WORK	
.....	110
 APPENDIX A: DISCRETIZATION OF PRESSURE EQUATIONS WITH GRAVITY EFFECT.....	112
 APPENDIX B-1: MODIFIED COREY RELATIVE PERMEABILITY MODEL ADJUSTMENT FOR SECTION 7.4.....	119
 APPENDIX B-2: MODIFIED COREY RELATIVE PERMEABILITY MODEL ADJUSTMENT FOR SECTION 7.6.....	122
 APPENDIX C: MATLAB PROGRAMMING CODES.....	125
 REFERENCES	151
 VITAE.....	160

LIST OF TABLES

Table 2.1	Comparison of some widely accepted models addressing wettability alterations	23
Table 6.1	Properties of the rock and fluids employed in the experiment	65
Table 6.2	Brine composition	65
Table 6.3	Fluid properties (core flooding experiment)	69
Table 6.4	Core plug effective porosities	70
Table 6.5	Brine flooding data	72
Table 6.6	Oil flooding data	72
Table 6.7	CO ₂ flooding data	73
Table 6.8	Contact angle values before and after CO ₂ flooding	74
Table 7.1	Variation of the contact angle with time	78
Table 7.2	Initial and final contact angles with stabilization time	80
Table 7.3	Simulation model input data in the displacement model comparison study	85
Table 7.4	Wettability alteration model input in the IMPES model	94
Table 7.5	Input data used for the displacement model verification	105

LIST OF FIGURES

Figure 1.1	2010 global EOR oil production rates	5
Figure 1.2	CO ₂ phase diagram	6
Figure 1.3	CO ₂ flooding process	9
Figure 4.1	Variation of CO ₂ compressibility factor	30
Figure 4.2	Variation of CO ₂ viscosity	30
Figure 4.3	Variation of $\frac{p}{z\mu_{CO_2}}$ for CO ₂	30
Figure 4.4	Variation of residual oil saturation with rock wettability	39
Figure 4.5	Proposed wettability alteration conditions in the porous medium	42
Figure 4.6	Contact angle variations with CO ₂ exposure time	43
Figure 5.1	Schematic of the one-dimensional flow system	47
Figure 5.2	Boundary conditions assumed in the model	47
Figure 5.3	Gas saturation for the first cell	48
Figure 5.4	Gas saturation for the cells from 2 to N-1	50
Figure 5.5	Gas saturation for the last cell	51
Figure 5.6	Pressure equation for the first cell	53
Figure 5.7	Pressure equation for the cells from 2 to N-1	55
Figure 5.8	Pressure equation for the last cell	57
Figure 6.1	Schematic of the experimental set-up	61
Figure 6.2	The windowed visual cell	62
Figure 6.3	Rock slice-hanger assembly	62
Figure 6.4	Visual cell components	66
Figure 6.5	Shape of the oil drop (a) before brine carbonation (b) after 44 minutes of brine carbonation	66
Figure 6.6	The three core plugs used in the core flooding experiment	67

Figure 6.7	Schematic of the core flooding experiment	68
Figure 6.8	Contact angle measurement setup	75
Figure 6.9	Contact angle measurement for core plug # 1 (view is inverted)	75
Figure 6.10	Contact angle measurement for core plug # 2 (view is inverted)	76
Figure 6.11	Contact angle measurement for core plug # 3 (view is inverted)	76
Figure 7.1	Raw experimental data for Run # 1 and Run # 2	79
Figure 7.2	Dimensionless experimental data for Run # 1 and Run # 2	80
Figure 7.3	Dimensionless experimental data for both Run # 1 and Run # 2	81
Figure 7.4	Impact of grid size on CO ₂ breakthrough time for the proposed model	88
Figure 7.5	Location of the CO ₂ flood front after injecting 0.1 PV of CO ₂	88
Figure 7.6	Location of the CO ₂ flood front after injecting 0.5 PV of CO ₂	89
Figure 7.7	Location of the CO ₂ flood front after injecting 1 PV of CO ₂	89
Figure 7.8	Location of the CO ₂ flood front after one injecting 2 PV of CO ₂	90
Figure 7.9	Location of the CO ₂ flood front after injecting 3 PV of CO ₂	90
Figure 7.10	CO ₂ breakthrough time	91
Figure 7.11	Variation of oil recovery factor with injected CO ₂ volume	91
Figure 7.12	Oil production rate	92
Figure 7.13	Variation of 1 st cell pressure with CO ₂ injection time	92
Figure 7.14	CO ₂ saturation profiles at three different flooding times	96
Figure 7.15	CO ₂ breakthrough time for with and without wettability alteration conditions	96
Figure 7.16	Oil recovery versus volume of CO ₂ injected	97
Figure 7.17	Oil production rate versus volume of CO ₂ injected	97
Figure 7.18	Contact angle variations at different injection times	98
Figure 7.19	Relative permeability curves	98

Figure 7.20	Variation of oil recovery with volume of CO ₂ injected	100
Figure 7.21	Variation of the contact angle with CO ₂ injection time	106
Figure 7.22	Oil recoveries for the CO ₂ core flooding experiment	106
Figure 7.23	Model predictions of oil recovery	107
Figure 7.24	Solubility of CO ₂ in various crudes	107
Figure 7.25	Volume change of crude saturated with CO ₂	108
Figure 7.26	Oil viscosity correction chart for CO ₂ –oil mixtures	108
Figure 7.27	Effect of solubility on oil recovery	109
Figure 7.28	Solubility effect on gas fractional flow	109

LIST OF ABBREVIATIONS

Latin

A	:	Cross-Sectional Area
A_{fc}	:	Deposition Volume of Asphaltene Covering all Pore Surfaces
A_c	:	Deposition Volume of Asphaltene Coating on Pore Walls
B	:	Formation Volume Factor, L ³ /std L ³
B_{co}	:	Conversion Factor for Oil Phase to Reservoir BBL, 1.127e-3
B_{cg}	:	Conversion Factor for Gas Phase to Reservoir BBL, 6.328e-3
c_t	:	Total Compressibility, psi ⁻¹
c_g	:	Gas Compressibility, psi ⁻¹
C_{pc}	:	Capillary Pressure Endpoint, m/t ²
C_{s,o}	:	Oil Spreading Coefficient
cc	:	Cubic Centimeter
cm	:	Centimeter
F	:	Fahrenheit
f_o	:	Oil Fractional Flow
f_{CO₂}	:	CO ₂ Fractional Flow

g	:	Gravitational Acceleration, L/t ²
g_c	:	Gravitational Conversion Factor, mL/t ² F
k_r	:	Relative Permeability
k_o	:	Oil Phase Effective Permeability, mD
k_{ro}	:	Oil Phase Relative Permeability
k_r^o	:	Endpoint Relative Permeability
k_{ro}^o	:	Oil Relative Permeability (at S _g = 0)
k_{rCO₂}^o	:	CO ₂ Relative Permeability (at S _g = 1 – S _{or})
K'_{rwja}/K'_{roja}	:	Relative Permeabilities after Asphaltene Deposition
K'_{rwj}/K'_{roj}	:	Relative Permeabilities as Asphaltene 100% Occupation
K_{rwj}/K_{roj}	:	Relative Permeabilities before Asphaltene Deposition
k_{rl}^{initial}	:	Initial Wettability Condition of Gridblock
k_{rl}^{final}	:	Initial Wettability Condition of Gridblock
k_{CO₂}	:	CO ₂ Phase Effective Permeability, mD
k_{rCO₂}	:	CO ₂ Phase Relative Permeability
MMBD	:	Millions Barrels Per Day
N_{Tl}	:	Trapping Number

n_l	:	Relative Permeability Exponent
n_o	:	Oil Phase Corey Exponent
n_g	:	Gas Phase Corey Exponent
$P_{c,ij}$:	Capillary Pressure, psi
P	:	Pressure, m/L t ²
p_{wf}	:	Bottom Flowing Pressure, psi
p_c	:	Capillary Pressure, psi
p_{CO_2}	:	CO ₂ Phase Pressure, psi
p	:	Pressure, psi
PI	:	Productivity Index
ppm	:	Particle Per Million
Q_g	:	Gas Injection Rate, ft ³ /day
q	:	Production/Injection Rate, L ³ /t
q_x	:	Total Production Rate, L ³ /t
q_o	:	Oil Production Rate, L ³ /t
q_{CO_2}	:	CO ₂ Production Rate, L ³ /t
r	:	Pore Throat Radius, ft

S_o	:	Oil Saturation
S_{CO_2}	:	CO ₂ Saturation
S	:	Saturation, fraction
S_{or}	:	Residual Oil Saturation
$(S_{or})_{ow}$:	Oil-Wet Residual Oil Saturation
$(S_{or})_{iw}$:	Intermediate-Wet Residual oil Saturation
S_{wi}	:	Initial Water saturation
S_{on}	:	Normalized Oil Saturation
s	:	Seconds
t	:	CO ₂ Exposure Time in Minutes
T	:	Input Trapping Number
T_2	:	Transverse relaxation time
T	:	Transmissibility
U_x	:	Total Velocity, L/t
u_o	:	Oil Phase Velocity, L/t
u_{CO_2}	:	CO ₂ Phase Velocity, L/t
V_p	:	Pore Volume

z : Compressibility Factor

Greek

σ_{ij} : Interfacial Tension, mt^2

θ_{ij} : Contact Angle between two fluid phases

τ_{m-f} : Matrix/Fracture Transfer Flow, L^3/t

ϕ : Porosity, fraction

λ : Transmissibility

ρ : Fluid Density, m/L^3

ω : Interpolation Scaling Factor

\Rightarrow
 \mathbf{k} : Permeability Tensor, L^2

\rightarrow
 $\nabla \Phi_1$: Flow Potential Gradient

Φ_1 : Potential, $ML^{-1}t^{-2}$

ρ_{CO_2} : CO_2 Density, m/L^3

μ_{CO_2} : CO_2 Viscosity, cP

Δx : Distance Step

ϕ : Porosity

ρ_o	:	Oil Density, m/L ³
μ_o	:	Oil Viscosity, cP
Δt	:	Time Step
θ	:	Contact Angle in Degrees

Subscripts

ij	:	ow, gw, go
α	:	Phase
m	:	Matrix
f	:	Fracture
l	:	Water
r	:	Residual
high	:	High Trapping Number
low	:	Low Trapping Number
'	:	Displacing Phase

ABSTRACT

Full Name : Saad Menahi Al-Mutairi

Dissertation Title: Modeling Wettability Alteration during Immiscible Carbon Dioxide Flooding

Major Field : Petroleum Engineering

Date of Degree : December 2013

A large number of laboratory experiments, including cores and micro-models, to investigate wettability alteration during CO₂ flooding had been reported in the literature. However, limited work on numerical and analytical modeling has been presented where continuous wettability alteration phenomena is addressed or incorporated. To the best of our knowledge, all published numerical and analytical models are time-independent solutions.

In this study, a comprehensive mathematical model is developed to describe CO₂-oil immiscible displacement process in porous media within a secondary recovery scheme. To allow continuous wettability alteration with the progress of the flood front, first an empirical relationship between contact angle and displacement time is developed. This relationship is derived from experiments in which the change in the contact angle between oil, carbonated brine and a slice of rock cut from a carbonate core plug are measured with time. The experimental results indicate that the rock wettability is altered from oil-wet to intermediate-wet and that the extent of the alteration depends on CO₂ concentration in the brine. Furthermore, it was observed that the contact angle decreases

exponentially with the time of exposure to the brine down to a stable value. Second, a novel modified Corey relative permeability model is developed and incorporated into the proposed comprehensive displacement model to calculate the phase relative permeability as a function of wettability.

The mathematical model equations are solved by a numerical, 1-dimensional, two-phase immiscible simulation scheme in which the equations are discretized using Implicit Pressure Explicit Saturation (IMPES) concept and solved numerically utilizing MATLAB programming. The numerical results show that the model is stable and can produce oil displacement. Numerical solution of the mathematical model proved to be stable and is close to the established models when tested on a hypothetical case – without wettability alteration. The displacement model with the inclusion of the continuous wettability alteration feature, predicts a much higher ultimate oil recovery which is confirmed by an actual core flooding experiment. The outcome of this study will enhance the understanding of the rheological behavior of the rock-fluid interaction during CO₂ flooding. In addition, the study proves that wettability alteration is one of the formation parameters which contribute to the ultimate oil recovery.

ملخص الرسالة

الاسم الكامل: سعد مناحي المطيري

عنوان الرسالة: نمذجة تغير خاصية التبلل خلال عملية الغمر بثاني اكسيد الكربون

التخصص: هندسة بترول

تاريخ الدرجة العلمية: ديسمبر 2013

بناءً على المراجعة الأكاديمية المكثفة التي اجريت لجمع احدث نتائج البحوث على تحول خاصية التبلل خلال عمليات الغمر بثاني اكسيد الكربون تبين انه تم تقرير عدد كبير من التجارب المختبرية للغمر، بما في ذلك العينات الصخرية والنماذج الدقيقة، لاستكشاف تحول خاصية التبلل خلال الغمر بثاني اكسيد الكربون. عدة بحوث سابقة في هذا المجال تشير إلى ان هناك دراسات محدودة على النماذج التحليلية والعديدية حيث أدرجت ظاهرة تحول خاصية التبلل المستمرة. وعلاوة على ذلك، وحسب معرفتنا، فإن النماذج العديدية والتحليلية الموجودة هي حلول غير معتمدة بشكل او بأخر على الزمن.

ولذلك، تم تطوير نموذج تحليل مرئي لتمثيل سريان امتزاج الزيت- ثاني اكسيد الكربون في مجال مسامي ضمن آلية استرداد ثانوي للمواد الهيدروكربونية الكامنة تحت الارض . أثناء عملية تطوير النموذج ، تم تطوير وادراج نموذج معدل فريد من نوعه لحساب النفاذية النسبية مقترنة بخاصية التبلل. أيضا، هذه الدراسة بحثت تجريبياً وبصفة مستمرة عن تغير خاصية التبلل خلال الغمر بثاني اكسيد الكربون. اجريت قياسات زاوية التلامس بين الزيت، ومحلول ملحي وشريحة من الصخر مقطوعة من عينة هيدروكربونية. وتشير النتائج إلى ان خاصية التبلل للصخور تتغير من زيت- مبلل إلى وسط- مبلل عندما يتعرض نظام زيت/صخر لثاني اكسيد الكربون المذاب. مدى تغير خاصية التبلل خاضعة لزمان التعرض لثاني اكسيد الكربون، كلما زاد الزمن، تغير خاصية التبلل تتقدم نحو حد واضح. أيضا، وجد أن كلما زاد تركيز ثاني اكسيد الكربون في المحلول الملحي ، تتغير خاصية التبلل بشكل ملحوظ. استنادا إلى الحقائق

التجريبية، تم تطوير نموذج تجريبي لوصف تغير خاصية التبلل المستمر. ويمكن تطبيق نتائج هذه الدراسة إلى حالات حيث يتم حقن ثاني أكسيد الكربون في مكامن نفطي رطب عند ضغط أقل من ضغط الامتزاج.

تم بناء نظام محاكاة غير ممتزج ثنائي الطور عددي احادي الابعاد بواسطة برنامج مات لاب لحل معادلات نموذج الازاحة. المعادلات المستخدمة في النموذج مبنية على مفهوم "الإمبيس" وحلها عددياً. تبين ان النموذج التحليلي قادر على تنبؤ كمية وكفاءة النفط المزاحة على قدر كبير من الواقعية بواسطة نموذج تغير خاصية التبلل المستمر.

CHAPTER 1

INTRODUCTION

Wettability has been recognized as one of the parameters that control the remaining oil-in-place. Knowledge of reservoir wettability is essential to understand the displacement mechanisms, and to develop strategies for achieving higher recovery factors. Since rock wettability has been known to be altered as a result of various substances introduced into the reservoir the causes and mechanism of such alteration need to be addressed properly for an effective approach to enhanced oil recovery.

This chapter starts with an overview of rock wettability discussing its definition, types, measurement techniques, modeling and importance. It then provides a brief background on enhanced oil recovery (EOR) processes with emphasis on the CO₂-EOR process. This includes the displacement mechanism operating within the process and the effects of CO₂ on oil properties.

1.1 Rock Wettability

Wettability is the relative preference for adhesion of two fluids to a solid surface [1]. The tendency of a liquid to spread over a solid surface can be expressed conveniently and in a more precise nature by measuring the angle of contact at the liquid-solid interface [2]. The contact angle is measured through the denser liquid phase and ranges from 0 to 180°

[3]. As the contact angle decreases the wettability of the liquid strengthens. Since wettability has been recognized as one of the parameters controlling the remaining oil-in-place [4], knowledge of the reservoir wettability is essential to develop good understanding of the displacement mechanisms and to recover oil efficiently.

There are four types of wettability: water-wet, oil-wet, fractional-wettability and mixed-wettability. The state of water-wetness occurs when the rock surface is wetted by water while the state of oil-wetness occurs when the rock surface is wetted by oil. The concept of fractional wettability visualizes that a fraction of the matrix surface is oil-wet and the remainder is water-wet [5]. Mixed wettability is a special type of fractional wettability in which the oil-wet surfaces form continuous paths through the large pores while the smaller pores remain water-wet and contain no oil [6]. When the rock has no strong preference for either oil or water, the system is said to be of neutral (or intermediate) wettability [6].

Wettability also plays a vital role in the electrical properties of fluid-saturated rocks [7]. These electrical properties control the location and distribution of fluids [6]. Wettability and saturation history are important factors in the determination of the electrical resistivity of a porous medium; and for the same reason the effect of wettability becomes larger when the pores are poorly connected [8]. In water-wet systems, water fills the small pores and spreads on the grain surfaces to form a film while the oil occupies the large pores and overlays the water film. Such a distribution preference also renders the relative permeability curves strongly influenced by wettability. The relative permeability to oil increases and the permeability to water decreases as wettability is varied from water-wet to oil-wet [1]. In an oil-bearing formation, the wettability can vary with depth

where a greater water-wetting preference is seen near the bottom of the transition zone and a greater oil-wetting preference is observed near the top [9].

Several methods have been devised to measure rock wettability. Anderson [6] classified such methods into quantitative and qualitative. The quantitative methods include contact angle, Amott and USBM. The qualitative methods include nuclear magnetic resonance relaxation techniques, inferring wettability through imbibition-rate measurements, relative permeability curves, permeability/saturation relationships, capillary pressure curves and reservoir logs [10].

1.2 Wettability Modeling

Rock wettability has been investigated by simulation models which, sometimes, utilized experimental data. Sharma et al. [4] conducted experiments on glass-bead packs and Berea cores. Their theoretical model was represented by a network of pore throats (bonds) and pore bodies (sites). The overall results showed that wettability had a large impact on the saturation exponent especially when the pores are poorly connected.

Blunt [11] devised a network model to study the effects of wettability on the pore level following Kovscek et al.'s [12] scenario. The model simulates three stages of depletion: primary, water flooding and oil re-injection. It was found that portions of rock surface were wetted by oil after primary drainage. In contrast, corners of the pore space filled by water were wetted by water. During water flooding, oil layers were bounded by water in the corners and in the center of the pore space. Different wettability conditions were

investigated and the residual oil saturation was found to display non-monotonic dependence on wettability.

Bona et al. [13] developed an integrated approach for estimating the rock wettability. The dielectric constant of the sample in a wide frequency interval was measured for different shapes of water phase. The principle is that the dielectric behavior of the rock is controlled by the shape of the water phase, which may vary from very elongated films to spherical drops depending on the wettability of the system. The technique had the ability to detect the heterogeneous wetting states.

1.3 Enhanced Oil Recovery (EOR)

When water flooding no longer provides economic oil recovery, tertiary processes are needed to boost oil recovery through improved displacement mechanisms. EOR is defined as oil recovery by the injection of materials not normally present in the reservoir [14], and comes usually after the secondary recovery. Almost all EOR methods have been implemented in the field either on pilot or commercial scales. EOR methods are classified by the main mechanism of oil displacement [15-20] and are currently grouped into three classes which are well known to the oil industry. These are thermal, chemical and miscible – mainly CO₂ and hydrocarbon gas - flooding processes.

In recent years, 92% of all EOR projects are being executed mainly in the USA (153 projects), Canada (45 projects), Venezuela (41 projects), and China (39 projects) [21]. The total world oil production from EOR has remained relatively level over the years,

contributing about 3 MMBD which represents about 3.5% of the global daily oil production [22]. The bulk of EOR contribution comes from thermal flooding (~2 MMBD) followed by chemical, hydrocarbon gas and CO₂ flooding processes with contribution of 0.3 MMBD each (Figure 1.1) [21].

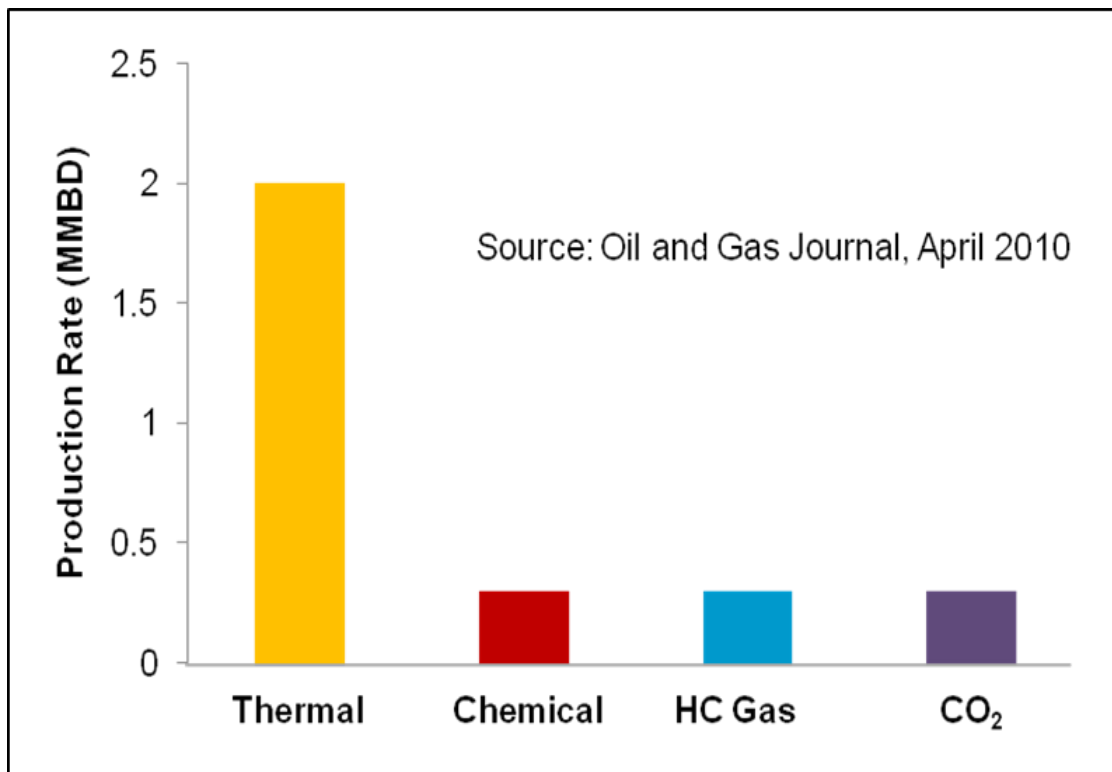


Figure 1.1 2010 global EOR oil production rates

1.4 CO₂ Properties

Carbon dioxide is a colorless, odorless, inert and non-combustible gas. It has a molecular weight of 44 and is 2 to 10 times more soluble in oil than in water. The viscosity of carbon dioxide is 0.0335 cP at its critical point (1070 psia and 87.8 °F). Its critical pressures fall within a relatively narrow range of 3.4-6.8 MPa (500-1000 psia) while its critical temperature is 87.8 °F/31.0 °C [14]. The density of carbon dioxide above its critical temperature at pressures between 6.9 and 27.6 MPa (1000-4000 psi) varies between 0.1 and 0.8 g/cm³ [23], which makes it close to that of a typical light oil (Figure 1.2) [24]. For example, under miscible displacement conditions in west Texas oil fields, the specific gravity of this dense carbon dioxide phase is typically 0.7 to 0.8 g/cm³ [25].

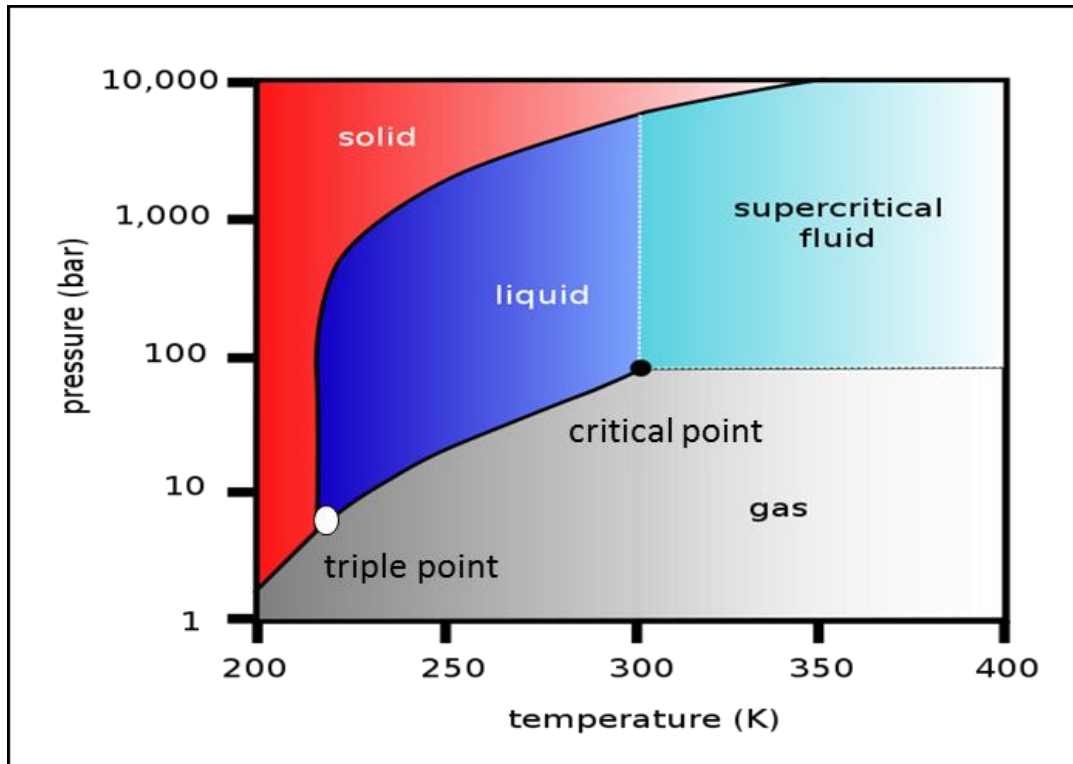


Figure 1.2 CO₂ phase diagram

1.5 Background of CO₂ Flooding

CO₂ flooding is a well-known EOR method established in the early 1960s. Along with thermal flooding, it is considered one of the most applied EOR processes around the world. Besides hydrocarbon gas floods, CO₂ floods in North America are the only EOR projects that have consistently and significantly increased annual EOR production since the 1986 crash in oil prices [26]. The American Petroleum Institute (API) states that the oil and gas industry has over 35 years of continuously developing experience in transporting and injecting CO₂ for EOR purposes [27].

There are two types of oil displacement mechanisms by CO₂: miscible and immiscible displacements.

1.6 CO₂ Miscible Displacement

Two fluids are said to be miscible when they can be mixed together in all proportions and all resulting mixtures remain in a single phase [28]. Miscibility between an injected fluid and the reservoir oil can be achieved through two mechanisms: first-contact and multiple-contact miscibility [25]. The first-contact miscible process is the simplest and most direct method for achieving miscible displacement. It requires injecting a solvent that mixes with the oil completely such that all mixtures become a single phase. Multiple-contact miscibility is achieved in stages involving contact between a progressively-modified fluid and the reservoir oil. CO₂ flooding involves a vaporizing-condensing process where CO₂ gas vaporizes the light to intermediate-molecular-weight hydrocarbons from the reservoir

oil into the CO₂ gas and later condenses into the oil phase (Figure 1.3) [25]. The extraction process occurs at temperatures where the fluid at the displacement front is a CO₂-rich liquid [28]. Oil recovery is also improved by reducing the oil viscosity caused by oil swelling as a result of CO₂ dissolution. Temperature and pressure are key parameters for miscibility development between oil and CO₂ where the local displacement efficiency is highly dependent on the minimum miscibility pressure (MMP) [29].

When the MMP is below the reservoir pressure, the flood will be miscible with higher oil recoveries. For the success of a miscible project a number of factors should be considered. These are: the injected solvent should be miscible with the oil, it should contact as much of the oil as possible, it should mobilize the contacted oil, and then it displaces it to the surface. Miscibility conditions can be obtained from laboratory experiments involving phase behavior studies and slim-tube tests. The sweep efficiency of a liquid CO₂ flood is generally better than a gas CO₂ flood because at the supercritical state CO₂ density is close to that of the liquid phase but with a lower viscosity.

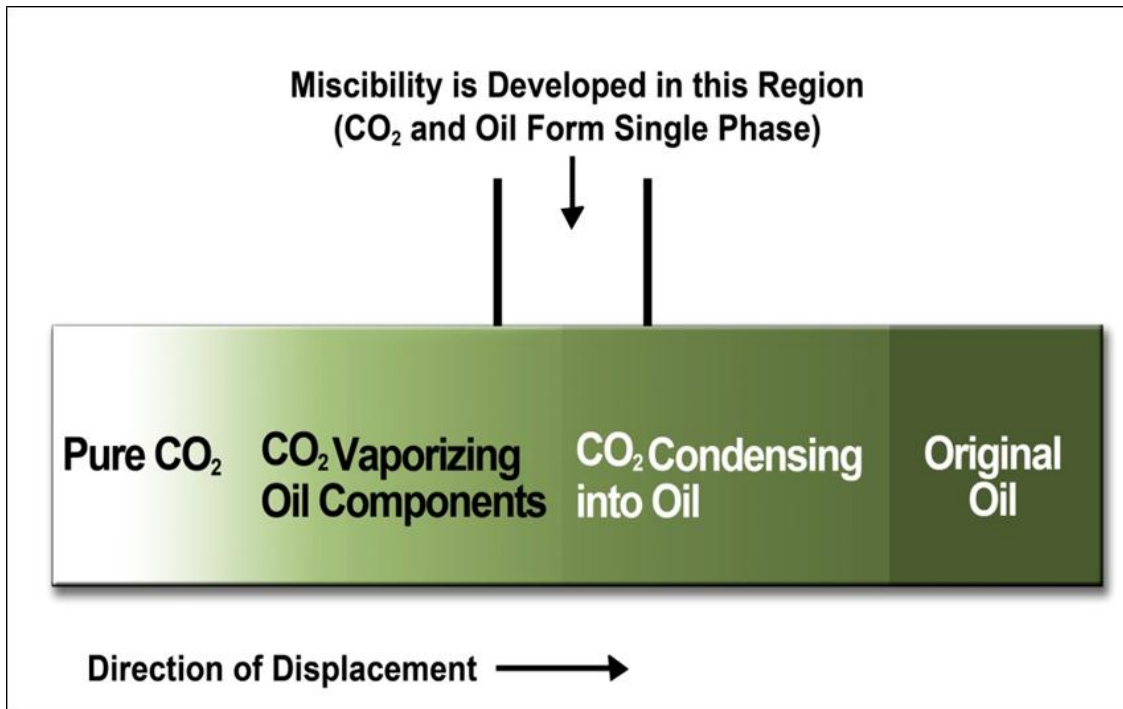


Figure 1.3 CO₂ flooding process

1.7 CO₂ Immiscible Displacement

Immiscible displacement, on the other hand, occurs when mixing produces two distinct fluid phases separated by a sharp interface [28]. When the MMP is above the reservoir pressure, CO₂ flooding will be immiscible resulting in generally lower ultimate oil recoveries. However, immiscible CO₂ flooding has a considerable potential for the recovery of moderately viscous oils, deep reservoirs and thin formations that are not suitable for thermal recovery techniques [30].

Three mass transfer mechanisms occur during this process: solubility, diffusion and dispersion. Solubility of CO₂ in oil is a function of temperature and pressure [14]. For low pressure applications (< 7 MPa) the major effect would be the dissolution of carbon dioxide in crude oil. Carbon dioxide is more soluble in hydrocarbons as a gas than as a liquid [31-32]. Carbon dioxide solubility increases as pressure increases and temperature decreases [33]. Carbon dioxide increases the viscosity of water slightly [34] but decreases its density [35]. Its effect on oil is discussed in the next section.

Diffusion is the macroscopic transport of mass due to random molecular motions and is independent of any convection within the system [35-36]. Diffusion helps carbon dioxide penetrate into heavy oil which may help reduce gravitational and viscous instabilities [30].

Dispersion is additional mixing of fluids that occurs in porous media due to velocity [30]. This additional mixing is due to the dispersive force of attraction which occurs in highly polarizable molecules such as hydrocarbons [37]. The dispersion is the results of the physical and chemical phenomena that take place within the pores during the travel of any particle through the pores.

Numerous laboratory experiments have been conducted to study various aspects of oil-CO₂ immiscible flow in porous media [24, 38-44]. However, little attention has been paid to model the process appropriately taking into account physical phenomena that are particular to this process. Grogen et al. [45] developed mathematical models to describe the diffusion processes occurring in secondary and tertiary CO₂ floods. Diffusivity of CO₂ in hydrocarbons and water was measured based on a direct observation of the

motion of an interface caused by the diffusion of CO₂ through oil or oil shielded by water. Diffusion coefficients were determined by fitting the mathematical model to the observed motion of the interfaces. Stokes-Einstein equation and McManamey and Woollen correlation were used to estimate diffusivity of CO₂ in water and in oil [46]. It was found that molecular diffusion plays an important role in the recovery of oil in secondary CO₂ floods. The diffusion coefficients of carbon dioxide in hydrocarbon at atmospheric conditions are in the range of 2.56×10^{-5} to $3.59 \times 10^{-5} \text{ cm}^2/\text{s}$ [21,47].

Numerical investigations of the two-phase flow in porous media for CO₂ sequestration applications have been studied by several authors in the recent years. Nordbotten and Dahle [48] derived closed-form constitutive functions for a vertically integrated model including gravitational and capillary forces which are appropriate to model CO₂ storage. The derived functions were used to show the impact of capillary forces on tip migration speed. The numerical results showed that the capillary forces which are dispersive on the fine scale led to self-sharpening behavior and slower tip speeds on the coarse scale.

Savioli and Santos [49] modeled brine-CO₂ flow in porous media to investigate the effectiveness of CO₂ sequestration over very long periods of time for the Sleipner field in the Utsira Sand aquifer (North Sea). The simultaneous flow of brine and CO₂ is described by the well-known Black-Oil formulation applied to two-phase, two components fluid flow. The solution of the Black-Oil fluid-flow model was obtained employing the public domain software BOAST, which solves the differential equations using IMPES, a semi implicit finite difference technique. Seismic monitoring is modeled using Biot's equations of motion describing wave propagation in fluid-saturated poro-viscoelastic solids. Numerical examples of CO₂ injection and time-lapse seismic using data of the

Utsira formation showed the capability of this methodology to monitor the migration and dispersal of CO₂ after injection.

Negara et al. [50] used pressure explicit saturation (IMPES) scheme with treating buoyancy and capillary forces to solve the two-phase water-CO₂ flow problem. They studied CO₂ plume in homogenous, layered and fractured porous media. The cell-centered finite difference (CCFD) technique was used to discretize the differential equation. The gravity force leads the injected CO₂ to rise buoyantly due to the density difference between CO₂ and water. Meanwhile, the capillary pressure compensates the upward migration of the CO₂ saturation distribution to the horizontal direction. The numerical results demonstrated the effects of the gravity and the capillary pressure on the flow for four different cases: gravity and capillarity are ignored, gravity only is ignored, capillarity only is ignored and both gravity and capillarity are considered.

The presented models were limited to the miscible CO₂ displacement process only and devoted to describe the flow of CO₂ into brine or water phase. These models were developed for CO₂ sequestration applications in aquifer formations. The authors addressed certain issues including the effectiveness of forces acting inside the aquifer and the monitoring CO₂ migration.

1.8 Effects of CO₂ on Oil Properties

Oil properties change when it dissolves CO₂. The literature highlights four main changes to oil properties: oil viscosity reduction, oil swelling, interfacial tension reduction and

asphaltene precipitation. First, the viscosity of oil is a function of temperature, pressure and concentration of dissolved CO₂ [30] with a large reduction in oil viscosity at lower operating temperatures [36]. Second, crude oil swells when contacted by CO₂. The amount of swelling increases with increased CO₂ dissolution [30]. Swelling factors increase dramatically at pressures below bubble point pressure [31]. The rapid increase in the swelling factor with continued carbon dioxide injection at pressures above 6 MPa is due to the formation of a liquid layer of carbon dioxide floating on top of the oil [30]. Third, the interfacial tension of oil is reduced in the presence of CO₂ [51] while it decreases moderately with increasing carbonation pressure of brine [36]. Fourth, asphaltene precipitation occurs when the hydrocarbons and polar fractions within the oil lose their ability to disperse the oil's asphaltene content colloiddally [52].

It has been shown that as the CO₂ pressure is increased, the tendency for asphaltene to flocculate from toluene solution in heavy oil increases [53]. For example, asphaltenes began to precipitate from a Lloydminster heavy oil sample at carbonation pressures greater than about 3.5 MPa without the addition of heptane [30]. Conversely, asphaltene precipitation decreases as the temperature is raised [30]. Asphaltene precipitation can cause serious problems in the reservoir. |

CHAPTER 2

LITERATURE REVIEW

Wettability alteration is an effective approach to enhance oil recovery significantly. The main factors affecting wettability alteration are oil composition, brine chemistry, rock surface mineralogy and the system temperature, pressure and saturation history. The adsorption of polar compounds and/or the deposition of organic matter that was originally present in the crude oil can alter most of the rock's surface chemistry. Polar compounds contain a polar end and a hydrocarbon end; the polar end adsorbs on the rock surface, exposing the hydrocarbon end and making the surface oil wet [6].

Brine chemistry plays a major role in altering the wettability of the rock where the brine's salinity and pH strongly affect the charge of the rock surface. The rock surface becomes positively charged when the pH is decreased and negatively charged when the pH is increased. Also, raising the temperature and pressure tends to promote the solubility of wettability-altering compounds. Such effect may explain why in an oil-bearing formation the wettability can vary with depth where a greater water-wetting preference is seen near the bottom of the transition zone and a greater oil-wetting preference is observed near the top [9]. Zones higher in the structure have a greater capillary pressure, which can counteract the disjoining pressure and destabilize the water film, allowing surface-active components in the oil to contact the solid. Lower in the structure, the solid surfaces mostly retain the water film [21].

Researchers have investigated rock wettability alteration during the CO₂ flooding process through conducting laboratory experiments and constructing numerical/analytical simulation models. The two sections below compile the up-to-date findings of those investigations.

2.1 Laboratory Experiments

Wettability alteration during the CO₂ flooding process has been investigated extensively in the laboratory. Several researchers measured wettability before and after CO₂ flooding in order to track any changes [54-57].

Shelton and Schneider [55] investigated the performance of miscible displacement of both the wetting and non-wetting phases with CO₂ flooding. The results suggested that the presence of water had adverse impact on the miscible displacement performance of both the wetting and non-wetting phases. A miscible CO₂ can displace tertiary oil. Also, oil trapping was developed in water-wet conditions while no oil trapping was observed in oil-wet conditions.

Tiffin and Yellig [57] conducted laboratory experiments to study the WAG option during CO₂ flooding of cores. They found that the oil recovery decreased as WAG ratio increased in the water-wet condition. In contrast, oil recovery increased as WAG ratio increased in oil-wet condition. It was reported that the decrease in oil recovery in a water-wet system was due to the presence of mobile water in the core isolating some oil from the injected CO₂.

Mathis [58] conducted a study investigating the effect of carbon dioxide injection on the total porosity in a dolomite reservoir in the Denver Unit of the Wason San Andres field in Texas. The collected cores were analyzed and the results indicated no porosity changes observed due to CO₂ injection.

Jackson et al. [59] conducted dimensionless scaled experiments to evaluate the effects of rock wettability on CO₂ flooding. Wettability was found to be a major factor affecting the flood performance. Gravity forces dominated the flooding in water-wet conditions while viscous (fingering) forces controlled the flooding in oil-wet conditions. Maximum recovery was achieved by gravity forces with continuous CO₂ injection.

Irani and Solomon [60] proposed a new, dual slug methodology of CO₂ injection based on the results obtained from slim tube tests. The methodology called for injecting a single surfactant slug first followed by continuous CO₂ injection. The results demonstrated that the foam front within the slim tube was totally displaced. The methodology helped optimize surfactant implementation and increase the gas mobility ratio in the areas located behind the foam front.

Lescure and Claridge [61] conducted laboratory experiments on the CO₂ foam process in a quarter 5-spot reservoir model investigating the effects of rock wettability and CO₂ slug size on the process performance. The results suggested that the oil recovery is higher in medium oil-wet than in medium water-wet systems due to larger surfactant adsorption in the latter case. Besides, injecting CO₂ as a slug is an optimal option over the WAG process resulting in higher oil recovery in the oil-wet case.

Potter [62] conducted experiments studying the effects of CO₂ flooding on the wettability of West Texas dolomitic cores. The selected cores represented three types of wettability states: intermediate oil-wet, intermediate and intermediate water-wet. Changes in relative permeability were examined before and after CO₂ flooding. Rock wettability was then inferred from changes in relative permeability trends. The results showed that the cores became slightly water-wet suggesting extraction of the rock surface caused by CO₂.

Yeh et al. [63] conducted a visual cell study evaluating the efficiency of fluid displacements with wettability alteration under CO₂ miscible flooding. The study showed that wettability was altered from initially water-wet to strongly oil-wet. When wettability alteration occurred, the extension of water blocking was over-predicted by water blocking measurement with refined oil. It was observed that water blocking was harsher in sandstone than carbonate rocks regardless of the wettability state. The results suggested that water blocking would not be a problem facing CO₂ miscible flooding.

Zekri and Natuh [64] tested the WAG technique for miscible CO₂ gas flooding to assess the overall oil recovery on laboratory scale. The cores were obtained from major sandstone and limestone Libyan reservoirs. Oil-wet condition was considered in the obtained cores for both reservoirs. The final laboratory results suggested that WAG ratio has no major effects on total oil recovery for the sandstone and limestone reservoirs.

Attanucci et al. [65] adapted new methods for managing the WAG process for the miscible CO₂ project that was initiated at the Rangely Weber Sand Unit in Colorado in 1986. The new methods were based on injection pattern performance and economics. Several scenarios of pilot tests associated with simulation modeling were conducted. The

results suggested that WAG tapering is a cost effective way to improve the recovery process.

Vives et al. [66] studied the effect of wettability on adverse mobility in immiscible flooding systems. A quarter 5-spot pattern experiment was used in both drainage and imbibition conditions and the macroscopic bypassing in adverse mobility immiscible floods was measured. The experimental results suggested that the macroscopic viscous fingering was present in adverse mobility immiscible floods. Viscous fingering and gravity override were larger for the drainage process than for imbibition process. In water-wet media, WAG injection is not better than continuous injection of CO₂ if the viscosity ratio of the oil-CO₂ mixture is about 20. However, at higher viscosity ratios and density differences a WAG ratio of 3 to 5 is more effective than continuous injection.

Wylie and Mohanty [67] studied the impact of wettability on oil bypassed during gas injection as a result of gravitational, viscous and heterogeneity effects. Mass transfer from the bypassed region to the flowing gas is dependent upon pressure-driven, gravity-driven and capillary-driven crossflows as well as diffusion and dispersion. Mass-transfer experiments eliminate viscous displacement and allow isolation of mass-transfer mechanisms. Gas floods are carried out to investigate viscous displacement and bypassing. The study showed that less bypassing occurred under strongly oil-wet than in water-wet condition for gravity-dominated, secondary gas floods. Also, mass transfer was improved under oil-wet conditions over water-wet conditions for diffusion and gravity dominated orientations.

Chalbaud et al. [68] addressed the role of wettability during CO₂ flooding. Core experiments were conducted on a carbonate reservoir for two wettability conditions: water-wet and intermediate-wet. CO₂ flooding was performed in glass micro-models to trace the distribution of fluids under the same conditions. The results showed that CO₂ did not contact the solids in water-wet media while for intermediate-wet media the CO₂ partially wetted the solids.

Zekri et al. [69] conducted a laboratory study evaluating the possible alteration of wettability for tight limestone cores. Changes in relative permeability due to CO₂ injection were used to recognize wettability alteration. The results suggested that CO₂ flooding changed water-wet limestone cores to more favorable condition of wettability, i.e., more water-wet condition. Also, CO₂ flooding caused another favorable effect by reducing the IFT between the employed crude oil and the brine.

Egermann et al. [70] proposed a novel experimental procedure to investigate rock-fluid interactions that occur in the far-field region during CO₂ injection. The experimental work showed that permeability evolution depended heavily on the pore structure. The pore network approach was then considered to interpret and analyze the evolution of rock properties. The pore network approach gave a first analysis of the evolution of the rock in terms of porosity and permeability at different dissolution regime. The reaction-limited regime is simulated by uniform dissolution while the reverse case is simulated by pore-body dissolution in diffusion predominant regime and by the pore-throat dissolution in the convection predominant regime. The quantitative comparison with the experimental results indicated the scenario that enables to reproduce satisfactorily the permeability evolution.

Fjelde and Asen [71] conducted spontaneous imbibition experiments to evaluate the wettability conditions for five core plugs obtained from a fractured chalk reservoir in the North Sea. The work was carried out at reservoir conditions during water and CO₂ flooding. The results showed that in the first cycle of a CO₂ WAG process, the wettability was changed from mixed-wet or preferential oil-wet to more water-wet. Wettability alteration was able to alter the saturation function and therefore affect the transport of CO₂ and water in the reservoir.

Yang et al. [72] investigated the efficiency of gas injection at the pore-scale for weak water-wet and weak oil-wet pores. A pore-scale network model was built using van Dijke and Sorbie model [73-74]. A Simulation approach was applied to test different water saturations with various wettability conditions. The results suggested that with gas injection, oil wetting films in gas-filled pores were present leading to higher oil recovery. The results also showed that continuous gas injection was a better mode than WAG.

2.2 Numerical/Analytical Simulation Models

While much of the research work on the influence of wettability during CO₂ flooding was carried out in laboratory experiments involving core flooding and micro-models, a limited number of numerical/analytical models has been reported.

Tehrani et al. [75] developed a mathematical network simulator representing all the significant physical flow processes involved in recovery by gas injection. The results obtained from the network model were compared with those of laboratory experiments

performed in micro-models of different wettabilities. The comparison showed that the simulator is very reliable in making prediction of real reservoir performance under gas injection operation. Table 2.1 presents four widely accepted models handling wettability alteration.

First, van Dijke and Sorbie [73] studied wettability effects through pore-scale network simulator models for porous media containing three phases. Wettability was specified by the cosine of the oil-water contact angle ($\cos \theta_{ow}$) where the sign of this parameter indicated the wetting order of the fluids (oil and water) in the pore. The capillary pressure in the porous medium was measured through the Young Laplace equations. Contact-angle relationships for all possible fluid-fluid interfaces with the solid were combined to develop a constraint on the three-phase contact angles and IFT [26,76-77]. The pore wettability was represented by measuring θ . Depending on the interfacial tensions, the ranges of the pore sizes and the degree of wettability of the pores, up to three regions in saturation space can be identified and related to the phase dependencies of three-phase capillary pressures and relative permeabilities.

Second, Delshad et al. [78] developed a new mathematical model to evaluate wettability alteration for a naturally fractured reservoir. Surfactants were used to change the wettability by increased imbibition of the water into the matrix rocks. Wettability alteration was modeled through measuring the changes in relative permeability and capillary pressure.

Third, Farhadinia and Delshad [79] modeled wettability alteration by chemical injection in naturally fractured reservoirs using dual porosity MINC (Multiple Interacting Continua) method. A fracture was modeled by a connected network of pores while the matrix was represented by discrete volumetric elements like sugar cubes. Two flow equations were applied, one for the matrix and one for the fracture. The two flow equations were tied through a transfer function. Two sets of relative permeabilities were required to model input corresponding to the initial and final wettability states for the rock. The relative permeability in each grid block was calculated while the relative permeabilities for each phase were assumed. The capillary pressure was modeled linearly as a function of wettability and was then scaled with IFT. The transfer function was calculated by solving the water pressure equation of the matrix. The transfer terms were then added to the fracture pressure equation to solve it implicitly. At the end of each time step, the fracture and matrix variables were obtained. The wettability alteration model updated the relative permeabilities and capillary pressures as input parameters.

Forth, Ju et al. [80] developed a new mathematical model handling wettability alteration assuming that relative permeabilities would be affected by asphaltene deposition. Thus, relative permeabilities would be modified. When the surfaces per unit bulk volume of the porous media are completely occupied by asphaltene, the modified relative permeabilities are taken. In addition, the numerical simulation results showed that wettability was changed from water-wet to oil-wet with asphaltene deposition resulting in less oil recovery by about 3% than without asphaltene deposition.

Table 2.1 Comparison of some widely accepted models addressing wettability alterations

Authors	Model	Remarks
Van Dijke and Sorbie (2002)	<p>In water wet pores: $0 \leq \cos \theta_{ow} \leq 1$</p> <p>In oil-wet pores: $-1 \leq \cos \theta_{ow} < 0$</p> $P_{c,ij} = \frac{2\sigma_{ij} \cos \theta_{ij}}{r}$ $\cos \theta_{go} = \frac{1}{2\sigma_{go}} \{C_{S,o} \cos \theta_{ow} + C_{S,o} + 2\sigma_{go}\}$ $\cos \theta_{gw} = \frac{1}{2\sigma_{gw}} \{(C_{S,o} + 2\sigma_{ow}) \cos \theta_{ow} + C_{S,o} + 2\sigma_{go}\}$	<ol style="list-style-type: none"> 1) Applied Young Laplace equations. 2) Wettability represented through contact angle measurements. 3) Incorporation of double and multiple displacements for mobilization of disconnected phase clusters. 4) Implemented outlet boundary conditions that are consistent with intra-system pressure changes.
Delshad et al. (2006)	$k_{rl} = k_{rl}^o \bar{S}_l^{n_l} \quad l = 1,2,3$ $\bar{S}_l = \frac{S_l - S_{lr}}{1 - \sum_{l=1}^3 S_{lr}} \quad l = 1,2,3$ $S_{lr} = \min \left[S_l \left(S_l^{high} + \frac{S_{lr}^{low} - S_{lr}^{high}}{1 + T_l N_{Tl}} \right) \right] \quad l = 1,2,3$ $N_{Tl} = \frac{\left -\vec{\nabla} \cdot \vec{\nabla} \phi_l - \frac{\vec{\nabla} \cdot [g(\rho_{l'} - \rho_l) \cdot \vec{\nabla} h]}{\sigma_{ll'}} \right }{\sigma_{ll'}}$ $k_{rl}^o = k_{rl}^{o,low} + \frac{S_{l'r}^{low} - S_{l'r}}{S_{l'r}^{low} - S_{l'r}^{high}} (k_{rl}^{o,high} - k_{rl}^{o,low}) \quad l = 1,2,3$ $n_l = n_l^{low} + \frac{S_{l'r}^{low} - S_{l'r}}{S_{l'r}^{low} - S_{l'r}^{high}} (n_l^{high} - n_l^{low}) \quad l = 1,2,3$ $k_{rl} = \omega k_{rl}^{final} + (1 - \omega) k_{rl}^{initial} \quad l = 1,2,3$ $P_c = \omega P_c^{final} + (1 - \omega) P_c^{initial}$	<ol style="list-style-type: none"> 1) Wettability represented through measuring the changes in relative permeability and capillary pressure. 2) Limited for natural fractured reservoirs.
Farhadinia and Delshad (2010)	<p>Matrix: $\tau_{am-f} = \frac{\partial}{\partial t} \left(\frac{\phi S_a}{B\alpha} \right)_m$</p> <p>Fracture: $\nabla \lambda_{af} \left(\nabla P_{af} - \rho_a \frac{g}{g_c} \nabla Z \right) = \frac{\partial}{\partial t} \left(\frac{\phi S_a}{B} \right)_f + q_{af} + \tau_{am-f}$</p> $k_{rl} = \omega k_{rl}^{final} + (1 - \omega) k_{rl}^{initial} \quad l = 1,2,3$ $k_{rl} = k_{rl}^o \left(\frac{S_l - S_{lr}}{1 - \sum_{l=1}^3 S_{lr}} \right)^{n_l} \quad l = 1,2,3$ $P_c = \omega P_c^{final} + (1 - \omega) P_c^{initial}$ $P_{clo} = C_{pc} \frac{\sigma_{ol}}{\sigma_{ow}} \left(1 - \frac{S_l - S_{lr}}{1 - \sum_{l=1}^3 S_{lr}} \right)^{E_{pc}} \quad l = 1 \text{ or } 3$	<ol style="list-style-type: none"> 1) Limited for natural fractured carbonate reservoirs only. 2) Using surfactants with a dual porosity model. 3) Applied discrete fracture approach.
Ju et al. (2010)	$K'_{rwja} = K_{rwj} + \frac{K'_{rwj} - K_{rwj}}{A_{fc}} A_c$ $K'_{roja} = K_{roj} + \frac{K'_{roj} - K_{roj}}{A_{fc}} A_c$	<ol style="list-style-type: none"> 1) Wettability represented through measuring the relative permeability. 2) Relative permeability is a function of volume of asphaltene precipitation.

]

CHAPTER 3

STATEMENT OF THE PROBLEM

3.1 Knowledge Gap

As evident from the literature survey reported in Chapter 2, a few numerical/analytical models have been developed that incorporate the influence of wettability during CO₂ flooding. Moreover, it is noticed that the solutions presented to these models consider rock and fluid properties to vary with space only [81-82] and are, thus, time-independent. This shortcoming creates a significant knowledge gap between the analytical/numerical solutions and reality since time is a crucial factor in the evolution of any rock and fluid property especially when mass transport between the phases is involved. Therefore, bridging this gap through development of a time-dependent model to trace the wettability alteration on continuous basis during CO₂ flooding process becomes necessary. If wettability alteration is handled properly, better prediction of CO₂ flooding performance will be achieved.

3.2 Objectives

The objectives of this work were as follows:

- To develop a new mathematical model to represent CO₂-oil displacement under immiscible conditions. The mathematical model is to include a representation of the relative permeabilities of the oil and CO₂ phases as functions of wettability.
- To solve the mathematical displacement model numerically using MATLAB program.
- To conduct a laboratory experiment to measure the change in wettability with time for a rock/oil/brine system exposed to CO₂.
- To conduct a laboratory core-flooding experiment with CO₂ under immiscible conditions.
- To verify the numerical model with data generated from all laboratory experiments.

3.3 Research Approach

Two approaches were employed in this work: analytical and experimental. In the first approach, a new mathematical model was developed to handle wettability alteration continuously during CO₂ flooding process. The mathematical model represents the CO₂-oil displacement system under immiscible conditions and includes a novel way of determining the relative permeabilities of the oil and CO₂ phases as functions of wettability. The mathematical model was solved numerically employing MATLAB

programming language. The assumptions made to the mathematical model were as follows:

- The reservoir has a known geometry and contains oil only.
- The pressure and oil saturation are uniform throughout the reservoir.
- The flow is assumed to be linear and parallel to the reservoir length (x-axis).
- CO₂ is injected at one end of the reservoir.
- CO₂ remains in the gas phase throughout the process.
- CO₂ injection rate is constant.
- The production rates of CO₂ and oil are measurable.
- The initial oil saturation and pressure are known.
- Flooding is immiscible with no gas slippage.
- Capillary pressure is neglected.
- The system is compressible and isothermal.
- The rock is initially strongly oil-wet.
- Connate water saturation is known.

In the second approach, a core flooding experiment was conducted with CO₂ under immiscible conditions at a pressure below the MMP. The experiment was conducted at a constant rate and temperature. The generated laboratory data was used to verify the displacement model developed in the first approach. Also, contact angle measurement experiments were conducted on a rock crystal in the presence of CO₂ to generate a contact angle versus CO₂ exposure time curve. All laboratory experiments were performed on samples obtained from a carbonate reservoir.

CHAPTER 4

MATHEMATICAL MODEL DEVELOPMENT

4.1 Background

In this chapter, a mathematical model is presented that describes rigorously immiscible CO₂-oil flow in porous media within a secondary recovery scheme. The model equation is based on one-dimensional, two-phase, immiscible fluid flow and accounts for alteration of rock wettability with time. Once discretized, the model equation can be solved numerically using MATLAB or any other programming language.

4.2 Model Assumptions

The porous medium is assumed to be an oil reservoir with linear geometry. The reservoir is initially saturated with oil at known immobile water saturation. The initial pressure and saturations are known and uniform throughout the reservoir. CO₂ is injected at one end and remains in the gas phase throughout the process which requires the flooding to be at low pressure (less than 1000 psi). The flow is assumed to be linear and parallel to the reservoir's main axis (x-axis) with constant CO₂ injection rate. Flooding is immiscible with no gas slippage, and the system is compressible and isothermal. Due to the large difference in densities between oil and CO₂, capillary pressure is neglected ($p_c \approx 0$).

Since gas compressibility will be dominant in the model, compressibility of oil and rock are neglected.

4.3 Development of CO₂-Oil Displacement Model

First, let us consider Darcy's law for a linear horizontal system.

$$q_x = -\frac{k_x A}{\mu_x} \frac{\partial p_x}{\partial x} \quad (4.1)$$

Under reservoir conditions, the oil and CO₂ velocities can be presented by:

$$u_o = -\frac{k_o}{\mu_o} \frac{\partial p}{\partial x} \quad (4.2)$$

and

$$u_{CO_2} = -\frac{k_{CO_2}}{\mu_{CO_2}} \frac{\partial p}{\partial x} \quad (4.3)$$

Due to the presence of immobile water saturation (s_{wi}) in the model, oil and CO₂ will flow in the porous medium with an effective porosity of $\phi^* = \phi(1 - s_{wi})$.

The continuity equation for the oil phase can be written as:

$$\frac{\partial}{\partial x}(\rho_o u_o) + \phi^* \frac{\partial}{\partial t}(\rho_o S_o) = 0 \quad (4.4)$$

Since oil can be regarded as an incompressible fluid, oil density remains constant. Thus, Eq. (4.4) becomes:

$$\frac{\partial u_o}{\partial x} + \phi^* \frac{\partial S_o}{\partial t} = 0 \quad (4.5)$$

The continuity equation for the CO₂ phase can be written as:

$$\frac{\partial}{\partial x}(\rho_{\text{CO}_2} u_{\text{CO}_2}) + \phi^* \frac{\partial}{\partial t}(\rho_{\text{CO}_2} S_{\text{CO}_2}) = 0 \quad (4.6)$$

However, the gas density is a function of pressure. The real gas density can be expressed as:

$$\rho_{\text{CO}_2} = \frac{pM_{\text{CO}_2}}{zRT} \quad (4.7)$$

Substituting Eq. (4.7) into Eq. (4.6) yields:

$$\frac{\partial}{\partial x} \left(\frac{pM_{\text{CO}_2}}{zRT} u_{\text{CO}_2} \right) + \phi^* \frac{\partial}{\partial t} \left(\frac{pM_{\text{CO}_2}}{zRT} S_{\text{CO}_2} \right) = 0 \quad (4.8)$$

M_{CO_2} , R and T are constants and can be eliminated:

$$\frac{\partial}{\partial x} \left(\frac{p u_{\text{CO}_2}}{z} \right) + \phi^* \frac{\partial}{\partial t} \left(\frac{p S_{\text{CO}_2}}{z} \right) = 0 \quad (4.9)$$

At low pressures (< 1000 psi) [25] and normal reservoir temperatures, the compressibility factor (z) of CO₂ varies slightly from about 0.96 to about 0.7 as depicted in Figure 4.1. Also, viscosity of CO₂ (μ_{CO_2}) is noticed to vary slightly from 0.016 cP at 500 psi to 0.02 cP at 900 psi as depicted in Figure 4.2. However, plotting $\left(\frac{p}{z\mu_{\text{CO}_2}} \right)$ shows rapid increase reaching about 80000 as depicted in Figure 4.3. Such physical behavior of CO₂ at low pressures suggests keeping the $\left(\frac{p}{z} \right)$ term in Eq. (4.9) coupled during the model development.

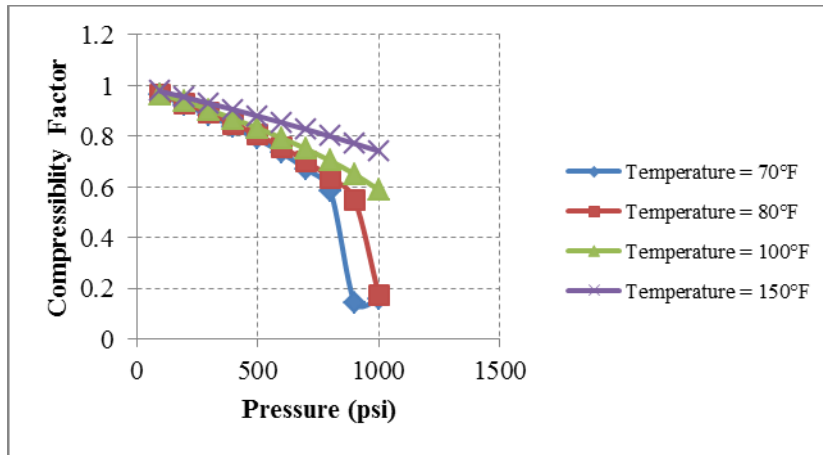


Figure 4.1 Variation of CO₂ compressibility factor

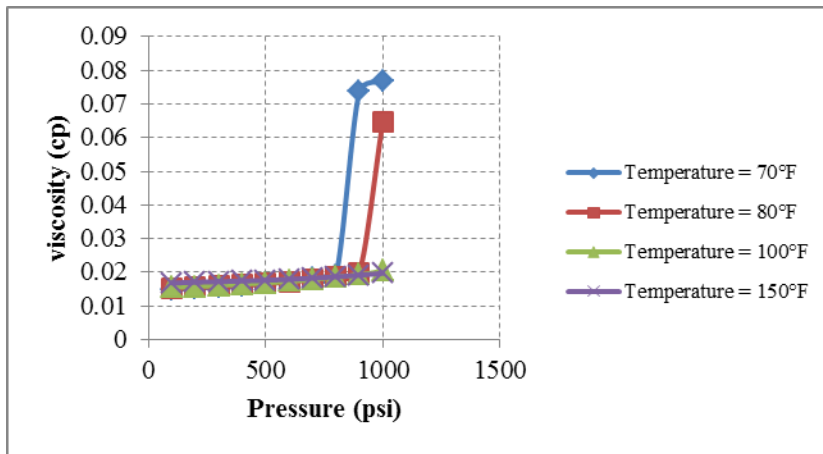


Figure 4.2 Variation of CO₂ viscosity

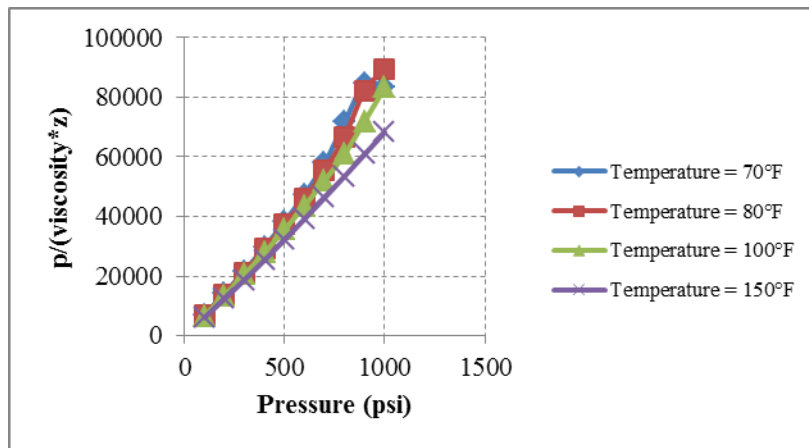


Figure 4.3 Variation of $\frac{p}{z\mu}$ for CO₂

Expanding the differentials of Eq. (4.9) yields:

$$\frac{p}{z} \frac{\partial u_{CO_2}}{\partial x} + u_{CO_2} \frac{\partial}{\partial p} \left(\frac{p}{z} \right) \frac{\partial p_{CO_2}}{\partial x} + \frac{\phi^* p}{z} \frac{\partial S_{CO_2}}{\partial t} + \phi^* S_{CO_2} \frac{\partial}{\partial p} \left(\frac{p}{z} \right) \frac{\partial p}{\partial t} = 0 \quad (4.10)$$

We know that:

$$\frac{\partial}{\partial p} \left(\frac{p}{z} \right) = \frac{z - p \frac{\partial z}{\partial p}}{z^2} \quad (4.11)$$

$$\frac{\partial}{\partial p} \left(\frac{p}{z} \right) = \frac{p c_{CO_2}}{z} \quad (4.12)$$

Substituting Eq. (4.12) into Eq. (4.10) yields:

$$\frac{p}{z} \frac{\partial u_{CO_2}}{\partial x} + u_{CO_2} \frac{p c_{CO_2}}{z} \frac{\partial p}{\partial x} + \frac{\phi^* p}{z} \frac{\partial S_{CO_2}}{\partial t} + \phi^* S_{CO_2} \frac{p c_{CO_2}}{z} \frac{\partial p}{\partial t} = 0 \quad (4.13)$$

Dividing Eq. (4.13) by $\frac{p}{z}$ yields:

$$\frac{\partial u_{CO_2}}{\partial x} + u_{CO_2} c_{CO_2} \frac{\partial p}{\partial x} + \phi^* \frac{\partial S_{CO_2}}{\partial t} + \phi^* S_{CO_2} c_{CO_2} \frac{\partial p}{\partial t} = 0 \quad (4.14)$$

Since we assumed no slip velocity exists between the two immiscible fluids, then:

$$U_x = u_o + u_{CO_2} \quad (4.15)$$

$$f_{CO_2} = \frac{u_{CO_2}}{U_x} \quad (4.16)$$

Substituting Eqs. (4.16) into Eq. (4.3) yields:

$$f_{CO_2} U_x = - \frac{k_{CO_2}}{\mu_{CO_2}} \frac{\partial p}{\partial x} \quad (4.17)$$

Substituting Eq. (4.16) into Eq. (4.14) yields:

$$\frac{\partial(f_{\text{CO}_2} U_x)}{\partial x} + f_{\text{CO}_2} U_x c_{\text{CO}_2} \frac{\partial p}{\partial x} + \phi^* \frac{\partial S_{\text{CO}_2}}{\partial t} + \phi^* S_{\text{CO}_2} c_{\text{CO}_2} \frac{\partial p}{\partial t} = 0 \quad (4.18)$$

Since capillary pressure is neglected, then:

$$U_x = - \left(\frac{k_{\text{CO}_2}}{\mu_{\text{CO}_2}} + \frac{k_o}{\mu_o} \right) \frac{\partial p}{\partial x} \quad (4.19)$$

Total mobility(γ_t) can be written as [83]:

$$\gamma_t = \left(\frac{k_{\text{CO}_2}}{\mu_{\text{CO}_2}} + \frac{k_o}{\mu_o} \right) \quad (4.20)$$

Substituting Eq. (4.20) into Eq. (4.19) yields:

$$U_x = -\gamma_t \frac{\partial p}{\partial x} \quad (4.21)$$

Substituting Eq. (4.21) into Eq. (4.18) yields:

$$- \frac{\partial \left(f_{\text{CO}_2} \left(\gamma_t \frac{\partial p}{\partial x} \right) \right)}{\partial x} - f_{\text{CO}_2} \left(\gamma_t \frac{\partial p}{\partial x} \right) c_{\text{CO}_2} \frac{\partial p}{\partial x} + \phi^* \frac{\partial S_{\text{CO}_2}}{\partial t} + \phi^* S_{\text{CO}_2} c_{\text{CO}_2} \frac{\partial p}{\partial t} = 0 \quad (4.22)$$

Expanding the differentials of Eq. (4.22) yields:

$$-f_{\text{CO}_2} \gamma_t \frac{\partial^2 p}{\partial x^2} - \gamma_t \frac{\partial p}{\partial x} \frac{\partial f_{\text{CO}_2}}{\partial x} - f_{\text{CO}_2} \frac{\partial p}{\partial x} \frac{\partial \gamma_t}{\partial x} - f_{\text{CO}_2} \gamma_t c_{\text{CO}_2} \left(\frac{\partial p}{\partial x} \right)^2 + \phi^* \frac{\partial S_{\text{CO}_2}}{\partial t} + \phi^* S_{\text{CO}_2} c_{\text{CO}_2} \frac{\partial p}{\partial t} = 0 \quad (4.23)$$

Equation (4.23) presents a CO₂-oil immiscible flow model in a one-dimensional porous medium.

4.3.1 Inspection of Displacement Model Dimensions

Dimensions of the displacement model – Eq. (4.22) – needs to be verified to make sure that all terms are consistent. Replacing the terms of Eq. (4.22) with respective dimensions yields:

$$\left(\frac{1}{L} \times \frac{L^2}{\frac{M}{Lt}} \times \frac{M}{L^2}\right) + \left(\frac{L^2}{\frac{M}{Lt}} \times \frac{M}{L} \times \frac{1}{L}\right) + \frac{1}{t} + \frac{1}{t} = 0$$

This simplifies to:

$$-\frac{1}{t} - \frac{1}{t} + \frac{1}{t} + \frac{1}{t} = 0$$

Where

$$p_{CO_2} \rightarrow \frac{M}{Lt^2}$$

$$x \rightarrow L$$

$$\gamma_t \rightarrow \frac{L^2}{\frac{M}{Lt}}$$

Since $L = \text{Length}$, $M = \text{Mass}$ and $t = \text{time}$

This confirms that all terms have a consistent dimension which is the inverse of time.

The field units considered in the displacement model are as follows:

$$\text{permeability} \rightarrow mD$$

pressure → psi

length → ft

viscosity → cP

time → Day

This requires introducing a conversion factor to be multiplied by the displacement model terms in order to ensure all terms have dimension of $\frac{1}{\text{Day}}$. This will be demonstrated for the first four terms of the displacement model.

For gas phase, the conversion factor will be computed as follows:

$$\frac{86400 \times 1.06 \times 10^{-14}}{1.45 \times 10^{-7}} \frac{ft^2}{in^2} \frac{lb}{in^2} \frac{s}{ft^2} \frac{Day}{s} = 6.3 \times 10^{-3} \frac{1}{Day}$$

For oil phase, the conversion factor will be as follows:

$$\frac{6.3 \times 10^{-3}}{5.615} = 1.1 \times 10^{-3} \frac{1}{Day}$$

The conversion factors for oil and gas phases are incorporated in the displacement model as follows:

$$\begin{aligned} & -f_{CO_2} \left(6.3 \times 10^{-3} \times \frac{k_{CO_2}}{\mu_{CO_2}} + 1.1 \times 10^{-3} \times \frac{k_o}{\mu_o} \right) \frac{\partial^2 p}{\partial x^2} - \left(6.3 \times 10^{-3} \times \frac{k_{CO_2}}{\mu_{CO_2}} + 1.1 \times 10^{-3} \times \right. \\ & \left. \frac{k_o}{\mu_o} \right) \frac{\partial p}{\partial x} \frac{\partial f_{CO_2}}{\partial x} - f_{CO_2} \frac{\partial p}{\partial x} \frac{\partial \left(6.3 \times 10^{-3} \times \frac{k_{CO_2}}{\mu_{CO_2}} + 1.1 \times 10^{-3} \times \frac{k_o}{\mu_o} \right)}{\partial x} - f_{CO_2} c_{CO_2} \left(6.3 \times 10^{-3} \times \frac{k_{CO_2}}{\mu_{CO_2}} + \right. \\ & \left. 1.1 \times 10^{-3} \times \frac{k_o}{\mu_o} \right) \left(\frac{\partial p}{\partial x} \right)^2 + \phi \frac{\partial S_{CO_2}}{\partial t} + \phi S_{CO_2} c_{CO_2} \frac{\partial p}{\partial t} = 0 \end{aligned} \quad (4.24)$$

4.3.2 Investigations of the Nonlinear Term in the Displacement Model

The displacement model - Eq. (4.24) - includes the following nonlinear term:

$$-f_{\text{CO}_2} c_{\text{CO}_2} \left(6.3 \times 10^{-3} \times \frac{k_{\text{CO}_2}}{\mu_{\text{CO}_2}} + 1.1 \times 10^{-3} \times \frac{k_o}{\mu_o} \right) \left(\frac{\partial p}{\partial x} \right)^2$$

This term should be investigated to determine its significance on the computation process. First, a relative comparison is made between the nonlinear term and one of the first three terms in Eq. (4.24) (i.e. the second term) as described below:

$$2^{\text{nd}} \text{ term} \rightarrow - \left(6.3 \times 10^{-3} \times \frac{k_{\text{CO}_2}}{\mu_{\text{CO}_2}} + 1.1 \times 10^{-3} \times \frac{k_o}{\mu_o} \right) \frac{\partial p}{\partial x} \frac{\partial f_{\text{CO}_2}}{\partial x}$$

$$\text{Nonlinear term} \rightarrow -f_{\text{CO}_2} c_{\text{CO}_2} \left(6.3 \times 10^{-3} \times \frac{k_{\text{CO}_2}}{\mu_{\text{CO}_2}} + 1.1 \times 10^{-3} \times \frac{k_o}{\mu_o} \right) \left(\frac{\partial p}{\partial x} \right)^2$$

Both terms can be expressed in terms of dimensions as follows:

$$2^{\text{nd}} \text{ term} \rightarrow \left(\gamma_c \frac{\Delta p}{L^2} \right)$$

$$\text{Nonlinear term} \rightarrow c_{\text{CO}_2} \left(\gamma_c \frac{\Delta p^2}{L^2} \right)$$

Where

γ_c = Characteristic mobility

$$\text{Ratio} = \frac{2^{\text{nd}} \text{ term}}{\text{Nonlinear term}} = \frac{\left(\gamma_c \frac{\Delta p}{L^2} \right)}{c_{\text{CO}_2} \left(\gamma_c \frac{\Delta p^2}{L^2} \right)}$$

$$Ratio = \frac{1}{c_{CO_2} \Delta p}$$

Typical values of c_{CO_2} at low reservoir pressures (<1000 psi) and $T = 75$ °F range from about 0.002 psi^{-1} at 500 psi to about 0.001 psi^{-1} at 900 psi. With the assumption of a porous medium with the following rock and fluid properties:

$$k = 600 \text{ mD} \qquad k_{rCO_2} = 0.70 (@ 1 - s_{or})$$

$$c_{CO_2} = 0.002 \text{ psi}^{-1} \qquad k_{rCO_2} = 0 (@ s_{wi})$$

$$\mu_{CO_2} = 0.02 \text{ cP} \qquad k_{ro} = 0 (@ 1 - s_{or})$$

$$\mu_o = 0.70 \text{ cP} \qquad k_{ro} = 0.90 (@ s_{wi})$$

$$L = 0.50 \text{ ft} \qquad Q_g = 0.25 \frac{\text{ft}^3}{\text{Day}}$$

$$Area = 0.01 \text{ ft}^2$$

the value of Δp with a low injection rate can be around 2.3 psi. Therefore

$$Ratio_{maximum} = \frac{1}{0.001 \times 2.3} = \frac{1}{0.04} \approx 434$$

$$Ratio_{minimum} = \frac{1}{0.002 \times 2.3} = \frac{1}{0.08} \approx 217$$

This shows that the second term will be greater than the nonlinear term by between 217 and 434 times at 500 and 900 psi, respectively.

Next, the absolute magnitude of the coefficient of the nonlinear term is also investigated.

Three conditions are considered:

Condition # 1: At $f_{CO_2} = 1$ (Maximum Value)

$$1 \times 0.002 \left(\frac{6.3 \times 10^{-3} \times 0.7 \times 600}{0.02} + 0 \right) \approx 0.266$$

Condition # 2: At $f_{CO_2} = 0.5$

$$0.5 \times 0.002 \left(\frac{1.1 \times 10^{-3} \times 0.45 \times 600}{0.70} + \frac{6.3 \times 10^{-3} \times 0.35 \times 600}{0.02} \right) \approx 0.07$$

Condition # 3: At $f_{CO_2} = 0$ (Minimum Value)

$$0 \times 0.002 \left(\frac{1.1 \times 10^{-3} \times 0.9 \times 600}{0.70} + 0 \right) = 0$$

Odeh and Babu [84] have shown that the practice of neglecting the nonlinear term in the PDE that describes the flow of slightly compressible fluids through porous media does not result in significant errors. This assumption is also valid during the flow of gases through porous media at low flow rates that results in small pressure gradients [85]. In summary, the investigation shows that the nonlinear term in Eq. (4.24) is negligible relative to the other terms. The coefficient of the nonlinear term varies between 0 and 0.266 which makes the significance of the nonlinear term even smaller. Besides, since the model deals with low pressure gradients, the magnitude of $\left(\frac{\partial p}{\partial x}\right)^2$ will be lowered. As a result, neglecting the nonlinear term in Eq. (4.24) will not introduce significant errors to the overall solution. Hence, Eq. (4.24) can be simplified to the following:

$$-f_{CO_2} \left(6.3 \times 10^{-3} \times \frac{k_{CO_2}}{\mu_{CO_2}} + 1.1 \times 10^{-3} \times \frac{k_o}{\mu_o} \right) \frac{\partial^2 p}{\partial x^2} - \left(6.3 \times 10^{-3} \times \frac{k_{CO_2}}{\mu_{CO_2}} + 1.1 \times 10^{-3} \times \frac{k_o}{\mu_o} \right) \frac{\partial p}{\partial x} \frac{\partial f_{CO_2}}{\partial x} - f_{CO_2} \frac{\partial p}{\partial x} \frac{\partial \left(6.3 \times 10^{-3} \times \frac{k_{CO_2}}{\mu_{CO_2}} + 1.1 \times 10^{-3} \times \frac{k_o}{\mu_o} \right)}{\partial x} + \phi^* \frac{\partial S_{CO_2}}{\partial t} + \phi^* S_{CO_2} c_{CO_2} \frac{\partial p}{\partial t} = 0 \quad (4.25)$$

This model is developed specifically to handle CO₂-oil displacement through a porous medium under the following conditions:

- An immiscible and compressible displacement process
- A low pressure system (< 1000 psi)
- Low gas flow rates
- Low pressure gradients

4.4 Development of a Modified Corey Relative Permeability Model

The phase relative permeability relationship is a necessary parameter in assessing the recovery efficiency for a particular reservoir. The normalized phase saturation is a well-established representation of phase relative permeability and can be expressed as [54]:

$$S_{on} = \frac{(S_o - S_{or})}{(1 - S_{or} - S_{wi})} \quad (4.26)$$

Corey [86] proposed the power law model for relative permeability of oil and gas as:

$$k_{ro} = k_{ro}^o S_{on}^{n_o} \quad (4.27)$$

$$k_{rCO_2} = k_{rCO_2}^o (1 - S_{on})^{n_g} \quad (4.28)$$

Core flooding experiments showed that the maximum oil recovery apparently occurs in neutral or slightly oil-wet cores [27]; [87]. Strong oil wettability results in low oil recovery because the wetting phase (oil) occupies the small pores, which leads to a high residual oil saturation. In contrast, the residual oil saturation in intermediate-wet rocks decreases since water shares those small pores with the oil. Therefore, it is theoretically plausible to speculate that the residual oil saturation will follow an exponential relationship with the rock wettability for rocks of the same type but with different states of wettability. The residual oil saturation will decrease exponentially as the rock wettability – represented by the contact angle - is changed from oil-wet to intermediate-wet as depicted in Figure 4.4 and expressed by Eq. (4.29).

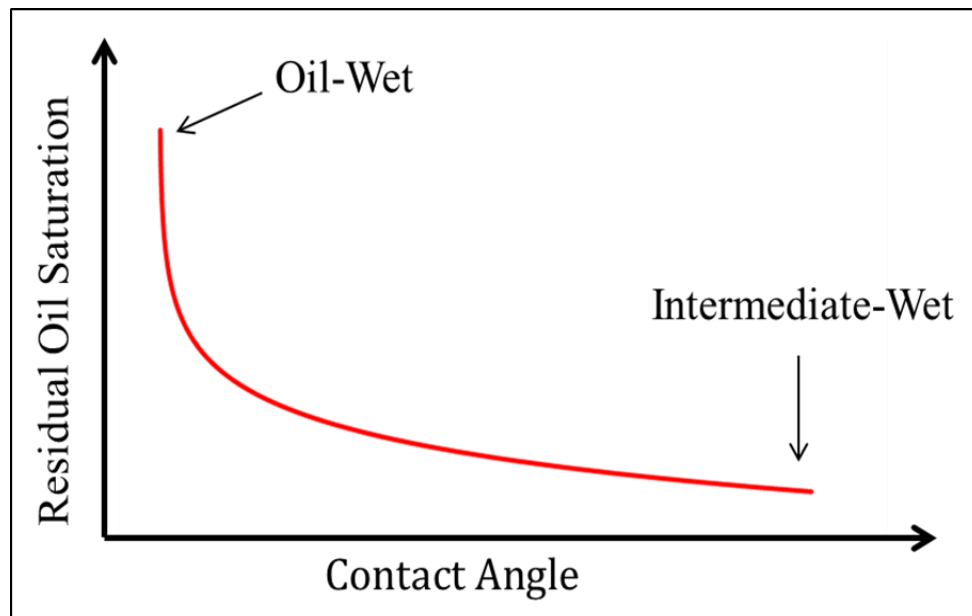


Figure 4.4 Variation of residual oil saturation with rock wettability

$$S_{or} = ae^{bcos\theta} \quad (4.29)$$

In CO₂-oil immiscible displacement process, the relationship between residual oil saturation and rock wettability presented in Figure 4.4 still applies. As the wettability is altered from oil-wet to intermediate-wet, the dispersed water drops that were restricted to large pores can now invade medium pores and, thus, vacate the large pores to the gas phase. Overall, the gas phase plays a major role in fluid re-distribution in pores as it becomes the continuous phase affecting rock wettability eventually.

Coefficients a and b in Eq. (4.29) can be determined through the following proposed boundary conditions:

For strongly oil-wet: ($\theta = 180^\circ$)

$$\cos(180^\circ) = -1 \quad (4.30)$$

For intermediate-wet: ($\theta = 90^\circ$)

$$\cos(90^\circ) = 0 \quad (4.31)$$

Substituting Eqs. (4.30) and (4.31) into Eq. (4.29) yields:

$$(S_{or})_{ow} = ae^{-b} \quad (4.32)$$

$$a = (S_{or})_{iw} \quad (4.33)$$

Substituting Eq. (4.33) into Eq. (4.32) yields:

$$(S_{or})_{ow} = (S_{or})_{iw}e^{-b} \quad (4.34)$$

Coefficient b can be obtained by taking the natural logarithm of Eq. (4.34):

$$b = \ln \left(\frac{(S_{or})_{iw}}{(S_{or})_{ow}} \right) \quad (4.35)$$

Substituting Eqs. (4.35) and (4.33) into Eq. (4.29) yields:

$$S_{or} = (S_{or})_{iw} e^{\ln \left(\frac{(S_{or})_{iw}}{(S_{or})_{ow}} \right) \cos \theta} \quad (4.36)$$

Re-arranging Eq. (4.36) yields:

$$S_{or} = (S_{or})_{iw} \left(\frac{(S_{or})_{iw}}{(S_{or})_{ow}} \right)^{\cos \theta} \quad (4.37)$$

Substituting Eq. (4.37) into Eq. (4.26) yields:

$$S_{on} = \frac{S_o - (S_{or})_{iw} \left(\frac{(S_{or})_{iw}}{(S_{or})_{ow}} \right)^{\cos \theta}}{1 - (S_{or})_{iw} \left(\frac{(S_{or})_{iw}}{(S_{or})_{ow}} \right)^{\cos \theta} - S_{wi}} \quad (4.38)$$

Substituting Eq. (4.38) into Eqs. (4.27) and (4.28) yields:

$$k_{ro} = k_{ro}^o \left[\frac{S_o - (S_{or})_{iw} \left(\frac{(S_{or})_{iw}}{(S_{or})_{ow}} \right)^{\cos \theta}}{1 - (S_{or})_{iw} \left(\frac{(S_{or})_{iw}}{(S_{or})_{ow}} \right)^{\cos \theta} - S_{wi}} \right]^{n_o} \quad (4.39)$$

$$k_{rCO_2} = k_{rCO_2}^o \left[1 - \left(\frac{S_o - (S_{or})_{iw} \left(\frac{(S_{or})_{iw}}{(S_{or})_{ow}} \right)^{\cos \theta}}{1 - (S_{or})_{iw} \left(\frac{(S_{or})_{iw}}{(S_{or})_{ow}} \right)^{\cos \theta} - S_{wi}} \right) \right]^{n_g} \quad (4.40)$$

Corey [86] measured gas (non-wetting phase) relative permeability to estimate the oil (wetting phase) relative permeability. He found that n_o and n_g can be 4 and 2, respectively. Equations (4.39) and (4.40) allow estimation of k_{ro} and k_{rCO_2} for any system with θ ranging between 90° and 180° .

4.5 Development of a Wettability Alteration Model

The argument presented to explain Fig. 4.4 can be extended to a given porous medium whose state of wettability is altered progressively from initially oil wet towards an intermediate-wet state. Suppose an oil-wet porous medium is initially fully saturated with oil at immobile water saturation. If CO_2 – whether dissolved in brine or as a free gas – is introduced into the medium, the medium’s wettability will be altered gradually from oil-wet to intermediate-wet as CO_2 diffuses through the oil to the solid surface (Figure 4.5). Since for a given system diffusion is controlled by the difference in concentrations, the rate of diffusion would decline exponentially with time as such difference diminishes [88]. As the change in contact angle is directly related to the concentration of CO_2 molecules at the oil/rock interface, and as the rate of build-up of such concentration is also diminishing exponentially with time, the contact angle would then be expected to decrease exponentially with CO_2 exposure time as conceptually depicted in Figure 4.6. However, such decrease would approach a certain limit asymptotically as the contact angle cannot drop below zero.

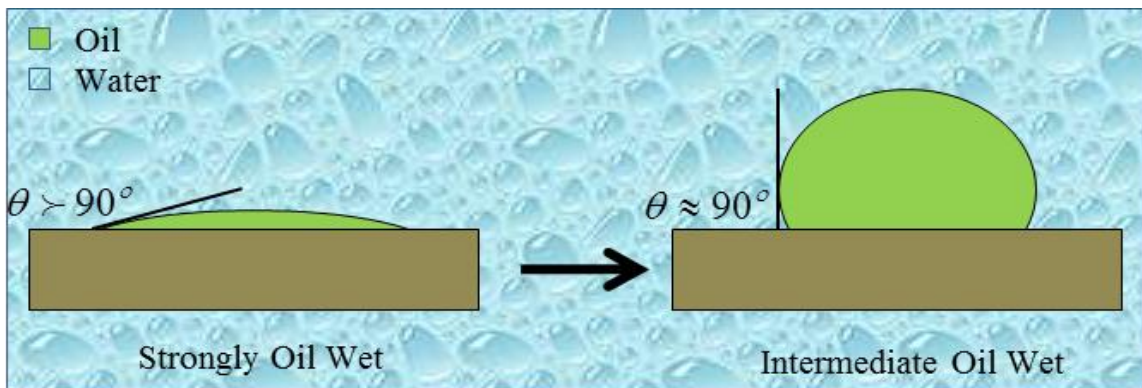


Figure 4.5 Proposed wettability alteration conditions in the porous medium

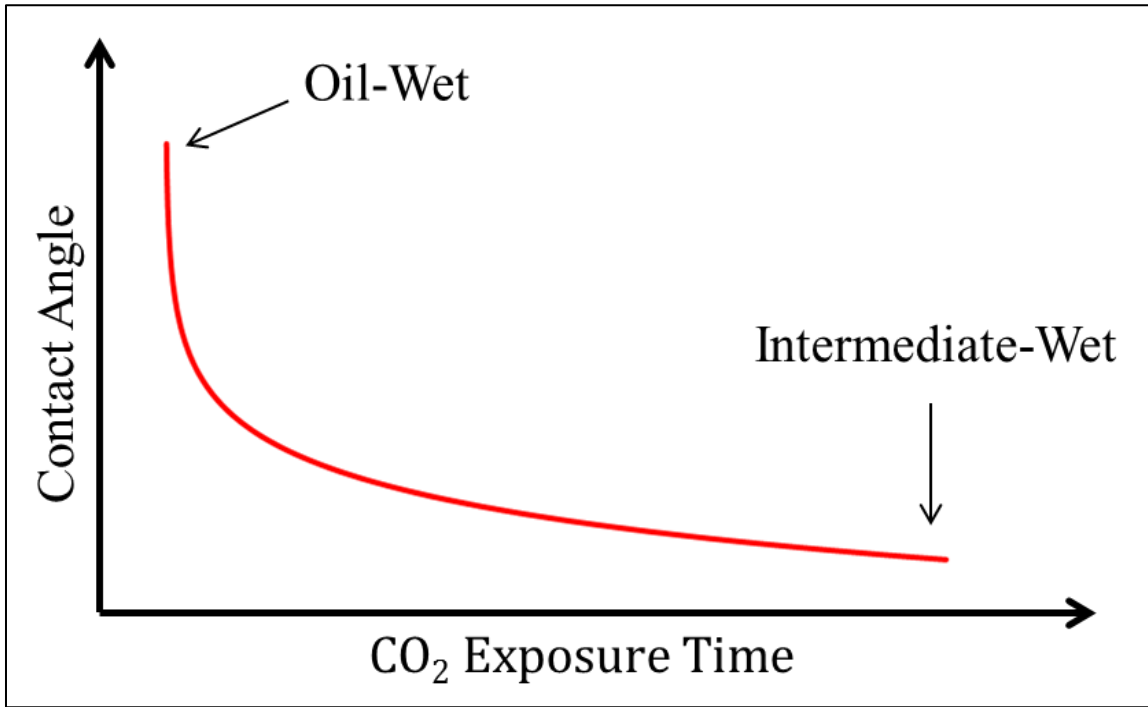


Figure 4.6 Contact angle variations with CO₂ exposure time

Based on the above concept, the relationships between wettability and CO₂ exposure time can be modeled as follows:

$$\theta = ae^{-bt} + c \quad (4.41)$$

Where

θ : Contact angle

t: time of exposure to CO₂

a, b and c: Constants related to rock and fluid compositions as well as aging history and process parameters.

Inspection of Eq. (4.41) reveals that “c” is the ultimate contact angle (θ_{\min}) reached – theoretically - at infinite exposure time (i. e., $t \rightarrow \infty$). The constant “a” then becomes the difference between the initial contact angle (θ_i) and (θ_{\min}). The constant “b” is related to the time when the contact angle is practically equal to (θ_{\min}). Such time shall be called stabilization time (t_{sb}) and, thus, “b” can be defined as $b = \xi/t_{sb}$ where ξ is a constant whose significance shall become evident in Section 7.1. Employing all the above definitions, Eq. (4.41) can then be rewritten in dimensionless form as:

$$\frac{\theta - \theta_{\min}}{\theta_{\min}} = \frac{\theta_i - \theta_{\min}}{\theta_{\min}} e^{-\xi t / t_{sb}} \quad (4.42)$$

Defining the dimensionless contact angle as $\theta_D = \frac{\theta - \theta_{\min}}{\theta_{\min}}$ and dimensionless time as

$t_D = \frac{t}{t_{sb}}$, Eq. (4.42) becomes:

$$\theta_D = \theta_{Di} e^{-\xi t_D} \quad (4.43)$$

Where

$$\theta_{Di} = \frac{\theta_i - \theta_{\min}}{\theta_{\min}}$$

All constants in Eq. (4.43) can be estimated experimentally as shall be demonstrated in Chapter 7.

4.6 Modeling Wettability Alteration on Continuous Basis during

Immiscible CO₂ Flooding Process

The three models represented by Eq. (4.25) and Eqs. (4.39-41) allow tracking the performance of the immiscible CO₂ flooding process where wettability is altered continuously. The wettability alteration model – Eq. (4.41) – estimates the shifted contact angle corresponding to the time of exposure to CO₂ for any given location in the system. The shifted contact angle is then fed to the modified Corey relative permeability model - Eqs. (4.39) and (4.40) - to calculate the new oil and CO₂ relative permeabilities at that location. Finally, the new relative permeability values are then employed by the displacement model represented by Eq. (4.25), which is solved numerically. The comprehensive model will be as follows:

$$\begin{aligned}
 & -f_{CO_2} \left(6.3 \times 10^{-3} \times \frac{k_{rCO_2}^o \left[1 - \left(\frac{S_o - (S_{or})_{iw} \left(\frac{(S_{or})_{iw}}{(S_{or})_{ow}} \right)^{\cos(ae^{-bt}+c)}}{1 - (S_{or})_{iw} \left(\frac{(S_{or})_{iw}}{(S_{or})_{ow}} \right)^{\cos(ae^{-bt}+c)} - S_{wi} \right)} \right]^{ng}}{\mu_{CO_2}} + 1.1 \times 10^{-3} \times \frac{k_{ro}^o \left[\frac{S_o - (S_{or})_{iw} \left(\frac{(S_{or})_{iw}}{(S_{or})_{ow}} \right)^{\cos(ae^{-bt}+c)}}{1 - (S_{or})_{iw} \left(\frac{(S_{or})_{iw}}{(S_{or})_{ow}} \right)^{\cos(ae^{-bt}+c)} - S_{wi} \right] k}{\mu_o} \right) \frac{\partial^2 p}{\partial x^2} \\
 & - \left(6.3 \times 10^{-3} \times \frac{k_{rCO_2}^o \left[1 - \left(\frac{S_o - (S_{or})_{iw} \left(\frac{(S_{or})_{iw}}{(S_{or})_{ow}} \right)^{\cos(ae^{-bt}+c)}}{1 - (S_{or})_{iw} \left(\frac{(S_{or})_{iw}}{(S_{or})_{ow}} \right)^{\cos(ae^{-bt}+c)} - S_{wi} \right)} \right]^{ng}}{\mu_{CO_2}} + 1.1 \times 10^{-3} \times \frac{k_{ro}^o \left[\frac{S_o - (S_{or})_{iw} \left(\frac{(S_{or})_{iw}}{(S_{or})_{ow}} \right)^{\cos(ae^{-bt}+c)}}{1 - (S_{or})_{iw} \left(\frac{(S_{or})_{iw}}{(S_{or})_{ow}} \right)^{\cos(ae^{-bt}+c)} - S_{wi} \right] k}{\mu_o} \right) \frac{\partial p}{\partial x} \frac{\partial f_{CO_2}}{\partial x} \\
 & - f_{CO_2} \frac{\partial p}{\partial x} \left(6.3 \times 10^{-3} \times \frac{k_{rCO_2}^o \left[1 - \left(\frac{S_o - (S_{or})_{iw} \left(\frac{(S_{or})_{iw}}{(S_{or})_{ow}} \right)^{\cos(ae^{-bt}+c)}}{1 - (S_{or})_{iw} \left(\frac{(S_{or})_{iw}}{(S_{or})_{ow}} \right)^{\cos(ae^{-bt}+c)} - S_{wi} \right)} \right]^{ng}}{\mu_{CO_2}} + 1.1 \times 10^{-3} \times \frac{k_{ro}^o \left[\frac{S_o - (S_{or})_{iw} \left(\frac{(S_{or})_{iw}}{(S_{or})_{ow}} \right)^{\cos(ae^{-bt}+c)}}{1 - (S_{or})_{iw} \left(\frac{(S_{or})_{iw}}{(S_{or})_{ow}} \right)^{\cos(ae^{-bt}+c)} - S_{wi} \right] k}{\mu_o} \right) \\
 & + \phi^* \frac{\partial S_{CO_2}}{\partial t} + \phi^* S_{CO_2} c_{CO_2} \frac{\partial p}{\partial t} = 0
 \end{aligned} \tag{4.44}$$

The numerical solution technique will be presented and discussed in detail in the next chapter.

CHAPTER 5

DEVELOPMENT OF THE NUMERICAL

SIMULATION MODEL

5.1 Model Description

The objective of the simulation model is to employ the three mathematical models developed in Chapter 4 in a numerical model that can predict the performance of immiscible displacement of oil by CO₂ in a linear system. A homogeneous, strongly-oil wet porous medium containing oil is considered where compressible and isothermal flow conditions prevail for all phases. The initial pressure and saturations are uniform throughout the medium and the volumetric flow is linear and parallel to the x-axis. The small pores are assumed to be completely filled with oil. CO₂ is injected at one end at a constant rate and remains in the gaseous state throughout the displacement process. An initially immobile water phase is also included. Figure 5.1 shows a schematic of the linear grid system adopted in the simulation model for the medium. The grid cell size is uniform. The Implicit Pressure Explicit Saturation (IMPES) approach is considered in the computation scheme, which means that the pressure was calculated implicitly while saturation was calculated explicitly. The gas saturation (S_{CO_2}) is then calculated after the pressure in each grid cell is obtained.

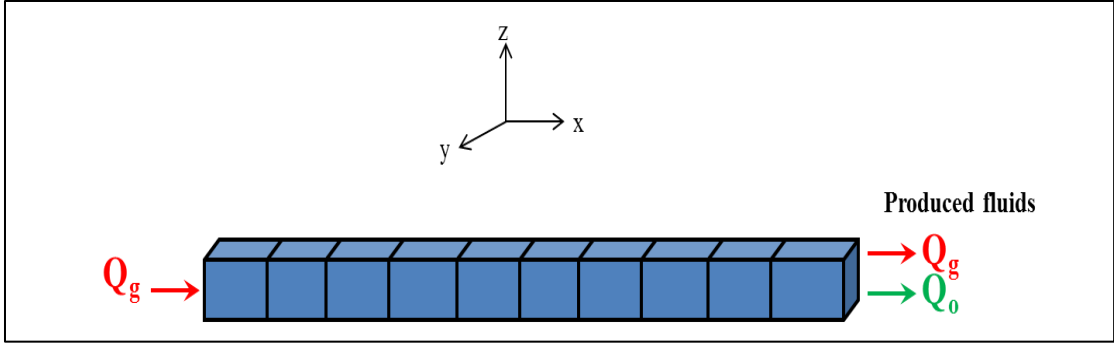


Figure 5.1 Schematic of the one-dimensional flow system

5.2 Boundary Conditions

The boundary conditions in the model are assumed to be fixed injection rate at the inlet and fixed pressure across the edge of the last cell as shown in Figure 5.2.

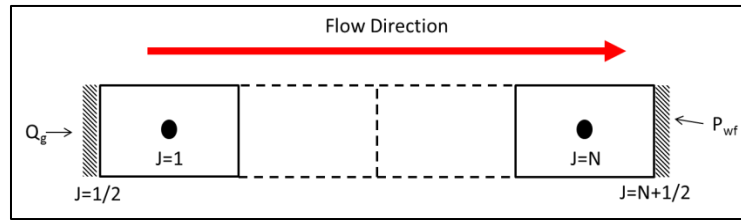


Figure 5.2 Boundary conditions assumed in the model

The inlet boundary condition at the edge of the first cell is represented as follows:

$$\left(\frac{\partial p}{\partial x}\right)_{\frac{1}{2}} = -\frac{Q_g \mu_g}{6.3 \times 10^{-3} \times k k_{rg} A} \quad (5.1)$$

At $i = \frac{1}{2}$, $f_g = 1$ and $k_{rg} = 1$

Eq. (5.1) can be simplified to:

$$\left(\frac{\partial p}{\partial x}\right)_{\frac{1}{2}} = -\frac{Q_g \mu_g}{6.3 \times 10^{-3} \times kA} \quad (5.2)$$

The outlet boundary condition at the last cell is represented as follows:

$$p_{N+\frac{1}{2}} = p_{wf} \quad (5.3)$$

These boundary conditions will be incorporated during the discretization process for gas saturation and pressure equations as will be presented in the next sections.

5.3 Discretization of the CO₂ Saturation Equation

For convenience, the total mobility can be expressed as follows [84]:

$$\gamma_t = 6.3 \times 10^{-3} \times \frac{k_{CO_2}}{\mu_{CO_2}} + 1.1 \times 10^{-3} \times \frac{k_o}{\mu_o} \quad (5.4)$$

Substituting Eq. (5.4) into Eq. (4.25) yields:

$$-f_{CO_2} \gamma_t \frac{\partial^2 p}{\partial x^2} - \gamma_t \frac{\partial p}{\partial x} \frac{\partial f_{CO_2}}{\partial x} - f_{CO_2} \frac{\partial p}{\partial x} \frac{\partial \gamma_t}{\partial x} + \frac{\phi^*}{5.615} \frac{\partial S_{CO_2}}{\partial t} + \frac{\phi^* S_{CO_2} c_{CO_2}}{5.615} \frac{\partial p}{\partial t} = 0 \quad (5.5)$$

For $i = 1$ (Figure 5.3):



Figure 5.3 Gas saturation for the first cell

Equation (5.5) will be re-arranged to solve for S_{CO_2} numerically at a new time step. First,

Eq. (5.5) is written as:

$$-\frac{\partial}{\partial x} \left(f_{CO_2} \gamma_t \frac{\partial p}{\partial x} \right) + \frac{\phi^*}{5.615} \frac{\partial S_{CO_2}}{\partial t} + \frac{\phi^* S_{CO_2} c_{CO_2}}{5.615} \frac{\partial p}{\partial t} = 0 \quad (5.6)$$

Expanding Eq. (5.6) for the first cell yields:

$$\begin{aligned} & \frac{1}{\Delta x} \left[- \left(f_{CO_2} \gamma_t \frac{\partial p}{\partial x} \right)_{\frac{3}{2}}^{n+1} + \left(f_{CO_2} \gamma_t \frac{\partial p}{\partial x} \right)_{\frac{1}{2}}^{n+1} \right] + \frac{\phi^*}{5.615} \left(\frac{S_{CO_2_1}^{n+1} - S_{CO_2_1}^n}{\Delta t} \right) + \\ & \frac{\phi^* S_{CO_2_1}^n c_{CO_2}}{5.615} \left(\frac{p_1^{n+1} - p_1^n}{\Delta t} \right) = 0 \end{aligned} \quad (5.7)$$

Substituting Eq. (5.2) into Eq. (5.7) yields:

$$\begin{aligned} & \frac{1}{\Delta x} \left[- \left(f_{CO_2} \gamma_t \frac{\partial p}{\partial x} \right)_{\frac{3}{2}}^{n+1} - \left(f_{CO_2} \gamma_t \right)_{\frac{1}{2}} \frac{Q_g \mu_g}{6.3 \times 10^{-3} \times kA} \right] + \frac{\phi^*}{5.615} \left(\frac{S_{CO_2_1}^{n+1} - S_{CO_2_1}^n}{\Delta t} \right) + \\ & \frac{\phi^* S_{CO_2_1}^n c_{CO_2}}{5.615} \left(\frac{p_1^{n+1} - p_1^n}{\Delta t} \right) = 0 \end{aligned} \quad (5.8)$$

At $t = \frac{1}{2}$, only the gas phase is flowing, which implies that:

$$\gamma_{t\frac{1}{2}} = \gamma_{CO_2\frac{1}{2}} = 6.3 \times 10^{-3} \times \frac{k}{\mu_g} \quad (5.9)$$

$$f_{CO_2\frac{1}{2}} = 1 \quad (5.10)$$

Substituting Eqs. (5.9) and (5.10) into Eq. (5.8) yields:

$$\begin{aligned} & \frac{5.615 \Delta t}{\phi^* \Delta x} \left[- \left(f_{CO_2} \gamma_t \frac{\partial p}{\partial x} \right)_{\frac{3}{2}}^{n+1} - \frac{Q_g}{A} \right] + S_{CO_2_1}^{n+1} - S_{CO_2_1}^n + S_{CO_2_1}^n c_{CO_2} (p_1^{n+1} - p_1^n) = 0 \end{aligned} \quad (5.11)$$

$$\frac{5.615f_{CO_2}^n \gamma_{t_1}^n \Delta t}{\phi^* \Delta x^2} (p_1^{n+1} - p_2^{n+1}) - \left(\frac{\Delta t}{\phi^* \Delta x} \frac{Q_g}{A} \right) + S_{CO_2}^{n+1} - S_{CO_2}^n + S_{CO_2}^n c_{CO_2} (p_1^{n+1} - p_1^n) = 0 \quad (5.12)$$

Solving Eq. (5.12) for $S_{CO_2}^{n+1}$ yields:

$$S_{CO_2}^{n+1} = S_{CO_2}^n - \frac{5.615f_{CO_2}^n \gamma_{t_1}^n \Delta t}{\phi^* \Delta x^2} (p_1^{n+1} - p_2^{n+1}) + \left(\frac{\Delta t}{\phi^* \Delta x} \frac{Q_g}{A} \right) - S_{CO_2}^n c_{CO_2} (p_1^{n+1} - p_1^n) \quad (5.13)$$

Eq. (5.13) solves for S_{CO_2} numerically at a new time step for $j = 1$.

For $i = 2: N - 1$ (Figure 5.4):

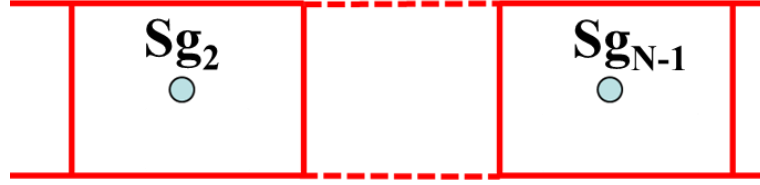


Figure 5.4 Gas saturation for the cells from 2 to N-1

Expanding Eq. (5.5) yields:

$$\begin{aligned} & -5.615f_{CO_2}^n \gamma_{t_i}^n \left(\frac{p_{i-1}^{n+1} - 2p_i^{n+1} + p_{i+1}^{n+1}}{\Delta x^2} \right) - 5.615\gamma_{t_i}^n \left(\frac{p_i^{n+1} - p_{i-1}^{n+1}}{\Delta x} \right) \left(\frac{f_{CO_2}^n - f_{CO_2}^{n-1}}{\Delta x} \right) - \\ & 5.615f_{CO_2}^n \left(\frac{p_i^{n+1} - p_{i-1}^{n+1}}{\Delta x} \right) \left(\frac{\gamma_{t_i}^n - \gamma_{t_{i-1}}^n}{\Delta x} \right) + \phi^* \left(\frac{S_{CO_2}^{n+1} - S_{CO_2}^n}{\Delta t} \right) + \phi^* S_{CO_2}^n c_{CO_2} \left(\frac{p_i^{n+1} - p_i^n}{\Delta t} \right) = 0 \end{aligned} \quad (5.14)$$

Solving Eq. (5.14) for $S_{CO_2}^{n+1}$ yields:

$$\begin{aligned}
S_{CO_2 i}^{n+1} = & S_{CO_2 i}^n + \frac{5.615 f_{CO_2 i}^n \gamma_{t_i}^n \Delta t}{\phi^* \Delta x^2} (p_{i-1}^{n+1} - 2p_i^{n+1} + p_{i+1}^{n+1}) + \frac{5.615 \gamma_{t_{i-1}}^n \Delta t}{\phi^* \Delta x^2} (p_i^{n+1} - \\
& p_{i-1}^{n+1}) (f_{CO_2 i}^n - f_{CO_2 i-1}^n) + \frac{5.615 f_{CO_2 i-1}^n \Delta t}{\phi^* \Delta x^2} (p_i^{n+1} - p_{i-1}^{n+1}) (\gamma_{t_i}^n - \gamma_{t_{i-1}}^n) - \\
& S_{CO_2 i}^n c_{CO_2} (p_i^{n+1} - p_i^n)
\end{aligned} \tag{5.15}$$

Eq. (5.15) solves for S_{CO_2} numerically at a new time step for cells ($i = 2: N - 1$).

For $i = N$ (Figure 5.5):



Figure 5.5 Gas saturation for the last cell

Expanding Eq. (5.6) for the last cell yields:

$$\begin{aligned}
\frac{1}{\Delta x} \left[- \left(f_{CO_2} \gamma_t \frac{\partial p}{\partial x} \right)_{N+\frac{1}{2}}^{n+1} + \left(f_{CO_2} \gamma_t \frac{\partial p}{\partial x} \right)_{N-\frac{1}{2}}^{n+1} \right] + \frac{\phi^*}{5.615} \left(\frac{S_{CO_2 N}^{n+1} - S_{CO_2 N}^n}{\Delta t} \right) + \\
\frac{\phi^* S_{CO_2}^n c_{CO_2}}{5.615} \left(\frac{p_N^{n+1} - p_N^n}{\Delta t} \right) = 0
\end{aligned} \tag{5.16}$$

Employing Eq. (5.3) yields:

$$\left(\frac{\partial p}{\partial x} \right)_{N+\frac{1}{2}} = \frac{p_{wf} - p_N}{\Delta x / 2} = \frac{2p_{wf} - 2p_N}{\Delta x} \tag{5.17}$$

Substituting Eq. (5.17) into Eq. (5.16) yields:

$$\frac{5.615\Delta t}{\phi^*\Delta x^2} \left[(f_{\text{CO}_2 N}^n \gamma_{t N}^n) (2p_N^{n+1} - 2p_{\text{wf}}) + (f_{\text{CO}_2 N-1}^n \gamma_{t N-1}^n) (p_N^{n+1} - p_{N-1}^{n+1}) \right] + S_{\text{CO}_2 N}^{n+1} - S_{\text{CO}_2 N}^n + S_{\text{CO}_2 N}^n c_{\text{CO}_2} (p_N^{n+1} - p_N^n) = 0 \quad (5.18)$$

Re-arranging Eq. (5.18) yields:

$$\frac{5.615f_{\text{CO}_2 N}^n \gamma_{t N}^n \Delta t}{\phi^*\Delta x^2} (2p_N^{n+1} - 2p_{\text{wf}}) + \frac{5.615f_{\text{CO}_2 N-1}^n \gamma_{t N-1}^n \Delta t}{\phi^*\Delta x^2} (p_N^{n+1} - p_{N-1}^{n+1}) + S_{\text{CO}_2 N}^{n+1} - S_{\text{CO}_2 N}^n + S_{\text{CO}_2 N}^n c_{\text{CO}_2} (p_N^{n+1} - p_N^n) = 0 \quad (5.19)$$

Solving Eq. (5.19) for $S_{\text{CO}_2 N}^{n+1}$ yields:

$$S_{\text{CO}_2 N}^{n+1} = S_{\text{CO}_2 N}^n - \frac{5.615f_{\text{CO}_2 N}^n \gamma_{t N}^n \Delta t}{\phi^*\Delta x^2} (2p_N^{n+1} - 2p_{\text{wf}}) - \frac{5.615f_{\text{CO}_2 N-1}^n \gamma_{t N-1}^n \Delta t}{\phi^*\Delta x^2} (p_N^{n+1} - p_{N-1}^{n+1}) - S_{\text{CO}_2 N}^n c_{\text{CO}_2} (p_N^{n+1} - p_N^n) \quad (5.20)$$

Eq. (5.20) solves for S_{CO_2} numerically at a new time step for $i = N$.

5.4 Discretization of the Pressure Equations

To solve the pressure equation, the total flux should be considered. First, the displacement of the oil phase - neglecting p_c - in the model can be obtained from Eq. (4.5) as follows:

$$-\frac{\partial}{\partial x} \left(f_o \gamma_t \frac{\partial p}{\partial x} \right) + \frac{\phi^*}{5.615} \frac{\partial S_o}{\partial t} = 0 \quad (5.21)$$

Adding Eqs. (5.6) and (5.21) yields:

$$-\frac{\partial}{\partial x} \left(f_{\text{CO}_2} \gamma_t \frac{\partial p}{\partial x} \right) + \frac{\phi^*}{5.615} \frac{\partial S_{\text{CO}_2}}{\partial t} + \frac{\phi^* S_{\text{CO}_2} c_{\text{CO}_2}}{5.615} \frac{\partial p}{\partial t} - \frac{\partial}{\partial x} \left(f_o \gamma_t \frac{\partial p}{\partial x} \right) + \frac{\phi^*}{5.615} \frac{\partial S_o}{\partial t} = 0 \quad (5.22)$$

Re-arranging Eq. (5.22) yields:

$$-\frac{\partial}{\partial x} \left((f_{\text{CO}_2} + f_o) \gamma_t \frac{\partial p}{\partial x} \right) + \frac{\phi^*}{5.615} \frac{\partial (S_{\text{CO}_2} + S_o)}{\partial t} + \frac{\phi^* S_{\text{CO}_2} c_{\text{CO}_2}}{5.615} \frac{\partial p}{\partial t} = 0 \quad (5.23)$$

Both oil and CO₂ phases are flowing in the system satisfying the equations below:

$$f_{\text{CO}_2} + f_o = 1 \quad (5.24)$$

$$s_{\text{CO}_2} + s_o = 1 \quad (5.25)$$

Employing Eqs. (5.24) and (5.25) into Eq. (5.23) yields:

$$-\frac{\partial}{\partial x} \left(\gamma_t \frac{\partial p}{\partial x} \right) + \frac{\phi^* S_{\text{CO}_2} c_{\text{CO}_2}}{5.615} \frac{\partial p}{\partial t} = 0 \quad (5.26)$$

Eq. (5.26) represents the general pressure equation for the model.

For $i = 1$ (Figure 5.6):

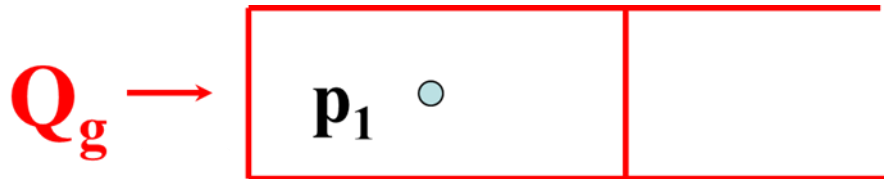


Figure 5.6 Pressure equation for the first cell

Expanding Eq. (5.26) for the first cell yields:

$$\frac{1}{\partial x} \left[- \left(\gamma_t \frac{\partial p}{\partial x} \right)_{\frac{3}{2}} + \left(\gamma_t \frac{\partial p}{\partial x} \right)_{\frac{1}{2}} \right] + \frac{\phi^* S_{CO_2} c_{CO_2}}{5.615} \frac{\partial p}{\partial t} = 0 \quad (5.27)$$

Applying the inlet boundary condition – Eq. (5.2) – into Eq. (5.27) yields:

$$\frac{1}{\Delta x} \left[- \left(\gamma_t \frac{\partial p}{\partial x} \right)_{\frac{3}{2}}^{n+1} - \frac{Q_g}{A} \right] + \frac{\phi^* S_{CO_2} c_{CO_2}}{5.615} \left(\frac{p_1^{n+1} - p_1^n}{\Delta t} \right) = 0 \quad (5.28)$$

Re-arranging Eq. (5.28) yields:

$$\frac{\gamma_{t_1}^{n+1} \Delta t}{\Delta x^2} (p_1^{n+1} - p_2^{n+1}) - \frac{Q_g \Delta t}{A \Delta x} + \frac{\phi^* S_{CO_2} c_{CO_2}}{5.615} (p_1^{n+1} - p_1^n) = 0 \quad (5.29)$$

Multiplying Eq. (5.29) by the cross sectional area (A) yields:

$$\frac{A \gamma_{t_1}^{n+1} \Delta t}{\Delta x^2} (p_1^{n+1} - p_2^{n+1}) - \frac{Q_g \Delta t}{\Delta x} + \frac{A \phi^* S_{CO_2} c_{CO_2}}{5.615} (p_1^{n+1} - p_1^n) = 0 \quad (5.30)$$

Expanding Eq. (5.30) yields:

$$\frac{A \gamma_{t_1}^{n+1} \Delta t}{\Delta x^2} p_1^{n+1} - \frac{A \gamma_{t_1}^{n+1} \Delta t}{\Delta x^2} p_2^{n+1} - \frac{Q_g \Delta t}{\Delta x} + \frac{A \phi^* S_{CO_2} c_{CO_2}}{5.615} (p_1^{n+1} - p_1^n) = 0 \quad (5.31)$$

The oil and CO₂ phase transmissibilities under reservoir conditions can be expressed, respectively, as:

$$T_o = \frac{1.1 \times 10^{-3} \times kA}{\mu_o \Delta x} \quad (5.32)$$

$$T_{CO_2} = \frac{6.3 \times 10^{-3} \times kA}{\mu_{CO_2} \Delta x} \quad (5.33)$$

Since the pore volume is:

$$V_p = \frac{A\phi^*\Delta x}{5.615} \quad (5.34)$$

Employing Eqs. (5.32), (5.33) and (5.34) into Eq. (5.31) yields:

$$\begin{aligned} & \left[\Delta t (T_{CO_2_1}^{n+1} k_{rCO_2_1}^{n+1}) + \Delta t (T_{O_1}^{n+1} k_{ro_1}^{n+1}) \right] p_1^{n+1} - \left[\Delta t (T_{CO_2_1}^{n+1} k_{rCO_2_1}^{n+1}) + \right. \\ & \left. \Delta t (T_{O_1}^{n+1} k_{ro_1}^{n+1}) \right] p_2^{n+1} - Q_g \Delta t + V_{p_1} c_{CO_2_1}^{n+1} (p_1^{n+1} - p_1^n) = 0 \end{aligned} \quad (5.35)$$

Re-arranging Eq. (5.35) yields:

$$\begin{aligned} & - \left[\Delta t (T_{CO_2_1}^{n+1} k_{rCO_2_1}^{n+1}) + \Delta t (T_{O_1}^{n+1} k_{ro_1}^{n+1}) \right] p_2^{n+1} + \left[\Delta t (T_{CO_2_1}^{n+1} k_{rCO_2_1}^{n+1}) + \right. \\ & \left. \Delta t (T_{O_1}^{n+1} k_{ro_1}^{n+1}) + c_{CO_2_1}^{n+1} V_{p_1} \right] p_1^{n+1} = Q_g \Delta t + V_{p_1} c_{CO_2_1}^{n+1} p_1^n \end{aligned} \quad (5.36)$$

Eq. (5.36) calculates the pressure for cell#1 at any given time.

For $i = 2: N - 1$ (Figure 5.7):

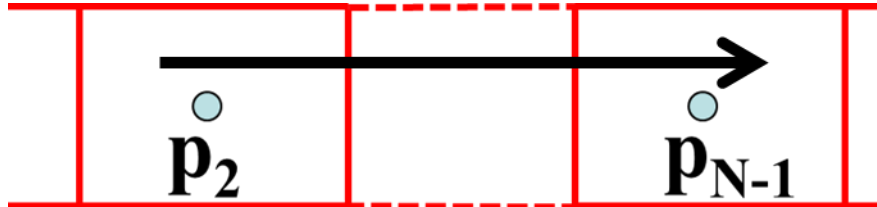


Figure 5.7 Pressure equation for the cells from 2 to N-1

The pressure equation for the cells from 2 to N-1 will be derived as follows.

Expanding Eq. (5.26) for the cells from 2 to N-1 yields:

$$-\frac{1}{\Delta x} \left[\left(\gamma_t \frac{\partial p}{\partial x} \right)_{i+\frac{1}{2}} - \left(\gamma_t \frac{\partial p}{\partial x} \right)_{i-\frac{1}{2}} \right] + \frac{\phi^* S_{CO_2} c_{CO_2}}{5.615} \frac{\partial p}{\partial t} = 0 \quad (5.37)$$

Since the flow is moving from cell i to cell $i+1$, upstream weighting can be applied as follows:

$$(\gamma_t)_{i+\frac{1}{2}} = (\gamma_t)_i \quad (5.38)$$

$$(\gamma_t)_{i-\frac{1}{2}} = (\gamma_t)_{i-1} \quad (5.39)$$

Employing Eqs. (5.38) and (5.39) into Eq. (5.37) and expanding it yields:

$$-\frac{1}{\Delta x^2} \left[(\gamma_t)_i^{n+1} (p_{i+1}^{n+1} - p_i^{n+1}) - (\gamma_t)_{i-1}^{n+1} (p_i^{n+1} - p_{i-1}^{n+1}) \right] + \frac{\phi^* c_{CO_2}^{n+1}}{5.615} \left(\frac{p_i^{n+1} - p_i^n}{\Delta t} \right) = 0 \quad (5.40)$$

Multiplying Eq. (5.40) by the cross sectional area (A) yields:

$$\frac{A}{\Delta x^2} \left[(\gamma_t)_i^{n+1} (p_i^{n+1} - p_{i+1}^{n+1}) + (\gamma_t)_{i-1}^{n+1} (p_i^{n+1} - p_{i-1}^{n+1}) \right] + \frac{A \phi^* c_{CO_2}^{n+1}}{5.615} \left(\frac{p_i^{n+1} - p_i^n}{\Delta t} \right) = 0 \quad (5.41)$$

Re-arranging Eq. (5.41) yields:

$$\frac{\Delta t}{\Delta x} [(\gamma_t)_i^{n+1} (p_i^{n+1} - p_{i+1}^{n+1}) + (\gamma_t)_{i-1}^{n+1} (p_i^{n+1} - p_{i-1}^{n+1})] + \frac{\Delta x A \phi^* c_{CO_2}^{n+1}}{5.615} (p_i^{n+1} - p_i^n) = 0 \quad (5.42)$$

Employing Eqs. (5.32), (5.33) and (5.34) for the cells from 2 to N-1 into Eq. (5.42) yields:

$$\begin{aligned} & \left[\Delta t (T_{CO_2 i}^{n+1} k_{rCO_2 i}^{n+1}) + \Delta t (T_{O_i}^{n+1} k_{ro_i}^{n+1}) \right] (p_i^{n+1} - p_{i+1}^{n+1}) + \left[\Delta t (T_{CO_2 i-1}^{n+1} k_{rCO_2 i-1}^{n+1}) + \right. \\ & \left. \Delta t (T_{O_{i-1}}^{n+1} k_{ro_{i-1}}^{n+1}) \right] (p_i^{n+1} - p_{i-1}^{n+1}) + V_{p_i} c_{CO_2 i}^{n+1} (p_i^{n+1} - p_i^n) = 0 \end{aligned} \quad (5.43)$$

Re-arranging Eq. (5.43) yields:

$$\begin{aligned} & - \left[\Delta t (T_{CO_2 i}^{n+1} k_{rCO_2 i}^{n+1}) + \Delta t (T_{O_i}^{n+1} k_{ro_i}^{n+1}) \right] p_{i+1}^{n+1} + \left[\Delta t (T_{CO_2 i}^{n+1} k_{rCO_2 i}^{n+1}) + \right. \\ & \left. \Delta t (T_{O_i}^{n+1} k_{ro_i}^{n+1}) \right] p_i^{n+1} + \left[\Delta t (T_{CO_2 i-1}^{n+1} k_{rCO_2 i-1}^{n+1}) + \Delta t (T_{O_{i-1}}^{n+1} k_{ro_{i-1}}^{n+1}) \right] p_{i-1}^{n+1} + V_{p_i} c_{CO_2 i}^{n+1} p_i^{n+1} - \\ & \left[\Delta t (T_{CO_2 i-1}^{n+1} k_{rCO_2 i-1}^{n+1}) + \Delta t (T_{O_{i-1}}^{n+1} k_{ro_{i-1}}^{n+1}) \right] p_{i-1}^{n+1} = V_{p_i} c_{CO_2 i}^{n+1} p_i^n \end{aligned} \quad (5.44)$$

Eq. (5.44) calculates the pressure for cells from 2 to N-1 at any given time.

For $i = N$ (Figure 5.8):

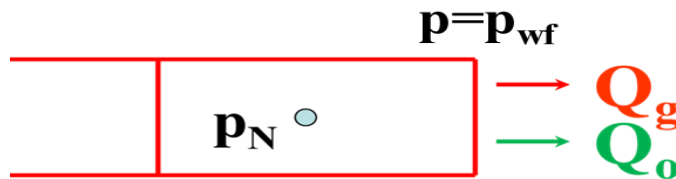


Figure 5.8 Pressure equation for the last cell

Expanding Eq. (5.27) for the last cell yields:

$$\frac{1}{\Delta x} \left[- \left(\gamma_t \frac{\partial p}{\partial x} \right)_{N+\frac{1}{2}} + \left(\gamma_t \frac{\partial p}{\partial x} \right)_{N-\frac{1}{2}} \right] + \frac{\phi^* S_{CO_2} c_{CO_2}}{5.615} \frac{\partial p}{\partial t} = 0 \quad (5.45)$$

Applying upstream weighting yields:

$$(\gamma_t)_{N+\frac{1}{2}} = (\gamma_t)_N \quad (5.46)$$

$$(\gamma_t)_{N-\frac{1}{2}} = (\gamma_t)_{N-1} \quad (5.47)$$

Applying the outlet boundary condition – Eq. (5.17), employing Eqs. (5.46) and (5.47) into Eq. (5.45) and expanding it yields:

$$\frac{1}{\Delta x^2} \left[(\gamma_t)_N^{n+1} (2p_N^{n+1} - 2p_{wf}) + (\gamma_t)_{N-1}^{n+1} (p_N^{n+1} - p_{N-1}^{n+1}) \right] + \frac{\phi^* c_{CO_2}^{n+1}}{5.615} \left(\frac{p_N^{n+1} - p_N^n}{\Delta t} \right) = 0 \quad (5.48)$$

Multiplying Eq. (5.48) by the cross sectional area (A) and re-arranging it yields:

$$\frac{\Delta t A}{\Delta x} \left[(\gamma_t)_N^{n+1} (2p_N^{n+1} - 2p_{wf}) + (\gamma_t)_{N-1}^{n+1} (p_N^{n+1} - p_{N-1}^{n+1}) \right] + \frac{\Delta x A \phi^* c_{CO_2}^{n+1}}{5.615} (p_N^{n+1} - p_N^n) = 0 \quad (5.49)$$

Employing Eqs. (5.32), (5.33) and (5.34) for the last cell into Eq. (5.49) yields:

$$\begin{aligned}
& \left[\Delta t \left(T_{\text{CO}_2 N}^{n+1} k_{\text{rCO}_2 N}^{n+1} \right) + \Delta t \left(T_{\text{o} N}^{n+1} k_{\text{ro} N}^{n+1} \right) \right] \left(2p_N^{n+1} - 2p_{\text{wf}} \right) + \\
& \left[\Delta t \left(T_{\text{CO}_2 N-1}^{n+1} k_{\text{rCO}_2 N-1}^{n+1} \right) + \Delta t \left(T_{\text{o} N-1}^{n+1} k_{\text{ro} N-1}^{n+1} \right) \right] \left(p_N^{n+1} - p_{N-1}^{n+1} \right) + V_{p_N} c_{\text{CO}_2 N}^{n+1} \left(p_N^{n+1} - \right. \\
& \left. p_N^n \right) = 0 \tag{5.50}
\end{aligned}$$

Re-arranging Eq. (5.50) yields:

$$\begin{aligned}
& \left[2 \left[\Delta t \left(T_{\text{CO}_2 N}^{n+1} k_{\text{rCO}_2 N}^{n+1} \right) + \Delta t \left(T_{\text{o} N}^{n+1} k_{\text{ro} N}^{n+1} \right) \right] + \left[\Delta t \left(T_{\text{CO}_2 N-1}^{n+1} k_{\text{rCO}_2 N-1}^{n+1} \right) + \right. \right. \\
& \left. \left. \Delta t \left(T_{\text{o} N-1}^{n+1} k_{\text{ro} N-1}^{n+1} \right) \right] + V_{p_N} c_{\text{CO}_2 N}^{n+1} \right] p_N^{n+1} - \\
& \left[\Delta t \left(T_{\text{CO}_2 N-1}^{n+1} k_{\text{rCO}_2 N-1}^{n+1} \right) + \Delta t \left(T_{\text{o} N-1}^{n+1} k_{\text{ro} N-1}^{n+1} \right) \right] p_{N-1}^{n+1} = 2 \left[\Delta t \left(T_{\text{CO}_2 N}^{n+1} k_{\text{rCO}_2 N}^{n+1} \right) + \right. \\
& \left. \Delta t \left(T_{\text{o} N}^{n+1} k_{\text{ro} N}^{n+1} \right) \right] p_{\text{wf}} + V_{p_N} c_{\text{CO}_2 N}^{n+1} p_N^n \tag{5.51}
\end{aligned}$$

Eq. (5.51) calculates the pressure for the last cell at any given time.

Equations 5.36, 5.44 and 5.51 can be solved numerically to produce the pressure profile as it varies with time in the linear system for any set of appropriate conditions. This will be presented in Chapter 7.

CHAPTER 6

EXPERIMENTAL WORK

This chapter presents two laboratory experiments that were conducted to test the wettability alteration and the displacement models derived in Chapter 4. The first experiment was carried out to prove the exponential relationship between contact angle and CO₂ exposure time (Eq. 4.41). It involved measurements of the change with time in the contact angle between oil, carbonated brine and a slice of rock cut from a carbonate core plug. The second one was carried out to verify the displacement model (Eq. 4.25). It involved core flooding with CO₂ under immiscible conditions and was conducted at a constant rate and temperature.

6.1 Wettability Alteration Experiment

This experiment was conducted to investigate wettability alteration during continuous contact with CO₂. A drop of oil placed on a slice of rock cut from an initially oil-wet core plug was exposed to carbonated brine, and the contact angle between oil, brine and the rock was monitored as it changed with exposure time.

6.1.1 Experimental Setup

The experimental set-up consists of eight components as shown in Figure 6.1. A CO₂ cylinder is connected to a 60-cc visual cell through a regulator to control CO₂ injection (Figure 6.2). The pressure and temperature of the visual cell are controlled and monitored throughout the experiment. The visual cell is made of stainless steel and can withstand high pressures and temperatures. A steel hanger is screwed to the roof of the cell on the inside to which a rock slice is attached (Figure 6.3). The visual cell is fitted with a glass window to allow monitoring the lower surface of the rock slice. A camera is placed horizontally to the level of the visual cell to allow taking photographs of the contents of the cell. The camera downloads the photographs to a personal computer where they are analyzed by special software to estimate the contact angle. The Drop Image software is provided by the manufacturer of the pendent drop IFT system.

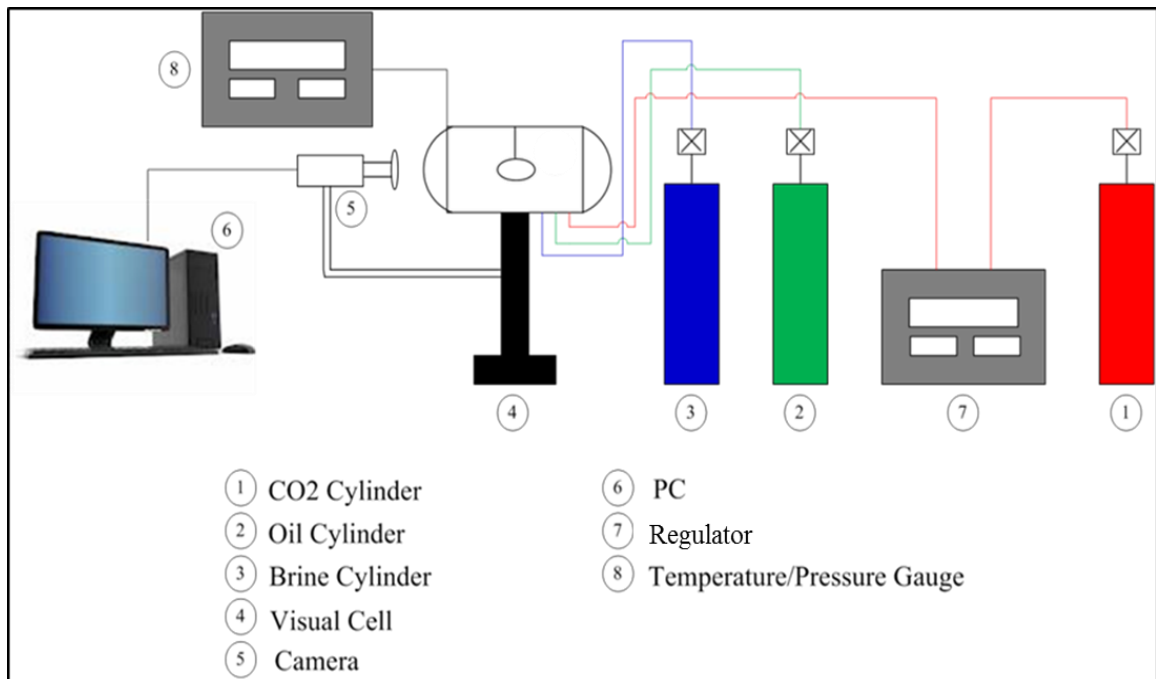


Figure 6.1 Schematic of the experimental set-up



Figure 6.2 The windowed visual cell



Figure 6.3 Rock slice-hanger assembly

6.1.2 Experimental Procedure

The carbonate core plug was cleaned and dried in an oven at 90 °C. The plug was then fully saturated with brine using the vacuum method followed by flooding the plug with dead oil in a core-flooding setup until no brine is produced. The plug's porosity, pore volume and final oil and water saturations were then computed by mass balance on oil and water. Properties of the rock and fluids employed in the experiment are presented in Tables 6.1 and 6.2.

A thin slice - 0.5 cm thick, 2.3 cm in diameter - was then cut from the core plug, submerged in the same oil and aged in a titanium cylinder at 85 °C and 2000 psig for two weeks to ensure oil wettability. After aging, the surface of the core slice was grinded to a uniform plane to allow accurate measurement of the contact angle. The polished core slice was then aged in the same oil under the same conditions to ensure oil wettability. The core slice was then attached to the hanger using special epoxy cement which has high resistance to temperature (Figure 6.3). The hanger was then mounted inside the visual cell. The cell was then filled completely with brine and heated to 70 °C and pressurized to 500 psig. A drop of the dead oil was then introduced to the cell through a vertical needle fitted to the bottom of the cell. The needle is positioned directly below the core slice so that when the drop enters the cell it rises through the brine and rests on the lower surface of the core slice (Figure 6.4). The contact angle between the rock surface, the oil drop and the surrounding brine was then measured.

CO₂ gas (99.5% pure with moisture content less than 120 ppm) was then rapidly charged to the cell until the cell's pressure rose to a pre-determined level (about 1000 psig); CO₂ injection was then stopped. When the cell's pressure dropped back to 500 psig, which usually took about 15 seconds, indicating complete dissolution of CO₂ in the brine, high-resolution photographs of the oil drop were then taken periodically until no noticeable change in the shape of the drop was observed. The photographs were then analyzed and values of the contact angle versus the drop's exposure time to the carbonated brine were recorded. Figure 6.5 depicts how the shape of the oil drop changed with time.

Calculation of the contact angle using the pendent drop method is a pure numerical technique. The camera's view finder shows a horizontal line on the screen along which the solid surface is aligned. The filter routine then gives a properly aligned drop profile and the contact angle is easily calculated by numerical derivation of the profile at the contact point. Because of reflection in the substrate and some diffraction, 2 to 3 data points closest to the contact point are neglected. In the Drop Image software the drop profile is established by a travelling secant method with linear extrapolation to the contact point. This method seems more robust than the ones that have been tried out. It gives values between a pure linear derivation, which underestimates the contact angle, and higher order (polynomial) methods that usually tend to overestimate the angle.

All experimental data and analysis will be presented in Chapter 7. Verification of the model proposed by Eq. (4.41) will also be established in Chapter 7.

Table 6.1 Properties of the rock and fluids employed in the experiment

Property	Value
Oil density (g/cc)	0.85
Brine density (g/cc)	0.99
Brine viscosity (cP)	0.56
Core permeability (mD)	5
Core porosity (%)	15

Table 6.2 Brine composition

Salt	Concentration g/L
Sodium Chloride (NaCl)	16.7
Calcium Chloride (CaCl ₂ .2H ₂ O)	3.62
Magnesium Chloride (MgCl ₂ .6H ₂ O)	1.28

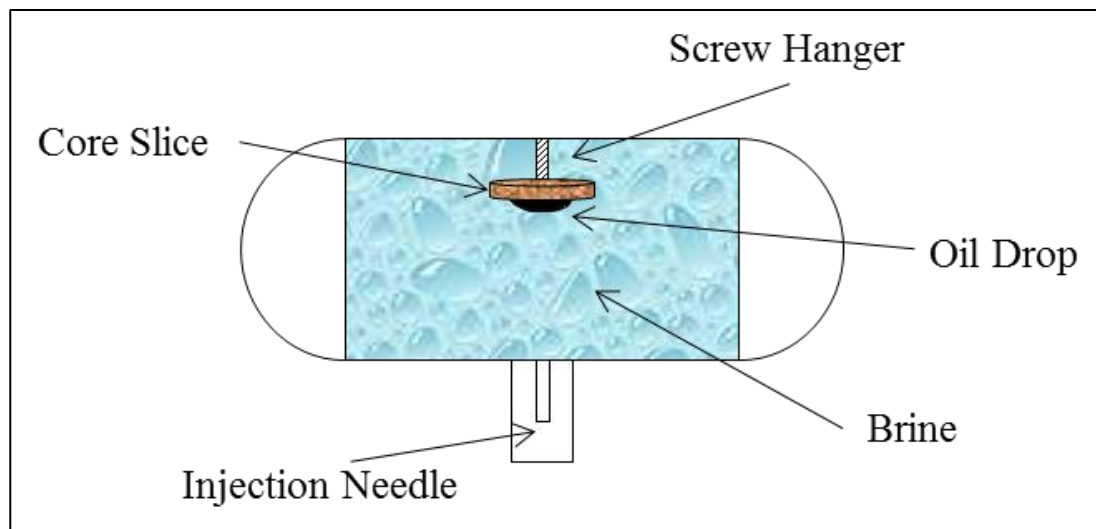


Figure 6.4 Visual cell components

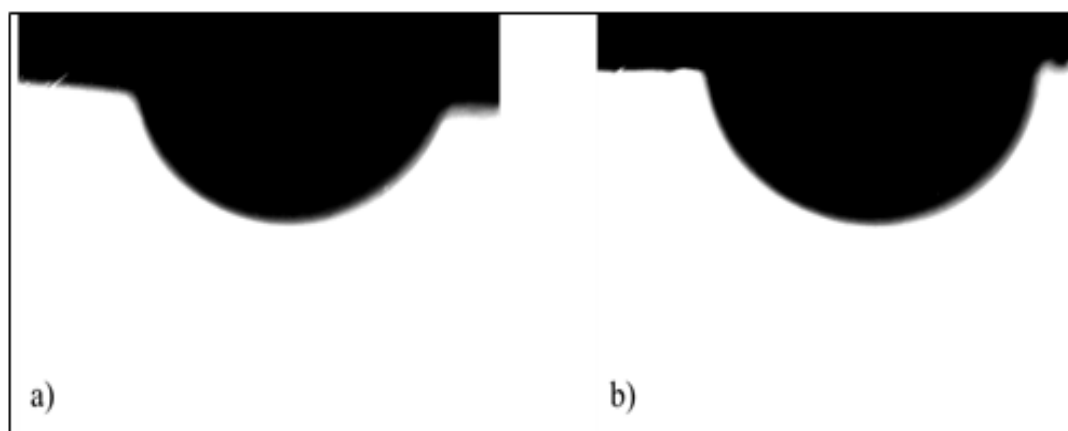


Figure 6.5 Shape of the oil drop (a) before brine carbonation (b) after 44 minutes of brine carbonation

6.2 Core Flooding Experiment

In this experiment a composite core sample was assembled of 3 core plugs (Figure 6.6) and flooded with CO₂ under immiscible conditions. All 3 core samples were initially oil wet and the experiment was carried out at conditions where CO₂ was in the gas state. The average value of $k_o @ S_{wi}$ – as measured and reported by the core samples supplier – was 90 mD.



Figure 6.6 The three core plugs used in the core flooding experiment

6.2.1 Experimental Setup

A schematic of the core-flooding experimental setup is shown in Figure 6.7. The core holder is Hassler-type with a Viton rubber sleeve that can hold 1.5 in. diameter, 12-in

long core samples. The core holder is rated for high pressure and high temperature operation and its wetted surfaces are made of corrosion-resistant Hastelloy C-4 alloy to withstand low pH fluids. The core holder was mounted vertically inside an air bath that maintained the core sample's temperature at the desired level. A hand pump was used to apply a suitable confining pressure on the core sample.

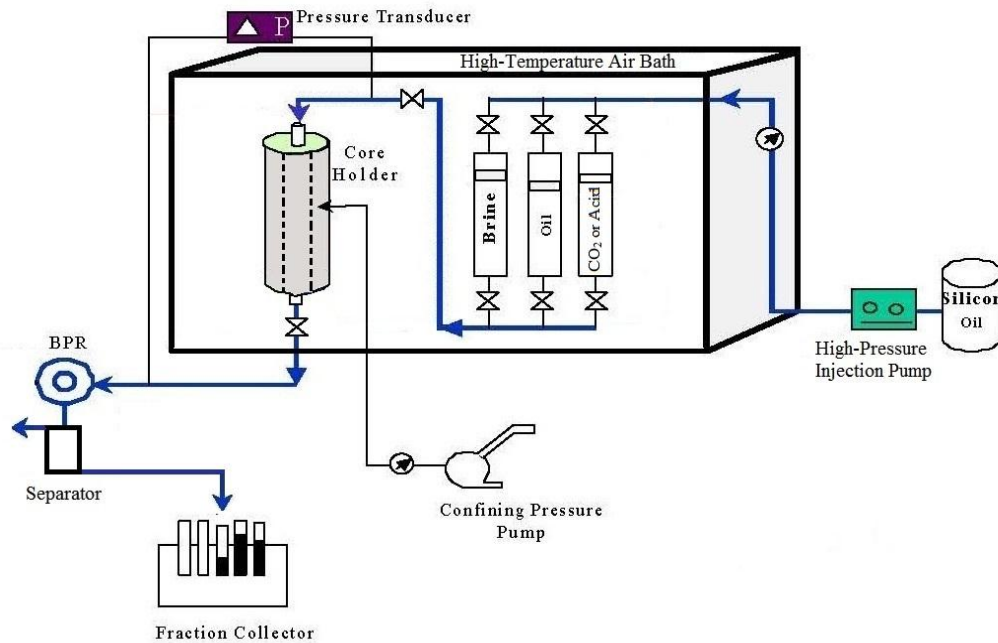


Figure 6.7 Schematic of the core flooding experiment

Three transfer cells that contained oil, brine, and CO₂ separately were connected through a manifold to a high-pressure, positive displacement, injection pump. The cells were connected to the core holder through another manifold. Both manifolds were configured in such a way that any of the three fluids could be delivered to the core holder individually as needed. The cell holding the CO₂ is also made of Hastelloy C-4 alloy, and

so is all the tubing that could come in contact with CO₂. The three transfer cells were also mounted inside the air bath to maintain thermal equilibrium between the injected fluids and the core sample. The brine and oil were loaded into their respective cells at atmospheric pressure while the CO₂ was loaded into its cell under the test pressure to ensure its gaseous state.

A back-pressure regulator was fitted to the outlet of the core holder to maintain the pressure at the desired level, and the total pressure drop across the core holder was measured by a pressure transducer. Fluids produced from the core holder passed through the regulator and were collected in a gas/liquid separator. The wetted parts of the regulator, transducer and the separator were made of a corrosion-resistant material. The following materials were used in the core-flooding experiment and their properties are presented in Table 6.3.

1. Reservoir core samples: These were obtained from an essentially limestone oil reservoir in the Middle East.
2. Brine: A 5% aqueous solution of KCl.
3. Oil: Dead Arabian Light crude oil.
4. Carbon Dioxide: Industrial grade CO₂ with less than 0.05% impurities.

Table 6.3 Fluid properties (core flooding experiment)

Fluid Property	Value
Oil density @ 55 °C	0.84 g/cc
Oil Viscosity @ 55 °C	6.7 cP
API Gravity	29° API

6.2.2 Experimental Procedure

6.2.2.1 Core Sample Saturation and Aging

1. The core plugs were cleaned of all fluids in a Soxhlet-type extractor. The extractor circulated hot toluene vapor through the pores of the rock specimen and cleaned them of any oil present. This was continued for about 10 days till clean toluene was seen in the extractor. The plugs were then cleaned with alcohol and dried in a vacuum oven at 90 °C for one day then weighed.
2. The plugs were then saturated under vacuum with the crude oil.
3. Each plug was then loaded into a permeameter and flooded with approximately 2 pore volumes of oil in each direction to ensure complete saturation.
4. The effective porosity of each plug was then calculated from the masses of the plug before and after saturation, bulk volume and oil density. These porosities are listed in Table 6.4.
5. The plugs were then aged in a bath of crude oil to ensure their oil wetness. Aging was carried out at 50 °C and atmospheric pressure for five days.

Table 6.4 Core plug effective porosities

Sample	Length (ft.)	Diameter (ft.)	Bulk Volume (cu ft.)	Dry Weight (pound)	Sat. Weight (pound)	Pore Volume (cu ft.)	Porosity (%)
1	0.121	0.125	0.00148	0.178	0.199	0.000415	0.28
2	0.137	0.125	0.00168	0.210	0.231	0.000453	0.26
3	0.125	0.125	0.00152	0.174	0.198	0.000448	0.29

6.2.2.2 Run Initialization

Initialization of the core flooding experiment followed the steps below:

1. The oil-saturated composite core sample was inserted into the Viton rubber sleeve, which was then loaded into the core holder. The core holder was then assembled and placed vertically inside the air bath.
2. The core holder was then connected to the transfer cell manifold (upper end), the effluent line (lower end) and the confining pressure line.
3. A confining pressure of 1180 psig was then applied.
4. The transfer cell containing brine was then connected to both the injection pump and core holder. Other transfer cells were isolated.
5. While the core holder outlet was opened to the atmosphere, the injection pump was started at a slow rate to purge all fluids (air, oil, brine) that were present within the core holder's lead and effluent lines.
6. The back-pressure regulator was set at the desired operating pressure. The air bath was set at the desired temperature (55 °C) and left on overnight. The core sample was ready for flooding.

6.2.2.3 Core Flooding

The first step was to flood the composite core with brine to residual oil saturation. The back-pressure regulator was set at 500 psig and 0.81 pore volumes of brine were injected through the core over a period of about 2.4 days at a rate of 0.00045 ft³/day. The residual

oil saturation was found to be about 43%. The composite core sample was then flooded with crude oil at the same conditions of pressure and temperature. About 1.40 pore volume of oil were injected through the core over nearly 4 days at a rate of 0.00045 ft³/day. The immobile water saturation was found to be 12%. The brine and oil flooding data are presented in Tables 6.5 and 6.6.

Table 6.5 Brine Flooding Data

Average Injection Flow	0.00045 ft ³ /day
Temperature	55 °C
Total Volume of Brine Injected	0.00108 ft ³
Cumulative Oil Produced	0.00076 ft ³

Table 6.6 Oil Flooding Data

Average Flow	0.00045 ft ³ /day
Temperature	55 °C
Total Volume of Oil Injected	0.0018 ft ³
Cumulative Brine Produced	0.0006 ft ³

The composite core sample was then flooded with about 5 PV of CO₂ at constant injection rate of 0.005 ft³/day for almost 1.3 day. The core outlet pressure was maintained at 500 psig to ensure immiscible displacement by gaseous CO₂. The temperature was maintained at 55 °C and the confining pressure was regulated at 1180 psig during the flooding process. The CO₂ flooding data is presented in Table 6.7.

Table 6.7 CO₂ Flooding Data

Cumulative Gas Injected (cu. ft.)	Cumulative Gas Injected (PV's)	Oil Produced (cu. ft.)	Oil Recovery (% IOIP)	Oil Recovery (PV's)
0.0000	0	0.00000	0.0	0.000
0.00014	0.11	0.00010	8.8	0.078
0.00032	0.24	0.00032	27.2	0.240
0.00037	0.29	0.00032	27.8	0.245
0.00041	0.31	0.00033	28.0	0.246
0.00064	0.49	0.00037	32.1	0.282
0.00533	4.10	0.00059	50.9	0.448
0.00535	4.11	0.00060	51.2	0.451
0.00537	4.13	0.00060	51.5	0.454
0.00540	4.15	0.00061	52.1	0.459
0.00620	4.77	0.00063	54.3	0.478
0.00630	4.85	0.00065	55.8	0.491
0.00634	4.87	0.00065	55.8	0.491
0.00637	4.90	0.00065	55.8	0.491
0.00641	4.93	0.00065	55.8	0.491
0.00644	4.96	0.00065	55.8	0.491

It should be noted that the CO₂ breakthrough occurred when 0.24 pore volumes of oil were produced against an injected CO₂ volume of 0.24 pore volumes, which agrees with the assumed steady state of the flood. Once gas breakthrough occurred, the data showed a normal trend toward the end of the run (oil recovery > 50%). These points reveal an ultimate oil recovery of about 56% which was achieved after about 5 pore volumes of CO₂ were injected.

6.2.2.4 Contact Angle Measurement

To test for any change in rock wettability, the contact angle between oil and brine was measured at 55 °C for each core plug before and after flooding with CO₂. Once the composite core was flooded with oil to immobile water saturation, each core plug was submerged into a glass beaker filled with brine (Fig. 6.8). A drop of oil was then placed with a needle on the lower face of the plug. High resolution pictures were then taken and the contact angle – as measured through the brine – was estimated as shown in Figs. 6.9, 6.10 and 6.11. The procedure was repeated with the core plugs after flooding with CO₂. The results of these measurements are presented in Table 6.8.

Table 6.8 Contact angle values before and after CO₂ flooding

Core Plug	Contact Angle Before CO₂ Flood	Contact Angle After CO₂ Flood
1	135°	110°
2	130°	120°
3	140°	120°

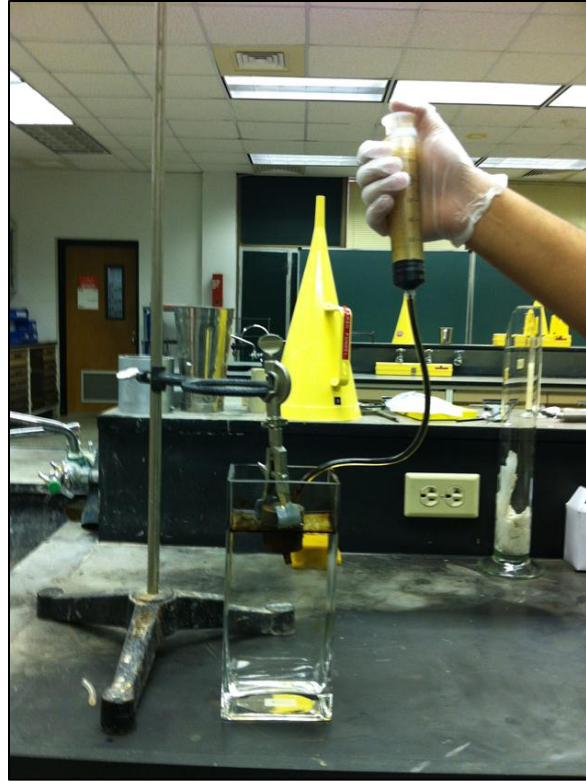


Figure 6.8 Contact angle measurement setup

Before CO₂ Flood



After CO₂ Flood

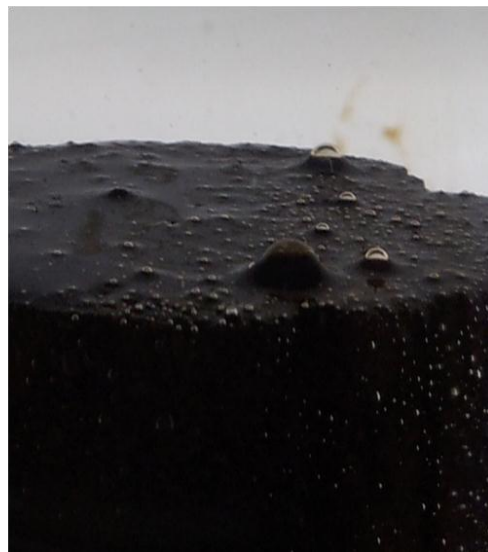


Figure 6.9 Contact angle measurement for core plug # 1 (view is inverted)

Before CO₂ Flood



After CO₂ Flood



Figure 6.10 Contact angle measurement for core plug # 2 (view is inverted)

Before CO₂ Flood



After CO₂ Flood



Figure 6.11 Contact angle measurement for core plug # 3 (view is inverted) |

CHAPTER 7

RESULTS AND DISCUSSION

This chapter discusses the results obtained from the numerical simulation models developed for the CO₂-oil immiscible displacement model, modified Corey relative permeability model and contact angle model. It also discusses the observations made with core flooding and wettability alteration experiments. Comparisons with two well-known displacement models are also made.

7.1 Wettability Alteration Model Calibration

The experiment described in Section 6.1 was run twice, each with a fresh slice of the same rock. Each run was conducted at a different brine CO₂ concentration: 0.0004 mole percent for Run # 1 and 0.0008 mole percent for Run # 2. The CO₂ concentration was calculated by volumetric balance on the cell's contents. Table 7.1 lists the data of both runs, which is also plotted in Figure 7.1.

The results demonstrate that the rock wettability in both runs was altered when the rock was exposed to CO₂. In Run # 1, the contact angle decreased from 101° initially to reach a stable value of about 83.9° after 44 minutes of exposure to the carbonated brine. The change in contact angle shows that the wettability of the core slice was altered from slightly oil-wet to intermediate-wet. In Run # 2, the stable value appeared to be 69.3 ° and

was attained in 52 minutes. When the exposure time was extended to 89 minutes in this run, no change was observed in the angle confirming the existence of a stable and new “equilibrium” value in the contact angle. The trend in both data sets reveals an asymptotic-exponential relationship between the contact angle and exposure time where the initial decrease in the angle was rapid followed by a gentle trend towards a stable value.

Table 7.1 Variation of the contact angle with time

Run#1		Run#2	
CO ₂ Exposure Time (min.)	Contact Angle (degree)	CO ₂ Exposure Time (min.)	Contact Angle (degree)
0	101.0	0	97.5
6	90.8	9	96.7
8	89.4	11	95.2
16	90.8	17	74.8
21	88.3	23	72.8
23	86.4	25	72.8
28	86.5	28	73.0
34	86.3	32	73.0
40	86.8	34	69.2
43	85.9	36	69.1
44	83.9	39	69.4
		44	69.4
		52	69.3
		76	69.3
		83	69.3
		89	69.3

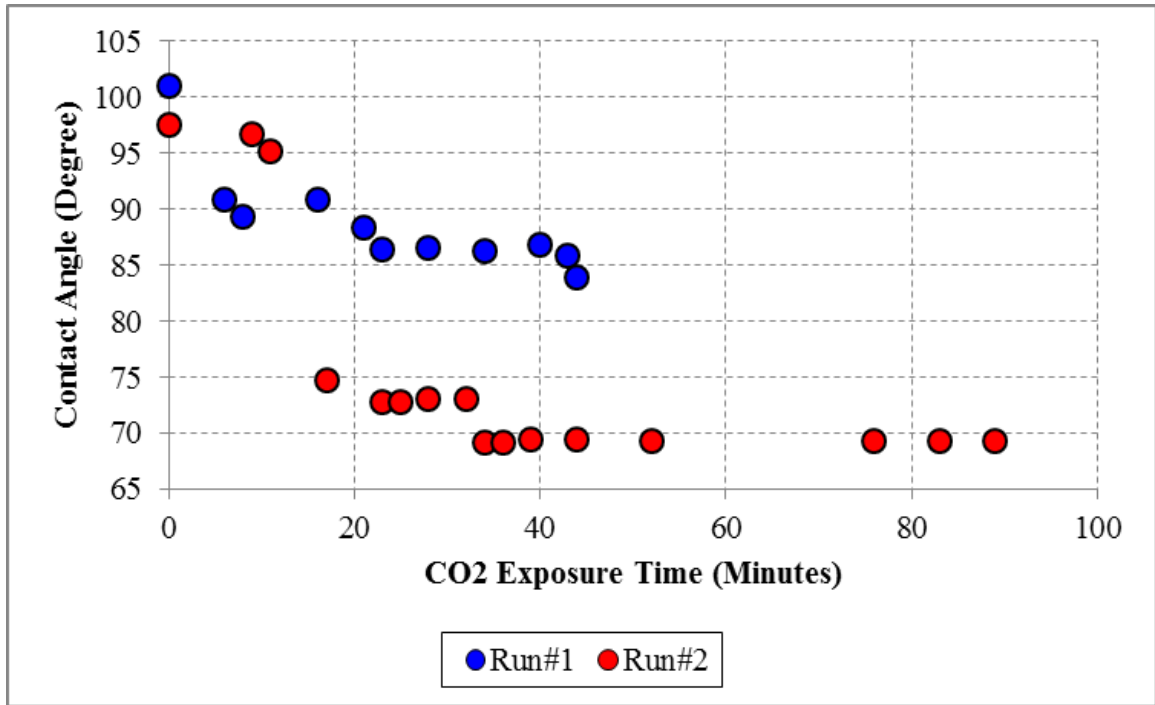


Figure 7.1 Raw experimental data for Run # 1 and Run # 2

The data of Figure 7.1 also reveals that the stable value depends on the CO₂ concentration of the brine in contact with the oil with a higher concentration causing a larger drop in the contact angle. However, the exposure time needed to reach a stable angle appears to be slightly dependent upon CO₂ concentration. One can then speculate that under the conditions of this experiment diffusion of CO₂ through the oil is fast enough even at relatively low concentrations. It remains to be seen whether at still higher concentrations the rock could be altered to a water-wet state. Table 7.2 summarizes Eq. (4.41) parameters as extracted from the data.

Table 7.2 Initial and final contact angles with stabilization time

Run No.	Brine CO ₂ Concentration (mole %)	θ_i (Degrees)	θ_{min} (Degrees)	t_{sb} (Minutes)
1	0.0004	101.0	83.9	44
2	0.0008	97.0	69.3	52

Based on the parameter values listed in Table 7.2, θ_D was computed and plotted vs. t_D for both runs in Fig. 7.2. All data points fall within one band indicating a common value of ξ for both runs.

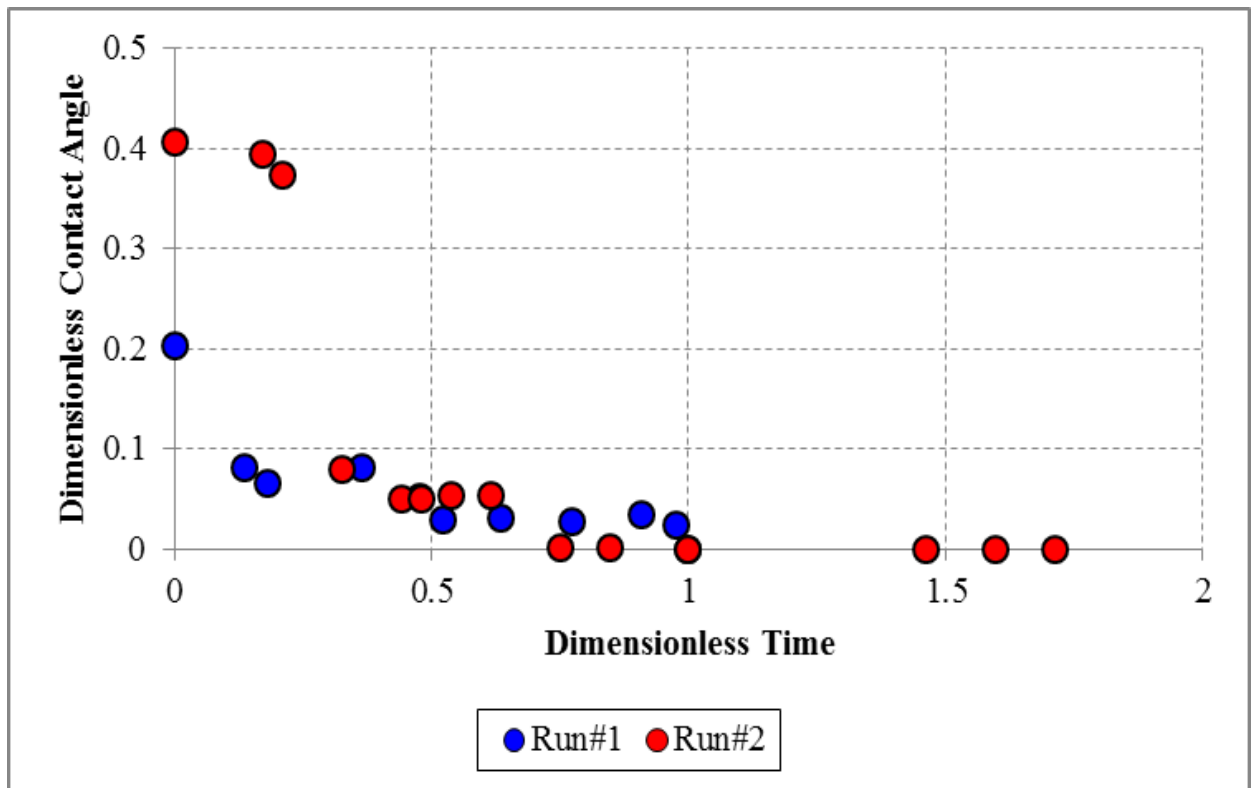


Figure 7.2 Dimensionless experimental data for Run # 1 and Run # 2

Taking \log_e of both sides of Eq. (4.43) yields

$$\log_e \theta_D = \log_e \theta_{Di} - \xi t_D \quad (7.1)$$

Re-plotting Figure 7.2 with semi-log axes (Figure 7.3) shows a reasonably linear trend. The four outlying data points are attributed to experimental error; however, the bulk of the data does fall on the same trend. Excluding those four data points, the slope of this line is 1.39 which is the value of ξ for the conditions of this experiment.

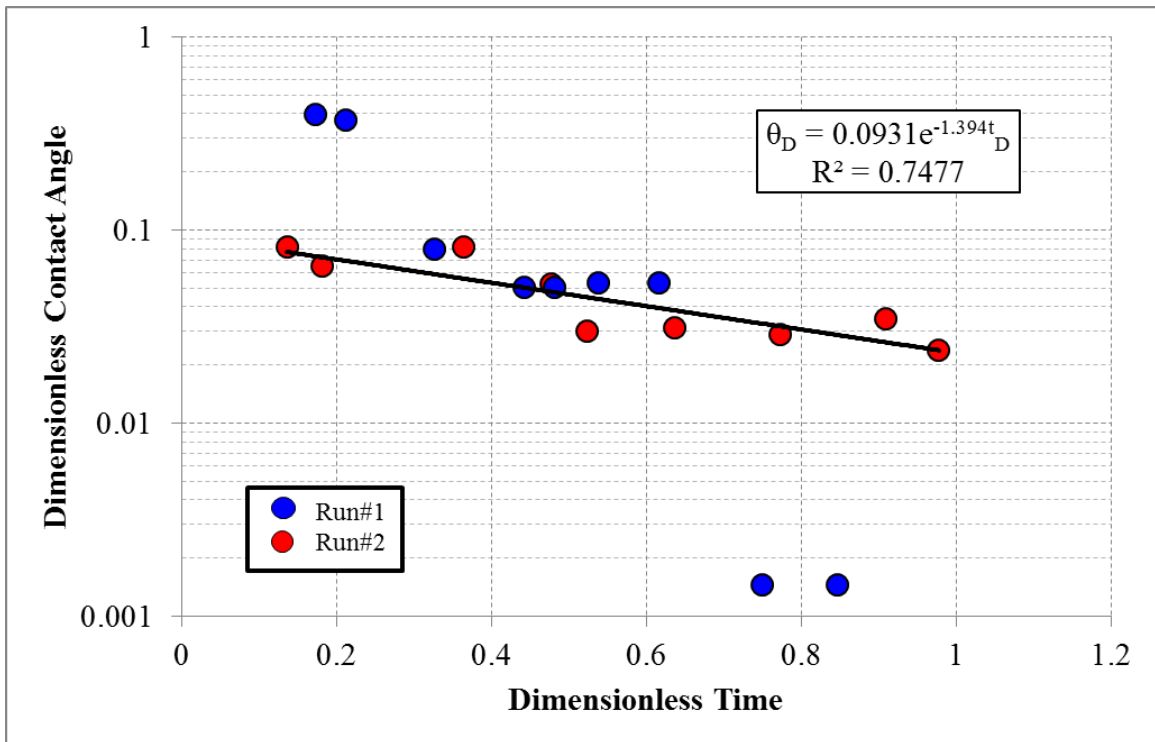


Figure 7.3 Dimensionless experimental data for both Run # 1 and Run # 2

Differentiating Eq. (4.43) with respect to t_D yields:

$$\frac{d\theta_D}{dt_D} = -\theta_{Di}\xi e^{-\xi t_D} \quad (7.2)$$

or

$$\frac{d\theta_D}{dt_D} = -\xi\theta_D \quad (7.3)$$

Eq. (7.3) shows that ξ controls the rate of decline of the dimensionless contact angle with dimensionless time. We can speculate that this parameter is similar for all other concentrations of CO₂, which makes predicting other minimum contact angles possible for the rock/oil system of this study.

The significance of this study can be related to cases where CO₂ is injected in a watered out, oil-wet reservoir at a pressure below the miscibility pressure. CO₂ diffusion through the oil can alter the rock wettability and render the residual oil mobile. In miscible CO₂ displacement processes, such phenomenon can still occur when CO₂ fingers advance ahead of the CO₂ slug and contact residual oil at low concentrations.

One might point that the relatively short time (less than one hour) it took to complete the wettability alteration as observed in the two runs is negligible in terms of the time scale of field applications. In flooding projects where the CO₂ flood front advances at a speed of feet per day wettability alteration is expected to appear almost instantaneously. However, in watered-out reservoir rock where oil exists as droplets trapped in small pores

with limited access by the reservoir brine, CO₂ gas needs to diffuse through the water phase then the oil droplets before reaching the rock surface. At low CO₂ concentrations, this diffusion process might take considerably longer time to complete, causing much slower wettability alteration.

7.2 Displacement Models Comparison

Performance of the displacement model (Eq. 4.25) presented in Section 4.3 was benchmarked against two displacement models. The first – the IMPES model – is based on the original form of the material balance equation (Eqs. 7.34 and 7.35) [89]. The second is the Buckley-Leverett displacement model – the BL model – (Eq. 7.36) [90].

$$S_{o_i}^{n+1} = S_{o_i}^n - S_{o_i}^n (c_o + c_r)_i^n (p_{o_i}^{n+1} - p_{o_i}^n) + \left(\Delta t T_{i+\frac{1}{2}} B_{o_i}^n \left(\frac{k_{ro}}{B_o} \right)_{i+\frac{1}{2}}^n [p_{o_{i+1}}^{n+1} - p_{o_i}^{n+1}] - \Delta t T_{i-\frac{1}{2}} B_{o_i}^n \left(\frac{k_{ro}}{B_o} \right)_{i-\frac{1}{2}}^n [p_{o_i}^{n+1} - p_{o_{i-1}}^{n+1}] \right) / V_{p_i}^n \quad (7.34)$$

$$S_{g_i}^{n+1} = 1 - S_{o_i}^{n+1} - S_{w_i} \quad (7.35)$$

$$S_{g_i}^{n+1} = S_{g_i}^n - \frac{Q_g \Delta t}{\phi A \Delta x} (f_{g_i}^n - f_{g_{i-1}}^n) \quad (7.36)$$

The wettability alteration phenomenon was eliminated during the comparison. The objective is to evaluate the reliability of the displacement model and benchmark it against the two other well-established displacement models. MATLAB programming was employed to run the models as detailed in Appendices C-1, C-2 and C-3. The rock and fluid properties assumed in all models are given in Table 7.3.

First, the optimum number of cells was examined with the proposed model prior to proceeding with the comparison study. Four different numbers were chosen: 20, 40, 60 and 80 cells. It was found that if the number of cells exceeded 60, the gas breakthrough time would not change significantly (Figure 7.4). In addition, a higher gas saturation profile was observed in the first few leading cells as the number of cells increased. This is due to their proximity to the gas inlet. For this reason, 60 cells were selected for the rest of the comparison study.

Table 7.3 Simulation model input data in the displacement model comparison study

Parameter	Value
Q_{gi}	0.2 ft ³ /day
k	300 mD
oil viscosity	2.0 cP
gas viscosity	0.03 cP
porosity	0.20
Δx	0.167 ft
Δy	0.1 ft
Δz	0.1 ft
Medium's Length	10 ft
S_{wi}	0.1
S_{gi}	0
S_{oi}	0.9
S_{or}	0.25
$k_{ro} @ S_{wi}$	1.00
$k_{rg} @ 1-S_{or}$	0.5
c_g	0.002 psi ⁻¹
c_r	0.000004 psi ⁻¹
c_o	0.000015 psi ⁻¹
Δt	0.0001 day

For the IMPES model, the saturation and pressure equations derived from the material balance equation were utilized in the model to calculate the pressure and saturation in each grid cell. The IMPES approach was considered in the computation scheme, which means that the pressure was calculated implicitly while saturation was calculated explicitly. The pressure equation in the IMPES scheme is obtained after summation of Darcy's laws and substituting them into the summation of the two mass conservation equations for each phase. The gas saturation (S_{CO_2}) is then calculated after obtaining the

pressure of each grid cell. On the other, the BL model depends on the relative permeability concept where gravitational and capillary forces are neglected [21].

The CO₂ saturation profile was investigated at 0.1, 0.5, 1, 2 and 3 pore volumes of CO₂ injected (Figures 7.5 to 7.9). Although the proposed model shows stable outputs and good predictive capability, it is noticed commonly that the CO₂ saturation is less compared to the other two models before and after gas breakthrough.

Initially, the differences in the gas saturation profiles are largest; then they decrease as larger pore volumes of gas are injected. At 3 pore volumes injected, the gas saturations predicted by the proposed model range from 0.44 in the first cell to 0.24 in the last cell. However, the gas saturations predicted by the other two models range from 0.48 in the first cell to 0.27 in the last cell. The gas breakthrough time occurred earlier in the proposed model, at about 0.0148 days of CO₂ injection, compared with about 0.0157 days of CO₂ injection in the other two models (Figure 7.10). The recovery factor in the proposed model is generally higher than the recovery factors in the other two models (Figure 7.11). The IMPES and BL models predict an oil recovery factor of about 36.3% after injecting 3 pore volumes of CO₂ compared with about 44% with the proposed model. Before breakthrough, the proposed model predicts a higher peak oil production rate compared with the other models (Figure 7.12). The oil production rate in the proposed model reaches up to 0.29 ft³/day compared to maxima of 0.24 ft³/day and 0.2 ft³/day for the IMPES and BL model, respectively. Beyond breakthrough, the oil production rate predicted by the proposed model remains higher than the oil production

rate of the other two models until the end of the run. The higher oil production rate of the proposed model explains the larger oil recovery observed in Figure 7.11.

The pressure at the first cell - as predicted by the proposed model - reaches a maximum of about 640 psi followed by a gradual drop after breakthrough until it reaches about 540 psi after 0.3 days of CO₂ injection (Figure 7.13). On the other hand, the IMPES model shows the pressure reaching above 670 psi followed by a gradual drop after breakthrough to about 520 psi towards the end of the flood.

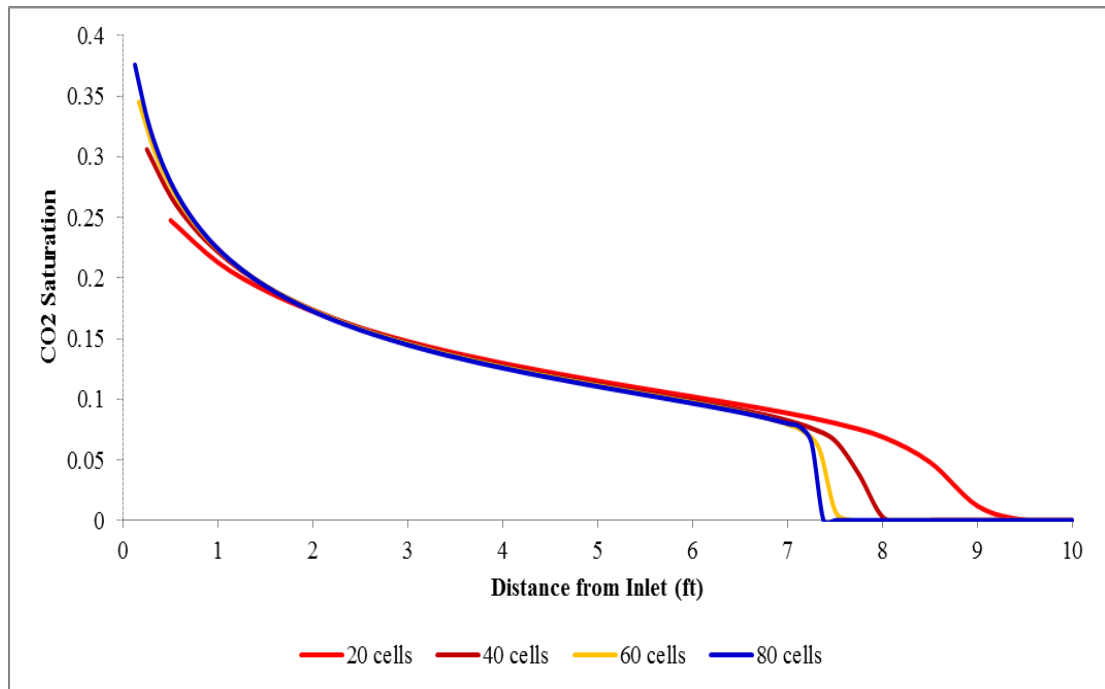


Figure 7.4 Impact of grid size on CO₂ breakthrough time for the proposed model

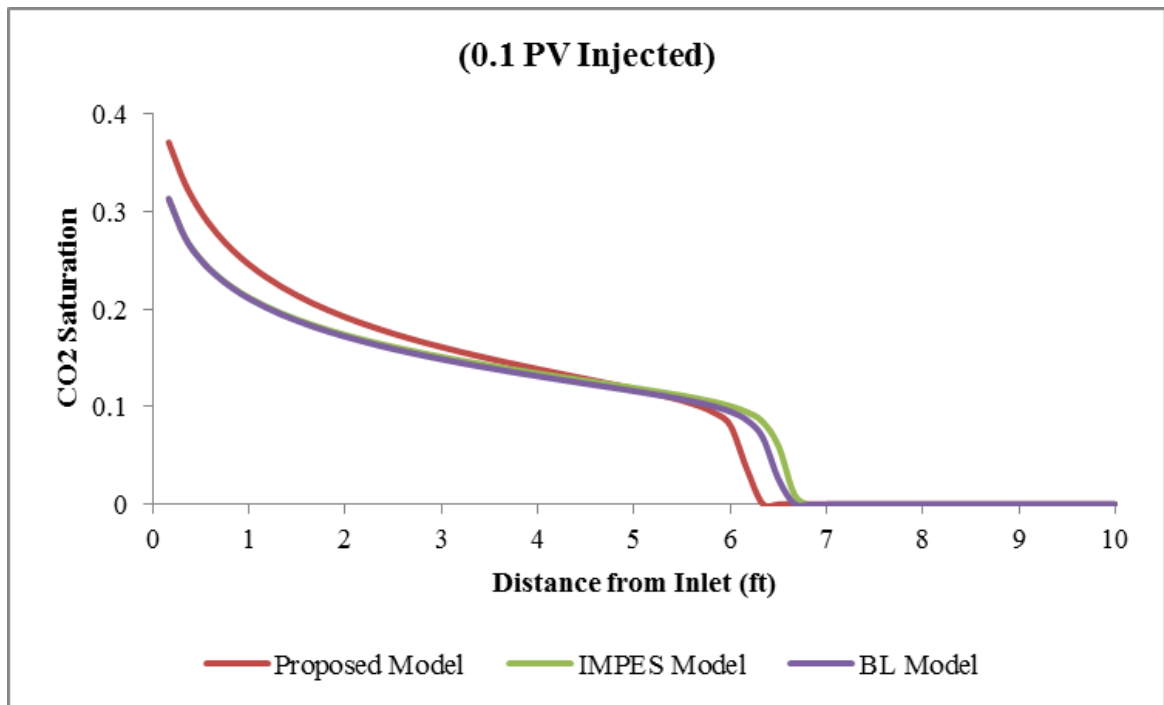


Figure 7.5 Location of the CO₂ flood front after injecting 0.1 PV of CO₂

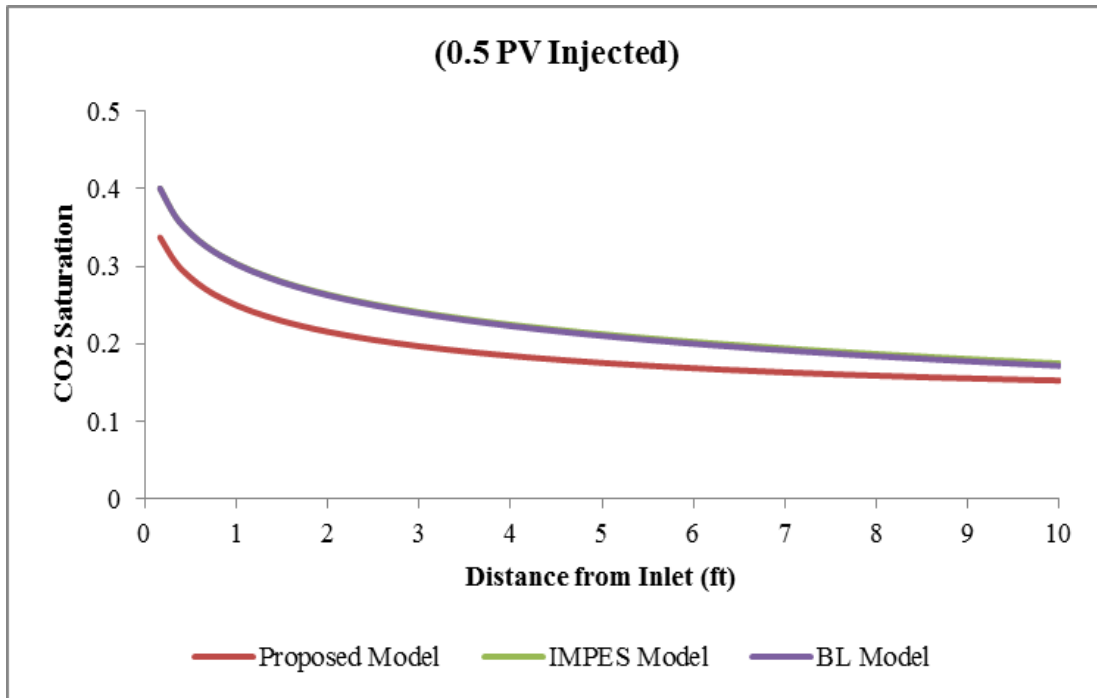


Figure 7.6 Location of the CO₂ flood front after injecting 0.5 PV of CO₂

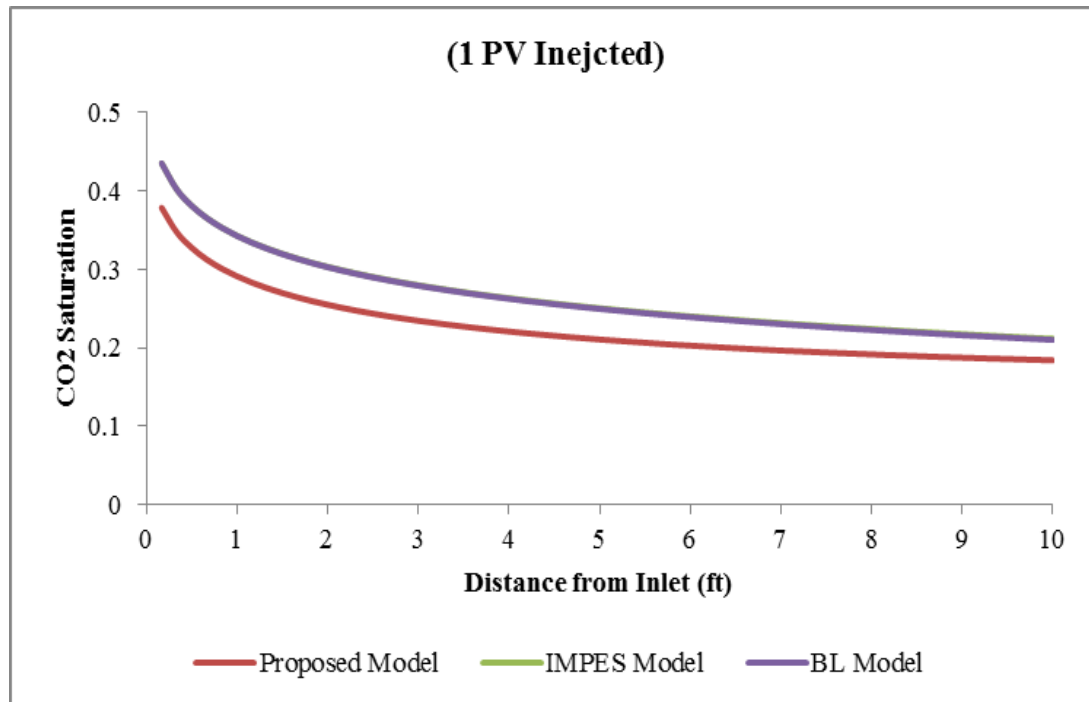


Figure 7.7 Location of the CO₂ flood front after injecting 1 PV of CO₂

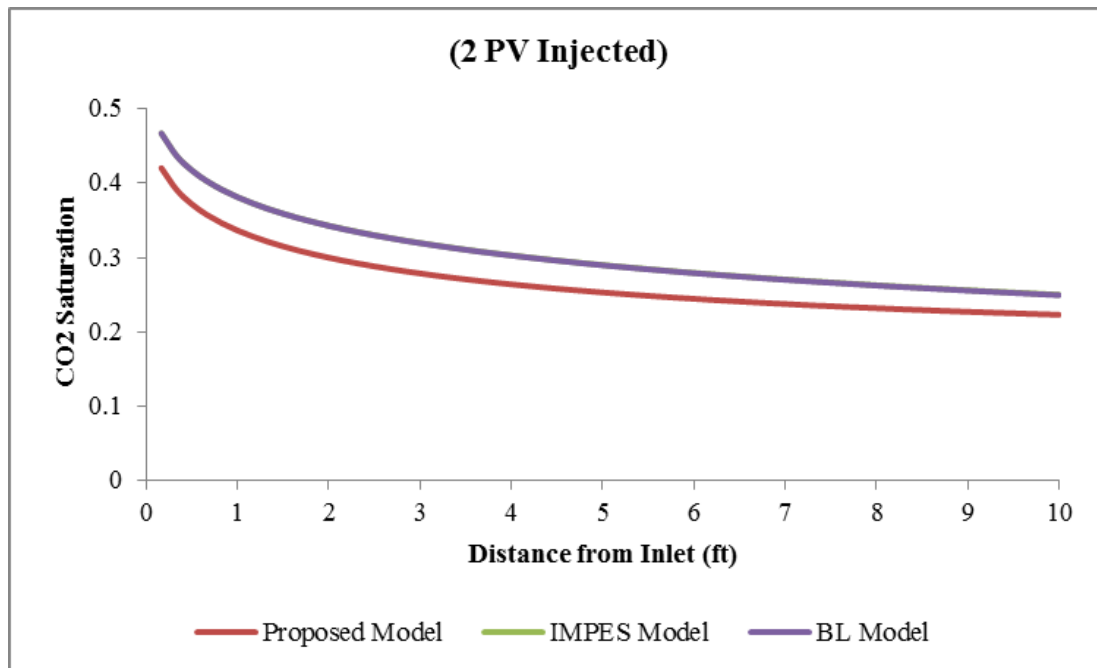


Figure 7.8 Location of the CO₂ flood front after one injecting 2 PV of CO₂

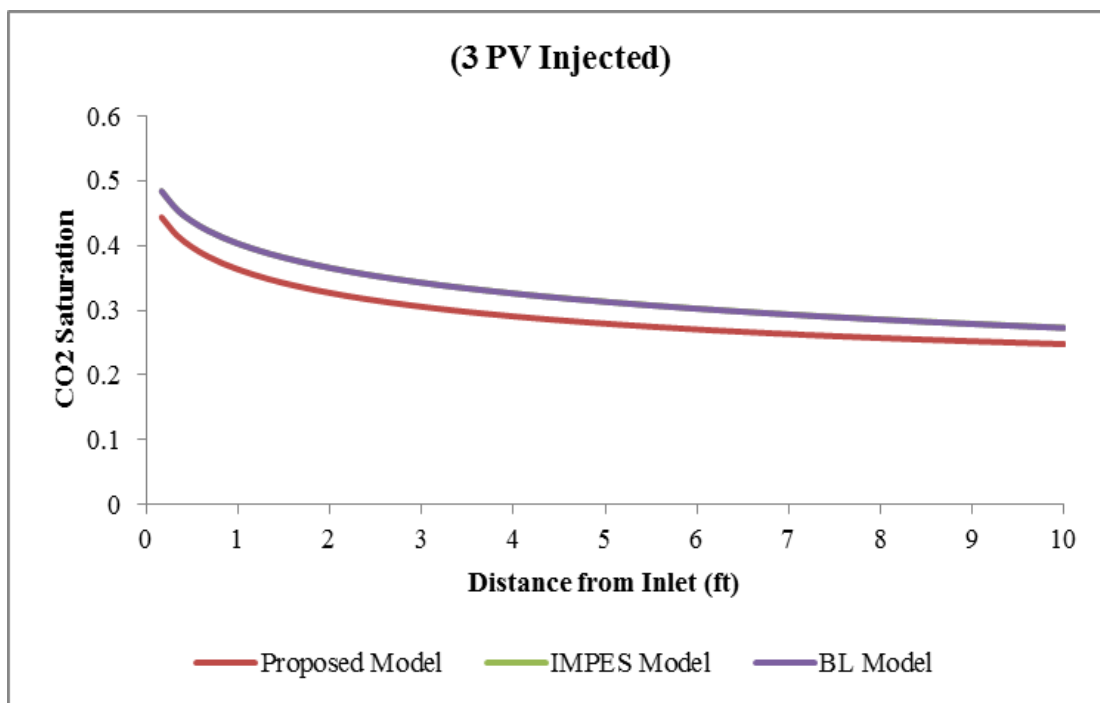


Figure 7.9 Location of the CO₂ flood front after injecting 3 PV of CO₂

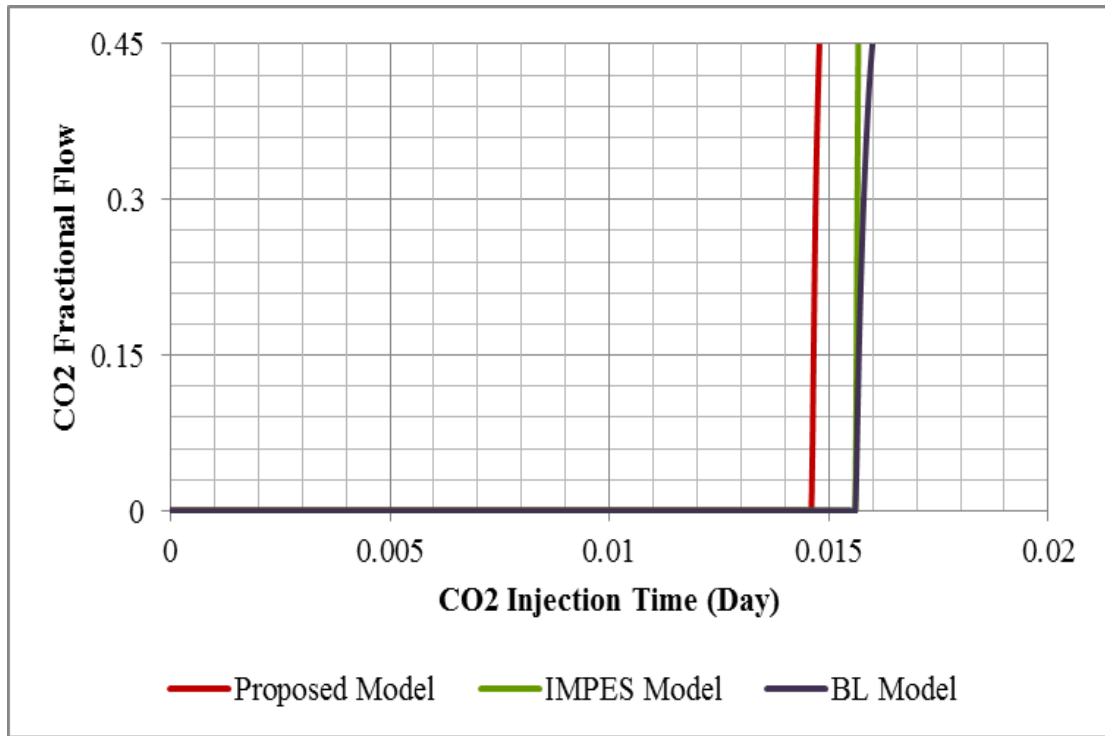


Figure 7.10 CO₂ breakthrough time

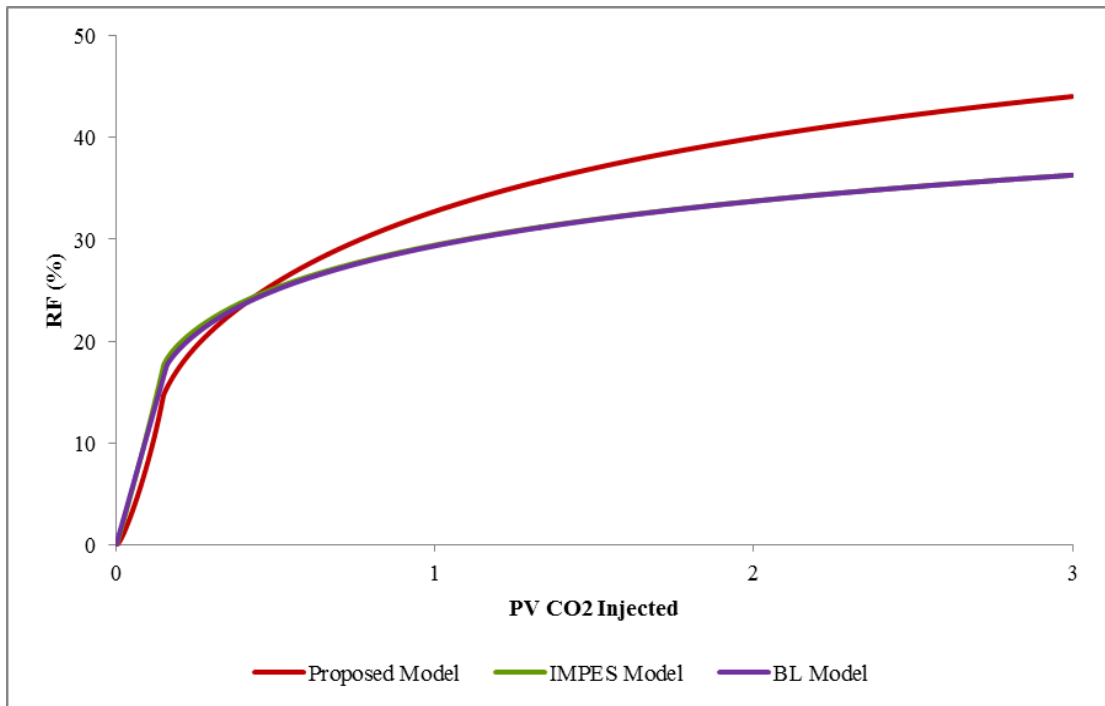


Figure 7.11 Variation of oil recovery factor with injected CO₂ volume

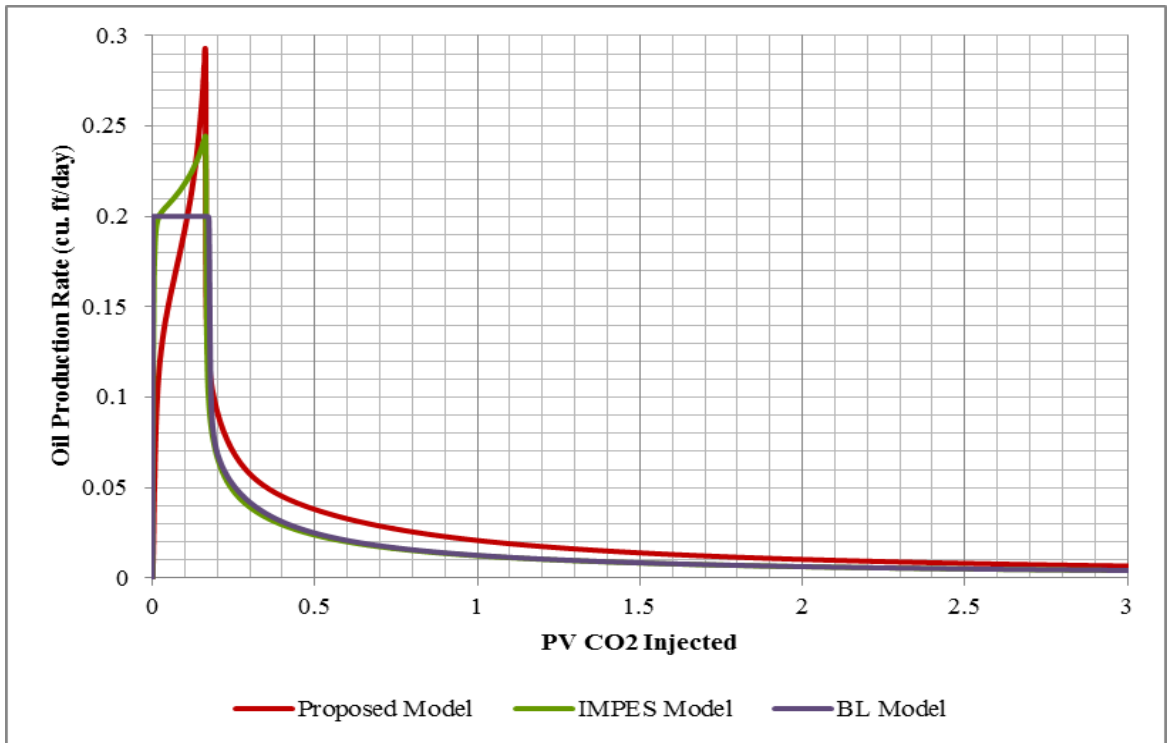


Figure 7.12 Oil production rate

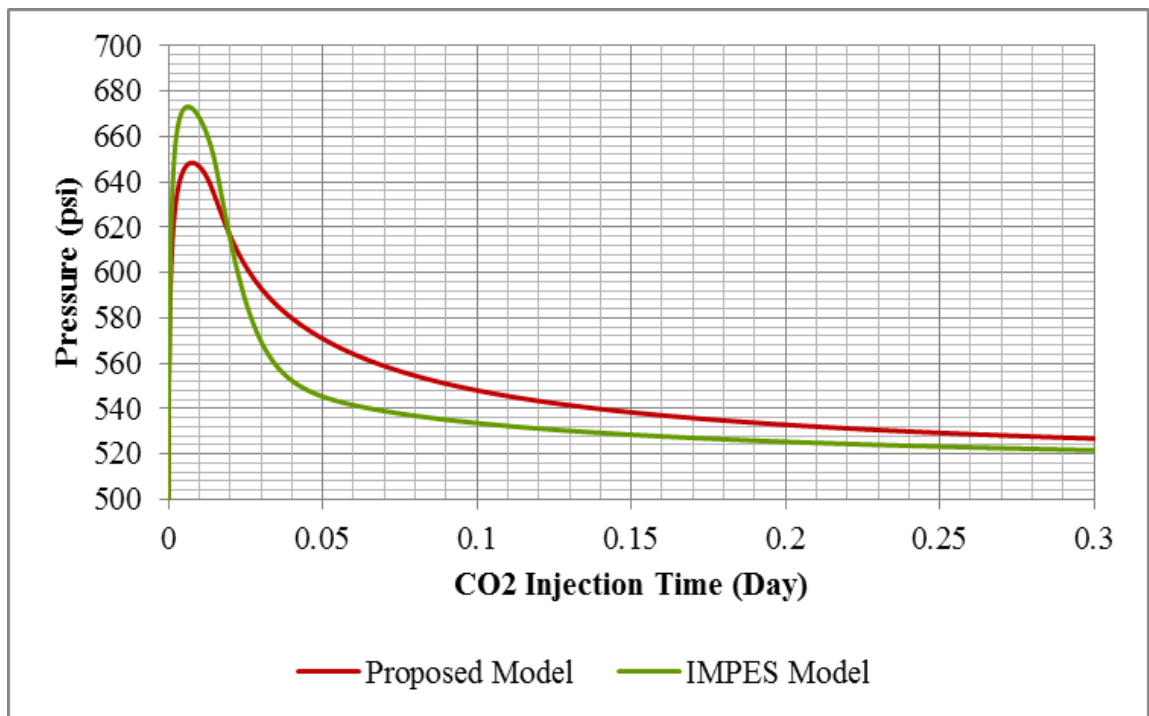


Figure 7.13 Variation of 1st cell pressure with CO₂ injection time

7.3 Limitations of the Proposed Model

Although the proposed model – Eq. (5.15) – produces stable results, its numerical scheme entails some material balance conservation errors as observed by the common discrepancy in plots presented in section (7.2) during the benchmark study. CO₂ saturations (Figures 7.5-7.9) predicted by the proposed model show a maximum absolute error of 7% which is equivalent to a relative error of about 17% in first cell after 0.5 PV of CO₂ injected. The material balance error leads the proposed model to predict a higher oil recovery with an absolute error of about 8% (21% relative error) when compared with the other models as observed in Figure 7.11. In addition, the proposed model could produce larger errors under some extreme conditions (e.g. a highly compressible system). For this reason, it was decided to carry out the wettability alteration analysis with the IMPES model as will be discussed in the following sections.

7.4 Incorporation of Wettability Alteration Phenomenon

Wettability alteration was incorporated in the IMPES model. The MATLAB programming code for the IMPES model incorporating wettability alteration is presented in Appendix C-4. The input parameters are the same as those listed in Table 7.3. Wettability alteration was assumed to follow Eq. (4.41). The parameters required for the wettability alteration model are listed in Table 7.4. Two cases were considered in the numerical simulation model: with wettability alteration and without. Based on the

assumed wettability conditions given in Table 7.4, the coefficients of the residual oil saturation model – Eq. (4.29) – and modified Corey relative permeability model for CO₂ and oil – Eqs. (4.39) and (4.40) – were adjusted as presented in Appendix B-1.

Table 7.4 Wettability alteration model input data in the IMPES model

Parameter	Value
Initial Contact Angle, θ_i	120°
Final Contact Angle, θ_f	100°
Stabilization Time	45 minutes
Final Residual Oil Saturation, S_{orf}	0.15

In each case, three CO₂ flooding times were investigated: 0.05, 0.10 and 0.30 days. Fig. 7.14 shows the CO₂ saturation profiles at the three CO₂ flooding times for both with wettability alteration and without wettability alteration conditions. It can be clearly noticed that the saturation profile is shifted higher for with-wettability alteration condition at all three times. For example, after 0.05 days of CO₂ flooding, the difference in gas saturation between the two conditions ranges between 0.05 at the first cell to 0.02 at the last cell.

The CO₂ breakthrough time was 0.014 days for the without-wettability alteration condition and 0.0151 days for the with-wettability alteration condition (Figure 7.15). The delay in breakthrough time for the with-wettability alteration condition is attributed to the lower CO₂ mobility caused by the shift in relative permeability curves.

The delay in breakthrough time and the shift in gas saturation profile results in a noticeable increase in oil recovery. Figure 7.16 shows an oil recovery of about 40% after injecting 3.3 pore volumes of CO₂ for the with-alteration condition compared with about 36% for the without-alteration condition. Oil production rate shows higher with the condition of with wettability alteration compared to the without wettability alteration condition (Figure 7.17). Figure 7.18 shows the changes in contact angle with respect to CO₂ exposure time. The drop in contact angle is higher for cells that are closer to the gas inlet indicating longer exposure time to CO₂. The contact angle of cell#1 drops the highest, from 120° to 100° after 45 minutes of CO₂ injection time. On the other hand, the contact angle of cell#60 drops the lowest, from 120° to 103° after 45 minutes of CO₂ injection time.

Inspecting the relative permeability curves for with and without-alteration conditions also shows a shift in the crossover point from $S_g = 0.27$ to 0.32 (Figure 7.19). This shift in the relative permeability curves can be explained physically by oil displacement from medium size pores caused by re-distribution of the water phase. As the wettability is altered from oil wet to intermediate wet, the residual water droplets that were restricted to large pores can now invade medium pores and, thus, vacate the large pores to the gas phase.

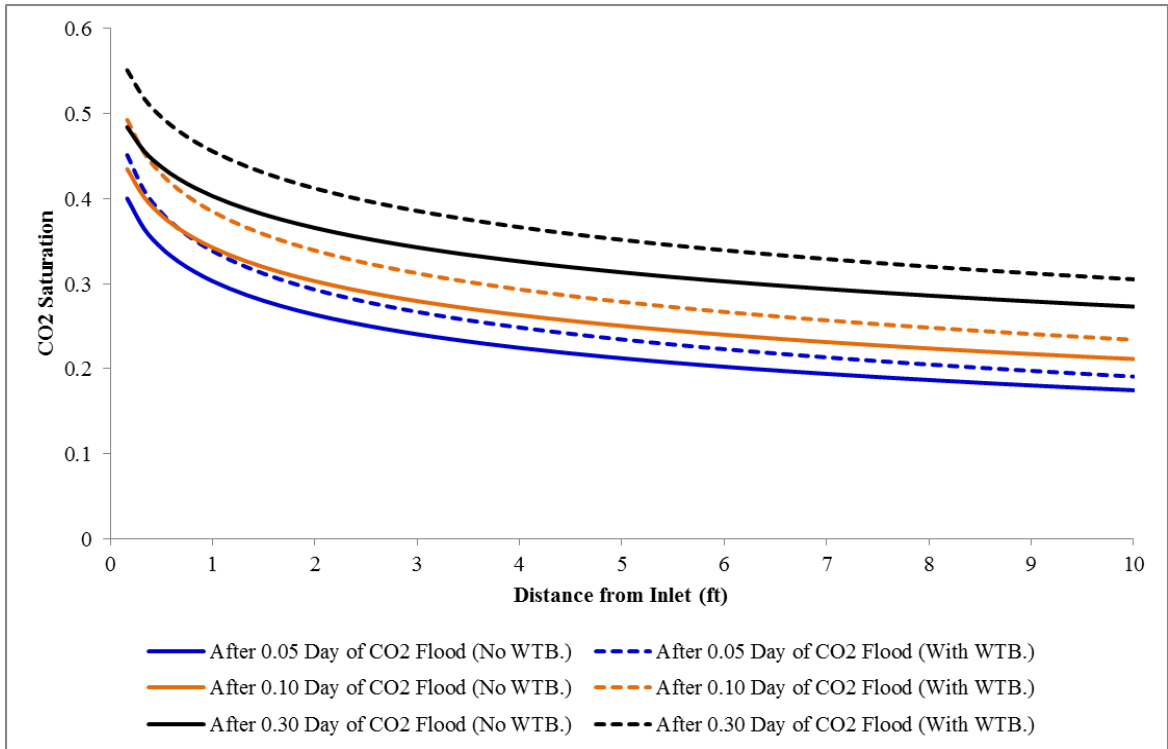


Figure 7.14 CO₂ saturation profiles at three different flooding times

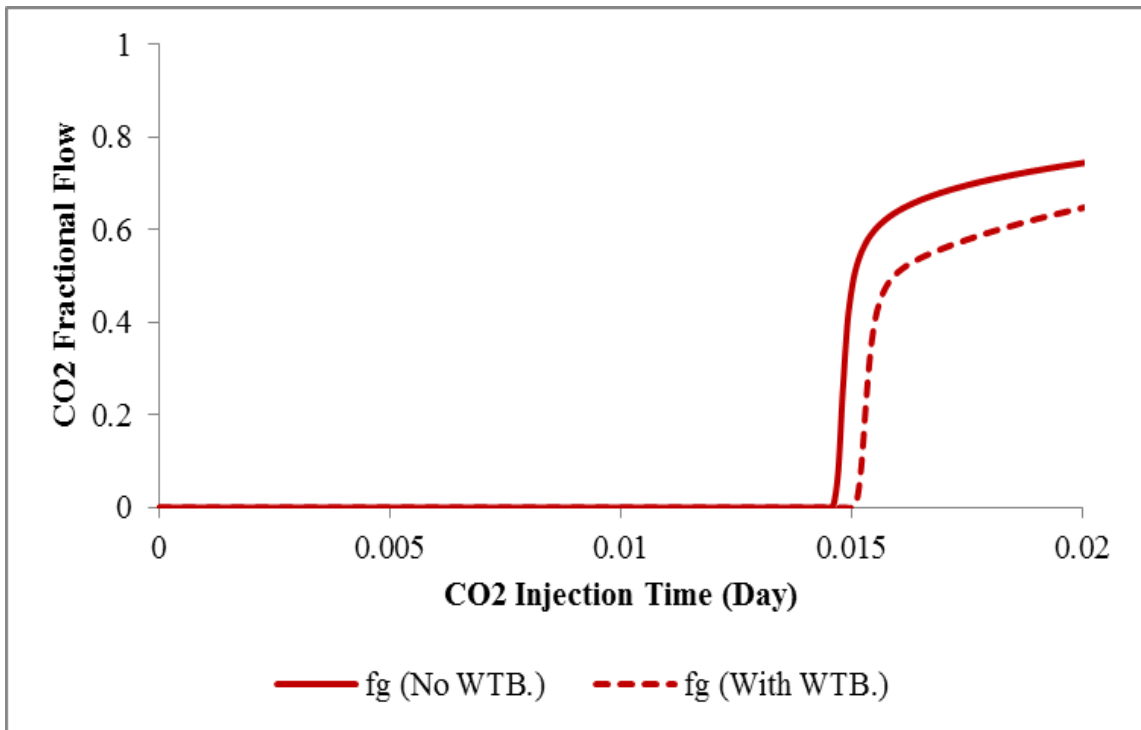


Figure 7.15 CO₂ breakthrough time for with and without wettability alteration conditions

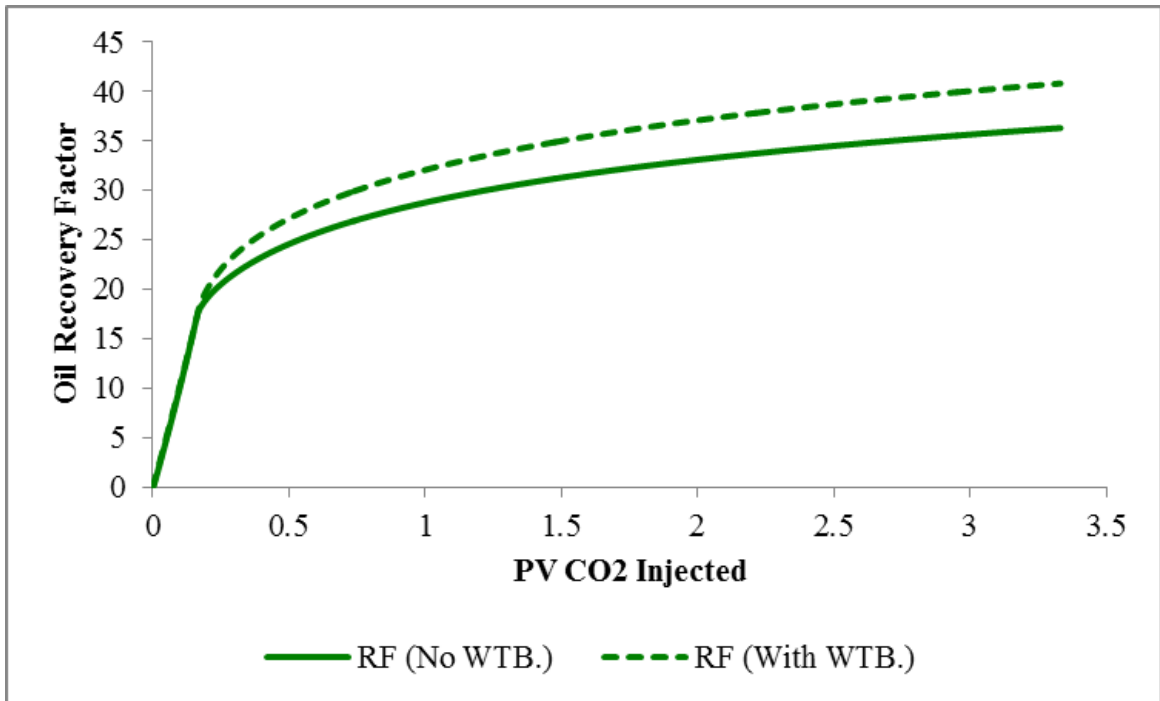


Figure 7.16 Oil recovery versus volume of CO₂ injected

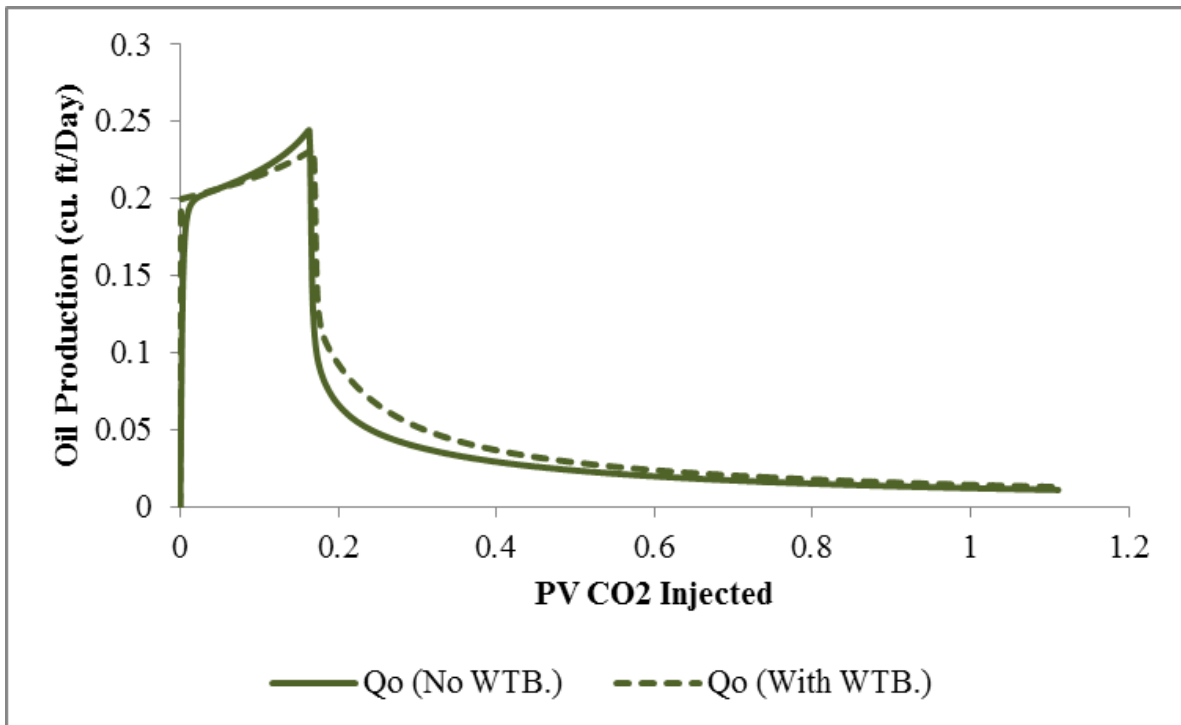


Figure 7.17 Oil production rate versus volume of CO₂ injected

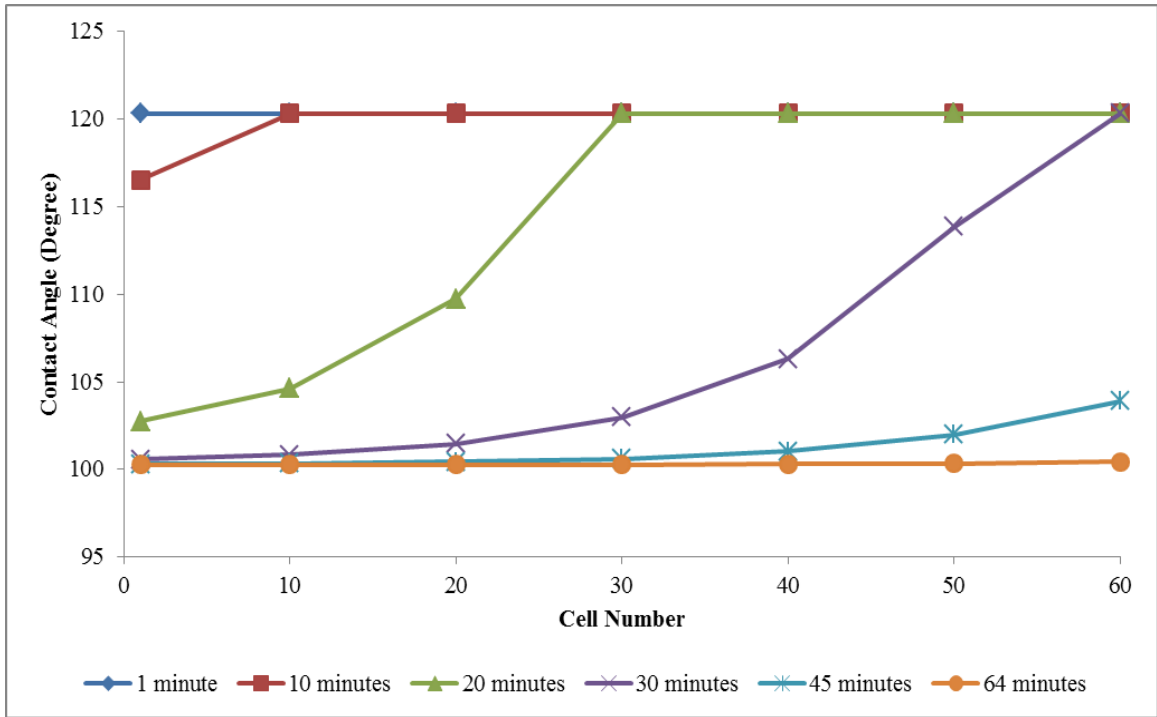


Figure 7.18 Contact angle variations at different injection times

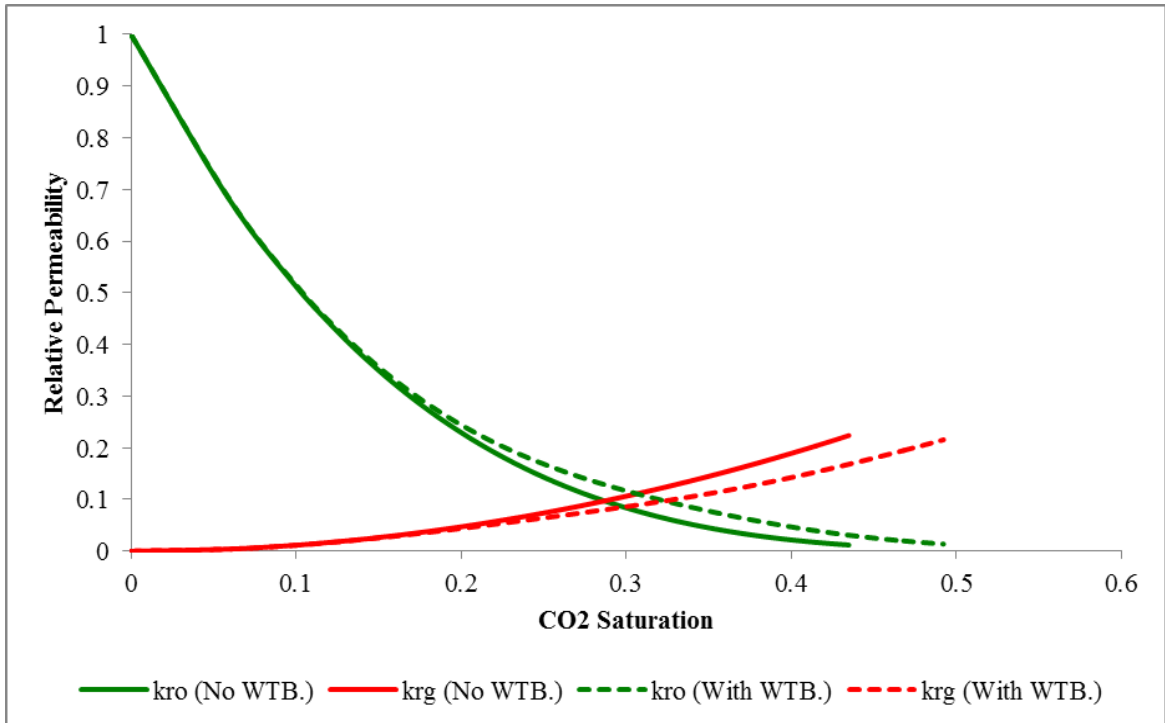


Figure 7.19 Relative permeability curves

7.5 Effect of Residual Oil Saturation on Oil Recovery

The wettability model was examined to evaluate the impact of residual oil saturation on oil recovery. Three cases were considered. The first two cases employ the IMPES model alone with residual oil saturations of 0.25 and 0.15. The third case includes wettability alteration in the IMPES model allowing the residual oil saturation to drop from 0.25 to 0.15.

Figure 7.20 shows variation in oil recovery with volume of CO₂ injected for the three cases up to 1 PV of CO₂. Naturally, the model predicts lower oil recovery with higher residual oil saturation. The oil recovery reaches 29% and 32% with S_{or} of 0.25 and 0.15, respectively. When wettability alteration is incorporated, the oil recovery shows a trend which is intermediate between the two no-wettability-alteration cases, starting slightly higher than the case with S_{or} = 0.25 and overlaps quickly with the case of S_{or} = 0.15 after about 0.34 PV CO₂ injected. This indicates that the wettability alteration model is capable of predicting the additional recovery as a result of drop in S_{or}; however, the extra oil recovery is not realized in a step fashion but rather in a gradual mode.

It is worth mentioning that it may not be economically feasible to inject large volumes of CO₂ in actual field applications. Nevertheless, account for wettability alteration is necessary because it could mean the difference between a viable and unviable recovery project. The results and analyses presented in this chapter demonstrate the potential of CO₂ as a wettability-alteration agent. A flooding process involving carbonated water or a water-driven slug of CO₂ could improve oil recovery significantly in an oil-wet reservoir even when the process is carried out under immiscible conditions.

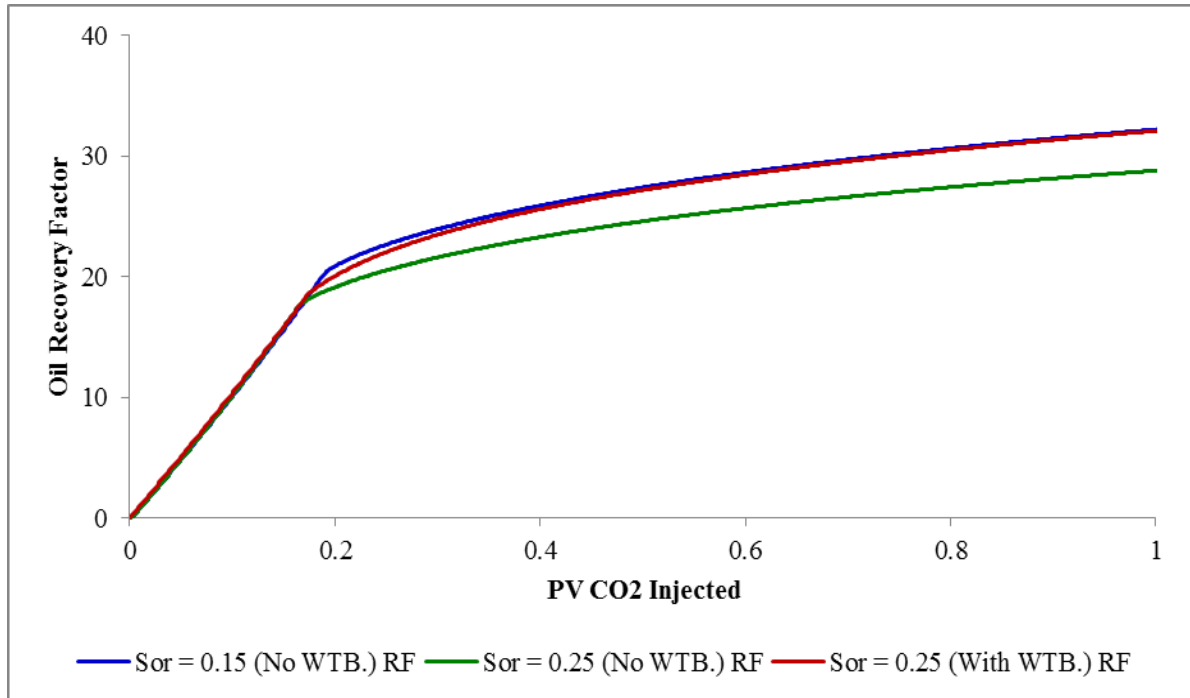


Figure 7.20 Variation of oil recovery with volume of CO₂ injected

7.6 CO₂-Oil Displacement Model Verification

This section presents verification of the displacement model that incorporates wettability alteration phenomenon. The gravity effect is also incorporated in the displacement model since the CO₂ core flooding experiment – described in Chapter 6 - was conducted in the vertical direction. The gravity effect is reflected in the pressure equation as presented in Appendix A.

The coefficients in the dynamic wettability alteration model – Eq. (4.41) – were estimated from the experimental data. Following the same procedure of section 7.1, those coefficients were estimated from the initial (135°) and final (115°) contact angles that

were measured before and after the CO₂ core flood. The stabilization time was assumed to be about 45 minutes. This assumption is based on experience with the carbonate rock used in the wettability alteration experiments of Chapter 6. The wettability alteration model for the CO₂ flood experiment was then found to be:

$$\theta = 20e^{-300t} + 115 \quad (7.37)$$

The final residual oil saturation was estimated from the oil recovery profile as it stabilized over the last hour of CO₂ flooding. The final residual oil saturation was found to be 0.389. Accordingly, the modified Corey relative permeability model was adjusted as presented in Appendix B-2. Table 7.5 presents the experimental conditions that were input into the numerical simulation model. This data represents the actual initial and operating conditions of the CO₂ core flooding experiment. In that table, the value of $k_o @ S_{wi}$ is the average value for the composite core as measured in the laboratory. Experiments on flooding oil-wet carbonate cores that are similar to the ones used in the flooding experiment of this study revealed values of $k_{rg} @ 1-S_{or}$ that ranged between 0.25 and 0.56 [98]. In those experiments, the relative permeability is based on $k_o @ S_{wi}$. Therefore, the value of $k_{rg} @ 1-S_{or}$ in Table 7.5 was selected to be within that range. The Corey oil saturation exponent is an altering parameter varying normally between 4 and 2. Since the core flooding experiments showed that wettability is shifted from oil-wet to less oil-wet, selecting a number falling between the two extreme wettability conditions (4 for strongly oil-wet and 2 for intermediate-wet) is acceptable and more representative for the actual core flooding experiments. This suggests a value of 3 for the Corey oil saturation exponent. MATLAB programming incorporating gravity effect and wettability alteration feature is shown in Appendix C-5.

Figure 7.21 shows variation of the contact angle with CO₂ injection time for each cell as predicted by the wettability alteration model. The choice of stabilization time does not change the simulation model's predictions noticeably. This is provided that both breakthrough time and total flood time are larger than the assumed stabilization time, which was the case with the experimental flooding run and should be the case in field operations. In the model, contact angle stabilization was noticed after injecting about 0.09 pore volumes of CO₂ while breakthrough was noticed later after injecting about 0.13 PV of CO₂.

Figure 7.22 shows a plot of the cumulative oil recovery vs. the pore volumes of CO₂ injected as observed in the core flood experiment. The experimental data shows that the breakthrough occurred when 0.24 PV of CO₂ was injected against 24% of oil recovery. The ultimate oil recovery reaches about 56% after injecting about 5 PV of CO₂.

Figure 7.23 shows the model's predictions of the flood performance for two cases: with wettability alteration (the upper curve) and without wettability alteration (the lower curve). For this particular core flooding experiment, the model predicts breakthrough to occur at about 0.13 PV of CO₂ injected. It also predicts an ultimate oil recovery of about 36% with wettability alteration against 34% if wettability alteration is ignored. Such a small difference in recovery is not insignificant considering that vertical gas/liquid displacement is normally highly efficient. The significant discrepancies between the laboratory data and the model's predictions are believed to be due to the effect of solubility, which is ignored in the model.

Under the conditions of the flooding experiment, solubility of CO₂ in oil is significant. As Figs. 7.24 and 7.25 [33] show, such solubility could reach 150 SCF/BBL causing the oil volume to swell by about 4%. Such swelling effect may be considered insignificant, but the consequent drop in oil viscosity is remarkable, typically around 70% as shown in figure 7.26 [14]. Therefore, the displacement model was adjusted to account for the effect of solubility – as presented in Appendix C-6 – as follows. When the CO₂ flood front reaches a cell, the oil viscosity will drop instantaneously to 2.1 cP and the oil saturation will increase by 4%. Simultaneously, wettability alteration takes place as modeled before.

At each time step – in the adjusted model – the gas saturation for any cell is examined if it is above 0.05 or not. If so, 0.04 of gas saturation is added to oil saturation and subtracted from gas saturation respectively. Within the same time step, relative permeability of each phase, fractional flow, total compressibility and pressures are calculated based on the new oil saturation. Then, oil saturation of the next time step is calculated based on new oil saturation followed immediately by calculation of the gas saturation at the next time step.

Figure 7.27 shows the oil recovery predicted by the adjusted model. If both solubility and wettability alteration effects are included, the model's prediction of the laboratory data improves considerably with an ultimate oil recovery of 45%. On the other hand, if only the solubility effect is included, the model's prediction of oil recovery drops to about 41%. For lack of data on the oil used in the study, the estimates for CO₂ solubility, oil swelling and drop in oil viscosity are based on data provided by the two references. Should they become available, employing measured values of those parameters in the model could lead to better – or worse – matches of the recovery data.

It is interesting to note that the incremental recovery caused by wettability alteration jumps remarkably from 2% to 4% when solubility is included. As shown in figure-7.28, the solubility effect shifts largely gas fractional flow curve to the right resulting in remarkable incremental oil recovery. It can be noticed also that the difference between fractional flow curves for with wettability alteration and without wettability alteration conditions – when solubility is included – is higher than the fractional flow curves when solubility is ignored which explains the jump observed in wettability alteration when solubility is included. This also could be explained physically by the huge reduction in oil viscosity which increases consequently oil mobility and improves oil displacement process efficiency.

Table 7.5 Input data used for the displacement model verification

Parameter	Value
Q_{gi}	0.005 ft ³ /day
$k_o @ S_{wi}$	90 mD
Oil Viscosity	6.70 cP
Gas Viscosity	0.02 cP
Porosity	0.28
Δx	0.0076 ft
Δy	0.112 ft
Δz	0.112 ft
Medium's Length	0.38 ft
S_{wi}	0.12
S_{gi}	0
S_{oi}	0.88
S_{ori}	0.43
$k_{ro} @ S_{wi}$	1.00
$k_{rg} @ 1-S_{or}$	0.3
c_g	0.002 psi ⁻¹
c_r	0.000004 psi ⁻¹
c_o	0.000015 psi ⁻¹
Δt	0.0001 day
Initial Contact Angle, θ_i	135°
Initial Contact Angle, θ_f	115°
Stabilization Time	45 minutes
S_{orf}	0.389

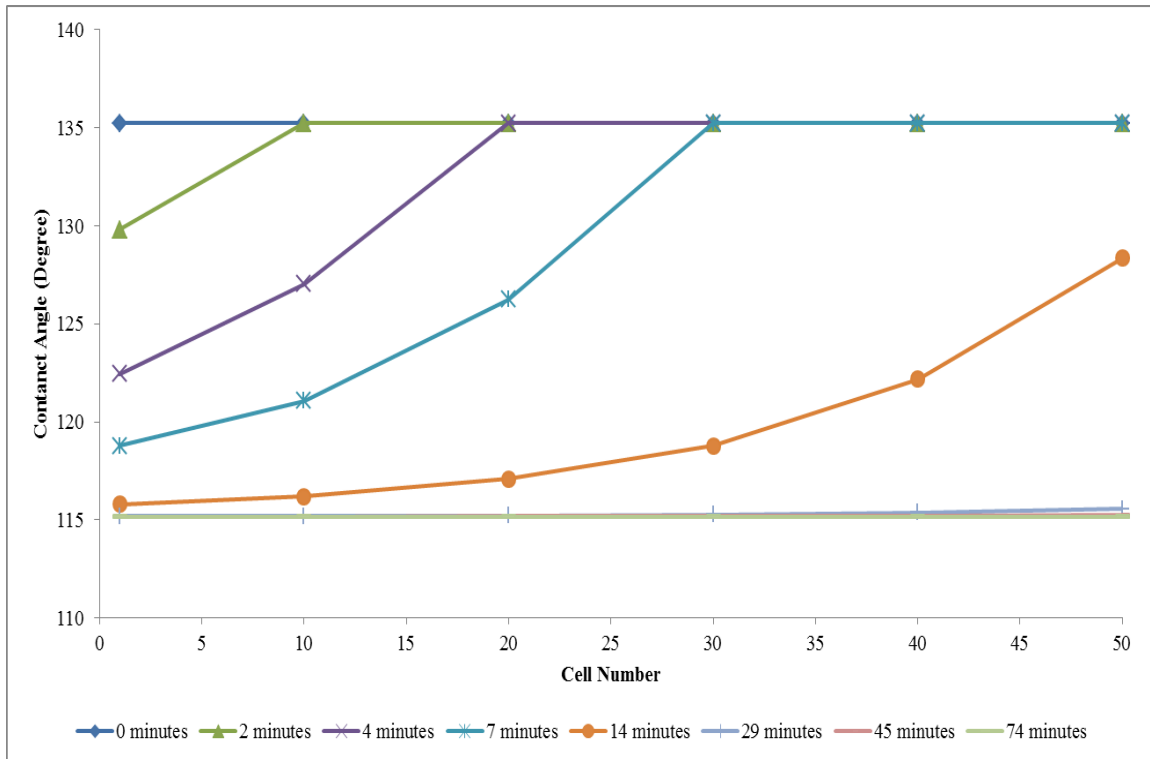


Figure 7.21 Variation of the contact angle with CO₂ injection time

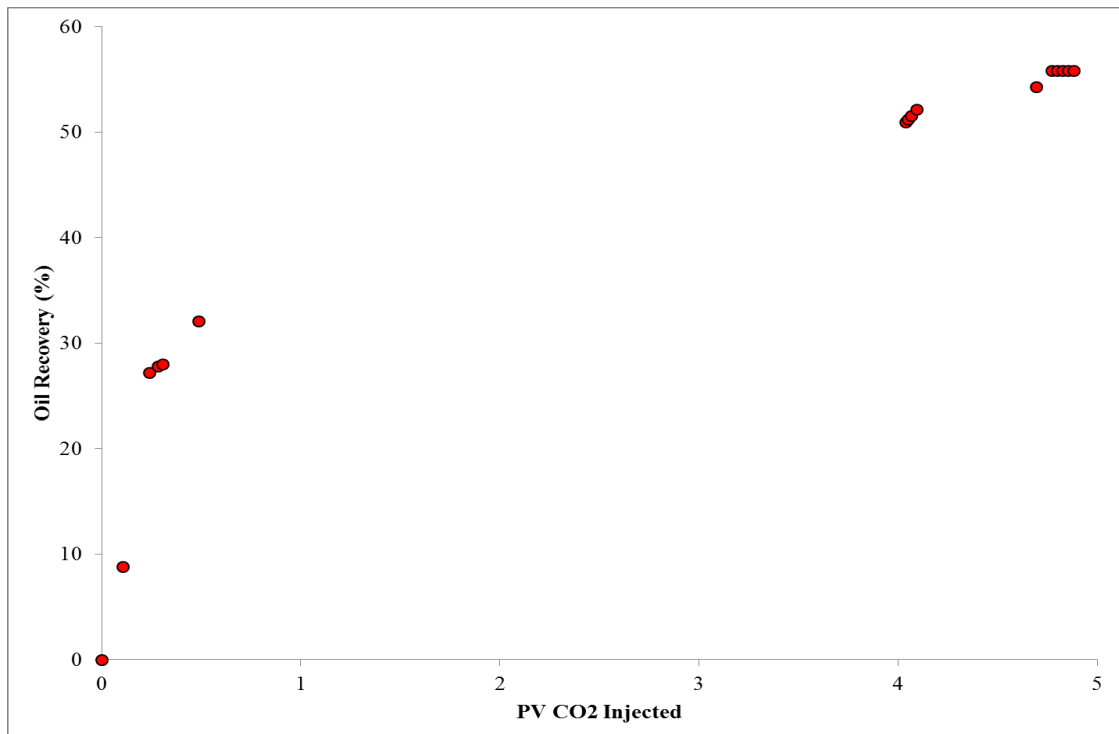


Figure 7.22 Oil recovery for the CO₂ core flooding experiment

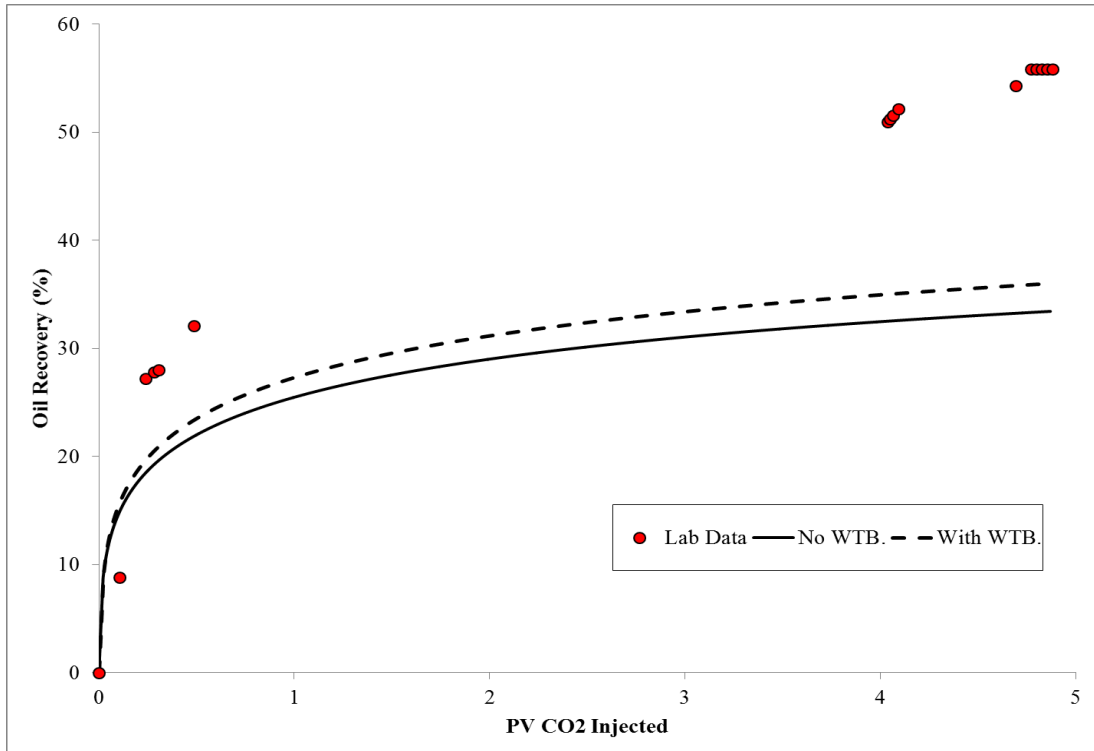


Figure 7.23 Model predictions of oil recovery

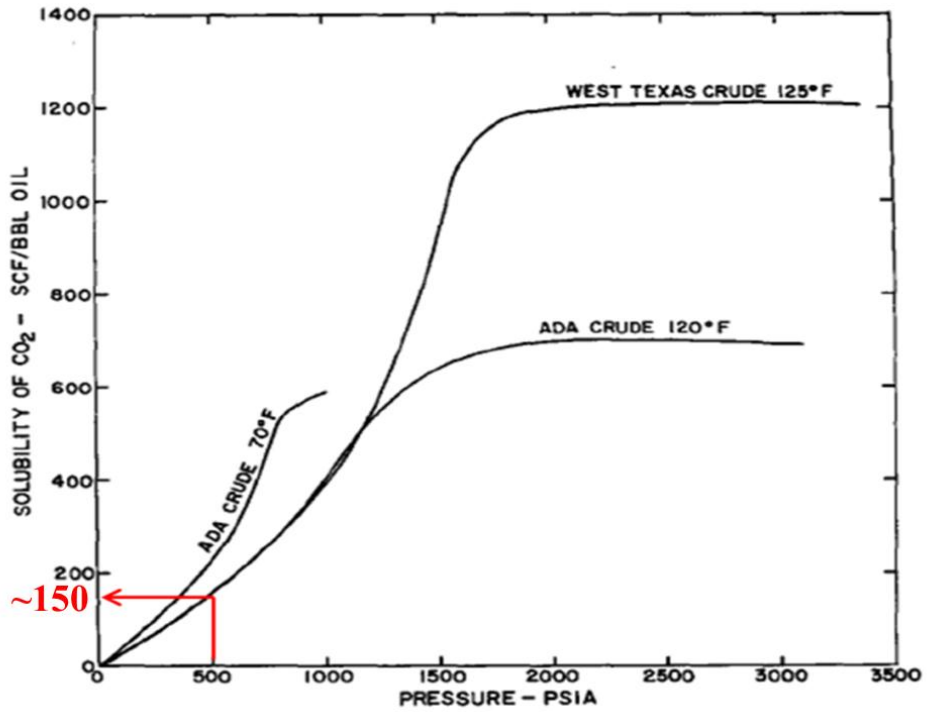


Figure 7.24 Solubility of CO₂ in various crudes

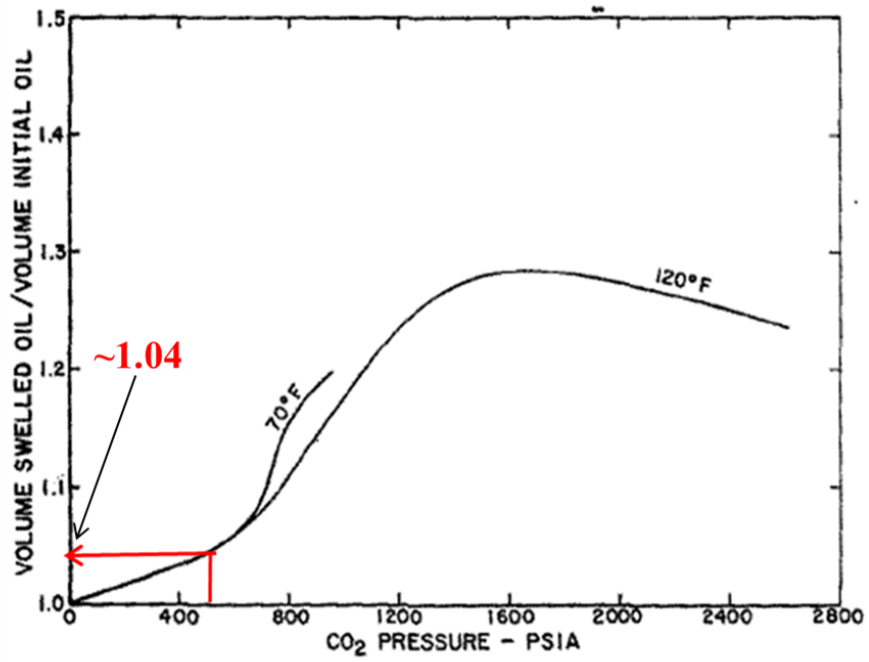


Figure 7.25 Volume change of crude saturated with CO₂

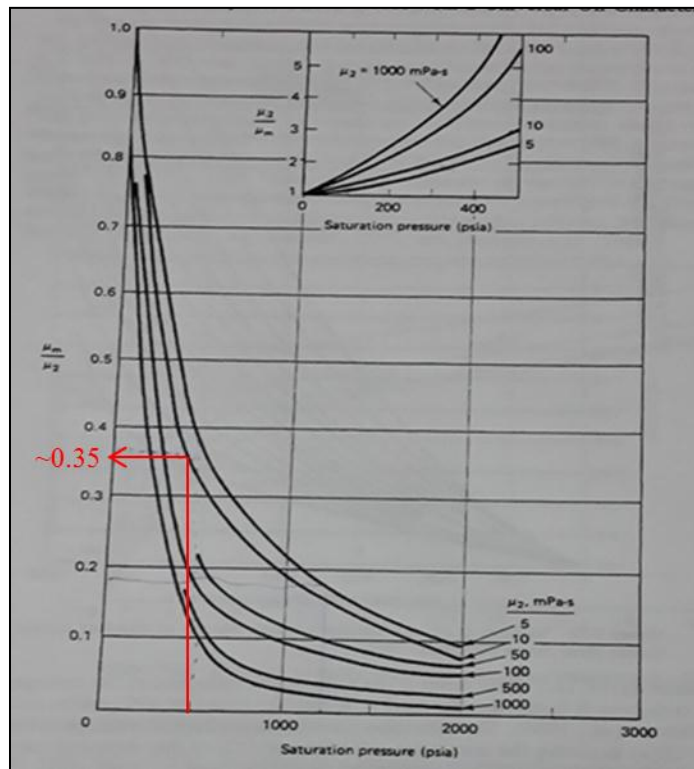


Figure 7.26 Oil viscosity correction chart for CO₂-oil mixtures

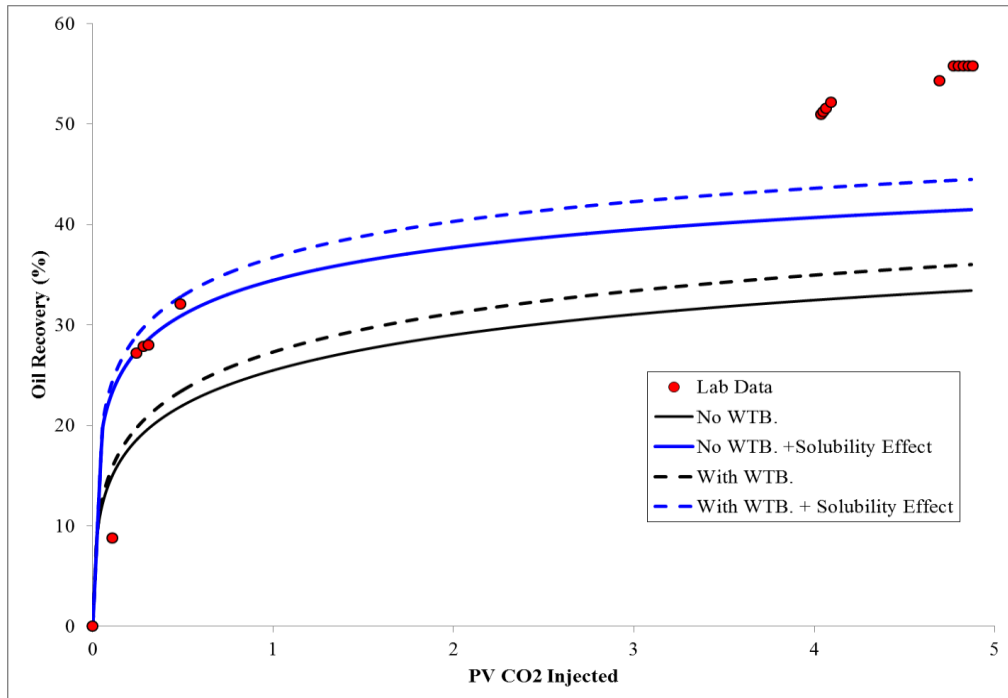


Figure 7.27 Effect of solubility on oil recovery

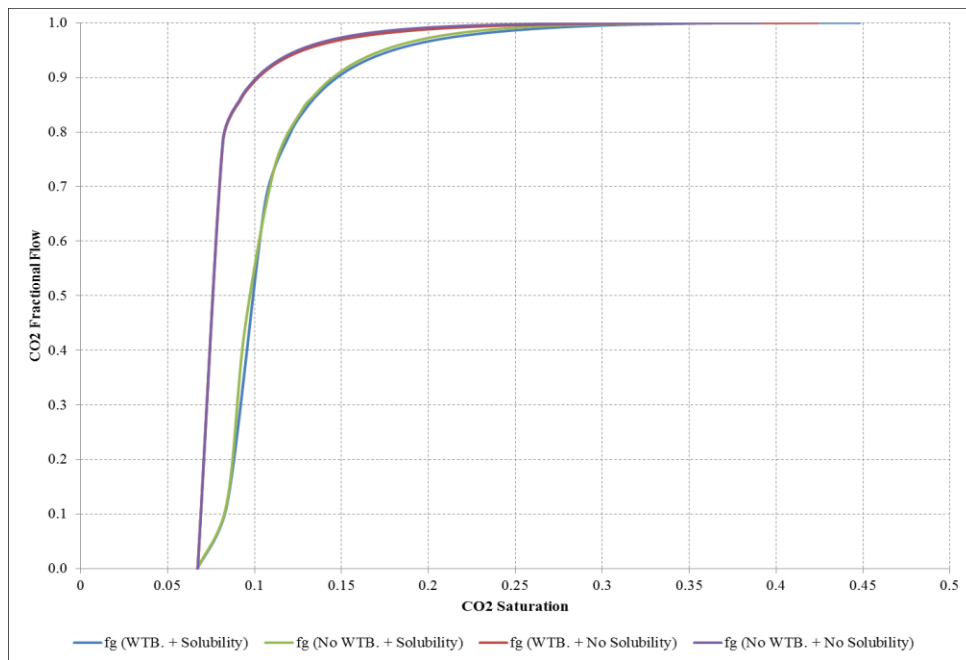


Figure 7.28 Solubility effect on gas fractional flow

CHAPTER 8

CONCLUSIONS & RECOMMENDATIONS FOR FUTURE

WORK

Conclusions from this study can be summarized as follows:

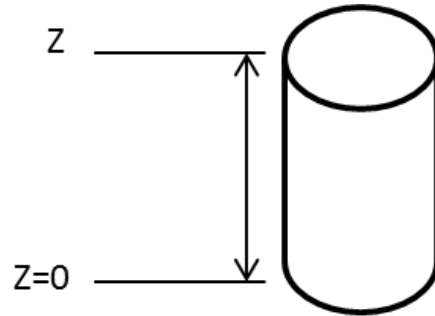
1. Exposing carbonate rock to brine containing CO₂ causes alteration of the rock wettability from an oil-wet to an intermediate-wet state.
2. Increasing CO₂ concentration in the brine results in larger alteration of wettability.
3. The oil-brine-rock contact angle decreases to a new stable value after a relatively short period of exposure to carbonated brine.
4. The change in contact angle can be modeled by an exponential function of time where a simple dimensionless relationship is controlled by a parameter, ξ , common to all CO₂ concentrations.
5. The Corey relative permeabilities of the oil and CO₂ phases can be modified to handle wettability alteration continuously during immiscible CO₂ flooding process.
6. A mathematical model has been developed to describe CO₂-oil immiscible displacement in porous media that allows continuous wettability alteration.
7. The modified Corey relative permeabilities have been incorporated in the displacement model.

8. Numerical solution of the developed model proved to be stable and the model's predictions are close to those of established models when tested on a hypothetical case.
9. The displacement model with wettability alteration compares with the core flood experiment data.
10. The wettability alteration and the displacement models will enhance understanding of the CO₂ flooding process and other EOR processes that involve wettability alteration.
11. The significance of this study can be related to cases where CO₂ is injected in a watered out, oil-wet reservoir at a pressure below the miscibility pressure. |

Recommendations for future work can be summarized as follows:

1. Wettability alteration experiments need to be conducted to establish a general wettability alteration model (Eq. 4.41) fitted for different rock/fluid systems under different conditions.
2. CO₂ Core flooding experiments need to be conducted on wide range of rock/fluid systems to verify the new comprehensive displacement model.
3. Other physical phenomena - such as gas solubility, precipitations, dispersion, etc. - need to be investigated and incorporated in the displacement model.

APPENDIX A: DISCRETIZATION OF PRESSURE EQUATIONS WITH GRAVITY EFFECT



The total flux - neglecting p_c - should be considered to solve the pressure equation as follows:

$$u_t = u_{CO_2} + u_o \quad (1)$$

Where

$$u_{CO_2} = -\frac{k_{CO_2}}{\mu_{CO_2}} \frac{\partial \phi_{CO_2}}{\partial z} \quad (2)$$

$$u_o = -\frac{k_o}{\mu_o} \frac{\partial \phi_o}{\partial z} \quad (3)$$

Gas potential can be written as:

$$\phi_{CO_2} = p + \rho_{CO_2} gZ \quad (4)$$

Differentiating Eq. (4) yields:

$$\frac{\partial \phi_{CO_2}}{\partial z} = \frac{\partial p}{\partial z} + \rho_{CO_2} g \quad (5)$$

Oil potential can be written as:

$$\phi_o = p + \rho_o gZ \quad (6)$$

Differentiating Eq. (6) yields:

$$\frac{\partial \phi_o}{\partial z} = \frac{\partial p}{\partial z} + \rho_o g \quad (7)$$

Substituting Eqs. (5) & (7) into Eq. (1) yields:

$$u_t = -\frac{k_{CO_2}}{\mu_{CO_2}} \left(\frac{\partial p}{\partial z} + \rho_{CO_2} g \right) - \frac{k_o}{\mu_o} \left(\frac{\partial p}{\partial z} + \rho_o g \right) \quad (8)$$

$$u_t = -\gamma_t \left(\frac{\partial p}{\partial z} \right) - g(\gamma_{CO_2} \rho_{CO_2} + \gamma_o \rho_o) \quad (9)$$

Incorporating Eq. (9) into Eq. (5.26) yields:

$$-\frac{\partial}{\partial z} \left(\gamma_t \frac{\partial p}{\partial z} + g(\gamma_{CO_2} \rho_{CO_2} + \gamma_o \rho_o) \right) + \frac{\phi^* S_{CO_2} c_{CO_2}}{5.615} \frac{\partial p}{\partial t} = 0 \quad (10)$$

Eq. (10) represents the general pressure equation with gravity effect.

For $i = 1$

Expanding Eq. (10) for the first cell yields:

$$\frac{1}{\Delta z} \left[- \left(\gamma_t \frac{\partial p}{\partial z} \right)_{\frac{3}{2}} + \left(\gamma_t \frac{\partial p}{\partial z} \right)_{\frac{1}{2}} - g(\gamma_{CO_2} \rho_{CO_2} + \gamma_o \rho_o)_{\frac{3}{2}} + g(\gamma_{CO_2} \rho_{CO_2})_{\frac{1}{2}} \right] + \frac{\phi^* S_{CO_2} c_{CO_2}}{5.615} \frac{\partial p}{\partial t} = 0 \quad (11)$$

Applying the inlet boundary condition into Eq. (11) yields:

$$\frac{1}{\Delta z} \left[- \left(\gamma_t \frac{\partial p}{\partial z} \right)_{\frac{3}{2}}^{n+1} - \frac{Q_g}{A} - g(\gamma_{CO_2} \rho_{CO_2} + \gamma_o \rho_o)_{\frac{3}{2}} + g(\gamma_{CO_2} \rho_{CO_2})_{\frac{1}{2}} \right] + \frac{\Phi^* S_{CO_2} c_{CO_2}}{5.615} \left(\frac{p_1^{n+1} - p_1^n}{\Delta t} \right) = 0 \quad (12)$$

Re-arranging Eq. (12) yields:

$$\frac{\gamma_{t_1}^{n+1} \Delta t}{\Delta z^2} (p_1^{n+1} - p_2^{n+1}) - \frac{Q_g \Delta t}{A \Delta z} - \frac{g \Delta t ((\gamma_{CO_2})_1^{n+1} \rho_{CO_2} + (\gamma_o)_1^{n+1} \rho_o)}{\Delta z} + \frac{\Delta t g \rho_{CO_2} (\gamma_{CO_2})_{\frac{1}{2}}^{n+1}}{\Delta z} + \frac{\Phi^* S_{CO_2} c_{CO_2}}{5.615} (p_1^{n+1} - p_1^n) = 0 \quad (13)$$

Multiplying Eq. (13) by the cross sectional area (A) yields:

$$\frac{A \gamma_{t_1}^{n+1} \Delta t}{\Delta z^2} (p_1^{n+1} - p_2^{n+1}) - \frac{Q_g \Delta t}{\Delta z} - \frac{g \Delta t A ((\gamma_{CO_2})_1^{n+1} \rho_{CO_2} + (\gamma_o)_1^{n+1} \rho_o)}{\Delta z} + \frac{\Delta t A g \rho_{CO_2} (\gamma_{CO_2})_{\frac{1}{2}}^{n+1}}{\Delta z} + \frac{A \Phi^* S_{CO_2} c_{CO_2}}{5.615} (p_1^{n+1} - p_1^n) = 0 \quad (14)$$

Expanding Eq. (14) yields:

$$\frac{A \gamma_{t_1}^{n+1} \Delta t}{\Delta z^2} p_1^{n+1} - \frac{A \gamma_{t_1}^{n+1} \Delta t}{\Delta z^2} p_2^{n+1} - \frac{Q_g \Delta t}{\Delta z} - \frac{g \Delta t A ((\gamma_{CO_2})_1^{n+1} \rho_{CO_2} + (\gamma_o)_1^{n+1} \rho_o)}{\Delta z} + \frac{\Delta t A g \rho_{CO_2} (\gamma_{CO_2})_{\frac{1}{2}}^{n+1}}{\Delta z} + \frac{A \Phi^* S_{CO_2} c_{CO_2}}{5.615} (p_1^{n+1} - p_1^n) = 0 \quad (15)$$

Re-writing Eq. (15) yields:

$$\begin{aligned}
& \left[\Delta t \left(T_{CO_2_1}^{n+1} k_{rCO_2_1}^{n+1} \right) + \Delta t \left(T_{O_1}^{n+1} k_{ro_1}^{n+1} \right) \right] p_1^{n+1} - \left[\Delta t \left(T_{CO_2_1}^{n+1} k_{rCO_2_1}^{n+1} \right) + \right. \\
& \left. \Delta t \left(T_{O_1}^{n+1} k_{ro_1}^{n+1} \right) \right] p_2^{n+1} - Q_g \Delta t - g \Delta t A \left((\gamma_{CO_2})_1^{n+1} \rho_{CO_2} + (\gamma_o)_1^{n+1} \rho_o \right) + \\
& \Delta t A g \rho_{CO_2} (\gamma_{CO_2})_{\frac{1}{2}}^{n+1} + V_{p_1} c_{CO_2_1}^{n+1} (p_1^{n+1} - p_1^n) = 0
\end{aligned} \tag{16}$$

Re-arranging Eq. (16) yields:

$$\begin{aligned}
& - \left[\Delta t \left(T_{CO_2_1}^{n+1} k_{rCO_2_1}^{n+1} \right) + \Delta t \left(T_{O_1}^{n+1} k_{ro_1}^{n+1} \right) \right] p_2^{n+1} + \left[\Delta t \left(T_{CO_2_1}^{n+1} k_{rCO_2_1}^{n+1} \right) + \right. \\
& \left. \Delta t \left(T_{O_1}^{n+1} k_{ro_1}^{n+1} \right) + c_{CO_2_1}^{n+1} V_{p_1} \right] p_1^{n+1} = Q_g \Delta t + g \Delta t A \left((\gamma_{CO_2})_1^{n+1} \rho_{CO_2} + (\gamma_o)_1^{n+1} \rho_o \right) - \\
& \Delta t A g \rho_{CO_2} (\gamma_{CO_2})_{\frac{1}{2}}^{n+1} + V_{p_1} c_{CO_2_1}^{n+1} p_1^n
\end{aligned} \tag{17}$$

Eq. (17) calculates the pressure for cell#1 at any given time.

For $i = 2: N - 1$

Expanding Eq. (10) for the cells from 2 to N-1 yields:

$$\begin{aligned}
& - \frac{1}{\Delta z} \left[\left(\gamma_t \frac{\partial p}{\partial z} \right)_{i+\frac{1}{2}} - \left(\gamma_t \frac{\partial p}{\partial z} \right)_{i-\frac{1}{2}} + g (\gamma_{CO_2} \rho_{CO_2} + \gamma_o \rho_o)_{i+\frac{1}{2}} - g (\gamma_{CO_2} \rho_{CO_2} + \gamma_o \rho_o)_{i-\frac{1}{2}} \right] + \\
& \frac{\phi^* S_{CO_2} c_{CO_2}}{5.615} \frac{\partial p}{\partial t} = 0
\end{aligned} \tag{18}$$

Expanding Eq. (18) yields:

$$-\frac{1}{\Delta z^2} [(\gamma_t)_i^{n+1} (p_{i+1}^{n+1} - p_i^{n+1}) - (\gamma_t)_{i-1}^{n+1} (p_i^{n+1} - p_{i-1}^{n+1})] - \frac{g((\gamma_{CO_2})_i^{n+1} \rho_{CO_2} + (\gamma_o)_i^{n+1} \rho_o)}{\Delta z} + \frac{g((\gamma_{CO_2})_{i-1}^{n+1} \rho_{CO_2} + (\gamma_o)_{i-1}^{n+1} \rho_o)}{\Delta z} + \frac{\Phi^* c_{CO_2}^{n+1}}{5.615} \left(\frac{p_i^{n+1} - p_i^n}{\Delta t} \right) = 0 \quad (19)$$

Multiplying Eq. (19) by the cross sectional area (A) yields:

$$\frac{A}{\Delta z^2} [(\gamma_t)_i^{n+1} (p_i^{n+1} - p_{i+1}^{n+1}) + (\gamma_t)_{i-1}^{n+1} (p_i^{n+1} - p_{i-1}^{n+1})] - \frac{gA((\gamma_{CO_2})_i^{n+1} \rho_{CO_2} + (\gamma_o)_i^{n+1} \rho_o)}{\Delta z} + \frac{gA((\gamma_{CO_2})_{i-1}^{n+1} \rho_{CO_2} + (\gamma_o)_{i-1}^{n+1} \rho_o)}{\Delta z} + \frac{A\Phi^* c_{CO_2}^{n+1}}{5.615} \left(\frac{p_i^{n+1} - p_i^n}{\Delta t} \right) = 0 \quad (20)$$

Re-arranging Eq. (20) yields:

$$\frac{A\Delta t}{\Delta z} [(\gamma_t)_i^{n+1} (p_i^{n+1} - p_{i+1}^{n+1}) + (\gamma_t)_{i-1}^{n+1} (p_i^{n+1} - p_{i-1}^{n+1})] - gA\Delta t \left((\gamma_{CO_2})_i^{n+1} \rho_{CO_2} + (\gamma_o)_i^{n+1} \rho_o \right) + gA\Delta t \left((\gamma_{CO_2})_{i-1}^{n+1} \rho_{CO_2} + (\gamma_o)_{i-1}^{n+1} \rho_o \right) + \frac{\Delta z A \Phi^* c_{CO_2}^{n+1}}{5.615} (p_i^{n+1} - p_i^n) = 0 \quad (21)$$

Re-writing Eq. (21) yields:

$$\left[\Delta t (T_{CO_2 i}^{n+1} k_{rCO_2 i}^{n+1}) + \Delta t (T_{O_i}^{n+1} k_{ro i}^{n+1}) \right] (p_i^{n+1} - p_{i+1}^{n+1}) + \left[\Delta t (T_{CO_2 i-1}^{n+1} k_{rCO_2 i-1}^{n+1}) + \Delta t (T_{O_{i-1}}^{n+1} k_{ro i-1}^{n+1}) \right] (p_i^{n+1} - p_{i-1}^{n+1}) - gA\Delta t \left((\gamma_{CO_2})_i^{n+1} \rho_{CO_2} + (\gamma_o)_i^{n+1} \rho_o \right) + gA\Delta t \left((\gamma_{CO_2})_{i-1}^{n+1} \rho_{CO_2} + (\gamma_o)_{i-1}^{n+1} \rho_o \right) + V_{p_i} c_{CO_2 i}^{n+1} (p_i^{n+1} - p_i^n) = 0 \quad (22)$$

Re-arranging Eq. (22) yields:

$$\begin{aligned}
& - \left[\Delta t \left(T_{CO_2 i}^{n+1} k_{rCO_2 i}^{n+1} \right) + \Delta t \left(T_{O_i}^{n+1} k_{ro_i}^{n+1} \right) \right] p_{i+1}^{n+1} + \left[\left[\Delta t \left(T_{CO_2 i}^{n+1} k_{rCO_2 i}^{n+1} \right) + \right. \right. \\
& \left. \left. \Delta t \left(T_{O_i}^{n+1} k_{ro_i}^{n+1} \right) \right] + \left[\Delta t \left(T_{CO_2 i-1}^{n+1} k_{rCO_2 i-1}^{n+1} \right) + \Delta t \left(T_{O_{i-1}}^{n+1} k_{ro_{i-1}}^{n+1} \right) \right] + V_{p_i} c_{CO_2 i}^{n+1} \right] p_i^{n+1} - \\
& \left[\Delta t \left(T_{CO_2 i-1}^{n+1} k_{rCO_2 i-1}^{n+1} \right) + \Delta t \left(T_{O_{i-1}}^{n+1} k_{ro_{i-1}}^{n+1} \right) \right] p_{i-1}^{n+1} = \\
& V_{p_i} c_{CO_2 i}^{n+1} p_i^n + gA\Delta t \left((\gamma_{CO_2})_i^{n+1} \rho_{CO_2} + (\gamma_o)_i^{n+1} \rho_o \right) - gA\Delta t \left((\gamma_{CO_2})_{i-1}^{n+1} \rho_{CO_2} + \right. \\
& \left. (\gamma_o)_{i-1}^{n+1} \rho_o \right) \tag{23}
\end{aligned}$$

Eq. (23) calculates the pressure for cells from 2 to N-1 at any given time.

For $i = N$

Expanding Eq. (10) for the last cell yields:

$$\begin{aligned}
& - \frac{\partial}{\Delta z} \left(\left(\gamma_t \frac{\partial p}{\partial z} \right)_{N+\frac{1}{2}} - \left(\gamma_t \frac{\partial p}{\partial z} \right)_{N-\frac{1}{2}} + g \left(\gamma_{CO_2} \rho_{CO_2} + \gamma_o \rho_o \right)_{N+\frac{1}{2}} - g \left(\gamma_{CO_2} \rho_{CO_2} + \gamma_o \rho_o \right)_{N-\frac{1}{2}} \right) + \\
& \frac{\Phi^* S_{CO_2} c_{CO_2}}{5.615} \frac{\partial p}{\partial t} = 0 \tag{24}
\end{aligned}$$

Re-writing Eq. (24) yields:

$$\begin{aligned}
& \frac{1}{\Delta z^2} \left[(\gamma_t)_N^{n+1} (2p_N^{n+1} - 2p_{wf}) + (\gamma_t)_{N-1}^{n+1} (p_N^{n+1} - p_{N-1}^{n+1}) \right] - \\
& \frac{g \left((\gamma_{CO_2})_N^{n+1} \rho_{CO_2} + (\gamma_o)_N^{n+1} \rho_o \right)}{\Delta z} + \frac{g \left((\gamma_{CO_2})_{N-1}^{n+1} \rho_{CO_2} + (\gamma_o)_{N-1}^{n+1} \rho_o \right)}{\Delta z} + \frac{\Phi^* c_{CO_2 N}^{n+1}}{5.615} \left(\frac{p_N^{n+1} - p_N^n}{\Delta t} \right) = 0 \tag{25}
\end{aligned}$$

Multiplying Eq. (25) by the cross sectional area (A) and re-arranging it yields:

$$\begin{aligned}
& \frac{\Delta t A}{\Delta z} \left[(\gamma_t)_N^{n+1} (2p_N^{n+1} - 2p_{wf}) + (\gamma_t)_{N-1}^{n+1} (p_N^{n+1} - p_{N-1}^{n+1}) \right] - \\
& gA\Delta t \left((\gamma_{CO_2})_N^{n+1} \rho_{CO_2} + (\gamma_o)_N^{n+1} \rho_o \right) + gA\Delta t \left((\gamma_{CO_2})_{N-1}^{n+1} \rho_{CO_2} + (\gamma_o)_{N-1}^{n+1} \rho_o \right) + \\
& \frac{\Delta z A \phi^* c_{CO_2 N}^{n+1}}{5.615} (p_N^{n+1} - p_N^n) = 0 \tag{26}
\end{aligned}$$

Re-writing Eq. (26) yields:

$$\begin{aligned}
& \left[\Delta t (T_{CO_2 N}^{n+1} k_{rCO_2 N}^{n+1}) + \Delta t (T_{o N}^{n+1} k_{ro N}^{n+1}) \right] (2p_N^{n+1} - 2p_{wf}) + \\
& \left[\Delta t (T_{CO_2 N-1}^{n+1} k_{rCO_2 N-1}^{n+1}) + \Delta t (T_{o N-1}^{n+1} k_{ro N-1}^{n+1}) \right] (p_N^{n+1} - p_{N-1}^{n+1}) - gA\Delta t \left((\gamma_{CO_2})_N^{n+1} \rho_{CO_2} + \right. \\
& \left. (\gamma_o)_N^{n+1} \rho_o \right) + gA\Delta t \left((\gamma_{CO_2})_{N-1}^{n+1} \rho_{CO_2} + (\gamma_o)_{N-1}^{n+1} \rho_o \right) + V_{p_N} c_{CO_2 N}^{n+1} (p_N^{n+1} - p_N^n) = 0 \tag{27}
\end{aligned}$$

Re-arranging Eq. (27) yields:

$$\begin{aligned}
& \left[2 \left[\Delta t (T_{CO_2 N}^{n+1} k_{rCO_2 N}^{n+1}) + \Delta t (T_{o N}^{n+1} k_{ro N}^{n+1}) \right] + \left[\Delta t (T_{CO_2 N-1}^{n+1} k_{rCO_2 N-1}^{n+1}) + \right. \right. \\
& \left. \left. \Delta t (T_{o N-1}^{n+1} k_{ro N-1}^{n+1}) \right] + V_{p_N} c_{CO_2 N}^{n+1} \right] p_N^{n+1} - \\
& \left[\Delta t (T_{CO_2 N-1}^{n+1} k_{rCO_2 N-1}^{n+1}) + \Delta t (T_{o N-1}^{n+1} k_{ro N-1}^{n+1}) \right] p_{N-1}^{n+1} = 2 \left[\Delta t (T_{CO_2 N}^{n+1} k_{rCO_2 N}^{n+1}) + \right. \\
& \left. \Delta t (T_{o N}^{n+1} k_{ro N}^{n+1}) \right] p_{wf} + V_{p_N} c_{CO_2 N}^{n+1} p_N^n + gA\Delta t \left((\gamma_{CO_2})_N^{n+1} \rho_{CO_2} + (\gamma_o)_N^{n+1} \rho_o \right) - \\
& gA\Delta t \left((\gamma_{CO_2})_{N-1}^{n+1} \rho_{CO_2} + (\gamma_o)_{N-1}^{n+1} \rho_o \right) \tag{28}
\end{aligned}$$

Eq. (28) calculates the pressure for the last cell at any given time.

Equations 17, 23 and 28 can be solved numerically to produce the pressure profiles with gravity effect as they vary with time in the linear system for any set of appropriate conditions.

APPENDIX B-1: MODIFIED COREY RELATIVE PERMEABILITY MODEL ADJUSTMENT FOR SECTION 7.4

$$s_{or} = ae^{bcos\theta} \quad (1)$$

Applying initial wettability condition on Eq. (1) yields

$$0.250 = ae^{bcos(120)} \quad (2)$$

$$0.250 = ae^{-0.50b} \quad (3)$$

Thanking natural logarithm of Eq. (3) yields:

$$\ln(0.250) = \ln(a) - 0.50b \quad (4)$$

$$-1.386 = \ln(a) - 0.50b \quad (5)$$

Re-arranging Eq. (5) yields:

$$0.50b = \ln(a) + 1.386 \quad (6)$$

$$b = \frac{\ln(a)}{0.50} + 2.773 \quad (7)$$

Applying final wettability condition on Eq. (1) yields

$$0.150 = ae^{bcos(100)} \quad (8)$$

Substituting Eq. (7) into Eq. (8) yields:

$$0.150 = ae^{-0.174\left(\frac{\ln(a)}{0.50}+2.773\right)} \quad (9)$$

Thanking natural logarithm of Eq. (9) yields:

$$-1.897 = \ln(a) - 0.174\left(\frac{\ln(a)}{0.50} + 2.773\right) \quad (10)$$

$$-1.897 = \ln(a) - 0.348 \ln(a) - 0.483 \quad (11)$$

$$-1.415 = \ln(a)(1 - 0.348) \quad (12)$$

$$-1.415 = 0.652 \ln(a) \quad (13)$$

$$\ln(a) = -2.170 \quad (14)$$

$$a = 0.114 \quad (15)$$

$$b = \frac{\ln(a)}{0.50} + 2.773 \quad (16)$$

Substituting Eq. (15) into Eq. (16) yields:

$$b = \frac{-2.170}{0.50} + 2.773 \quad (17)$$

$$b = -1.556 \quad (18)$$

Substituting Eqs. (15) & (18) into Eq. (1) yields:

$$S_{or} = 0.114e^{-1.556\cos\theta} \quad (19)$$

Substituting Eq. (19) into Eq. (4.26) yields:

$$S_{on} = \frac{(S_o - 0.114e^{-1.556\cos\theta})}{(1 - 0.114e^{-1.556\cos\theta} - S_{wi})} \quad (20)$$

Substituting Eq. (20) into Eqs. (4.27) & (4.28) yields:

$$k_{ro} = k_{ro}^o \left(\frac{(S_o - 0.114e^{-1.556\cos\theta})}{(1 - 0.114e^{-1.556\cos\theta} - S_{wi})} \right)^{no} \quad (21)$$

$$k_{rCO_2} = k_{rCO_2}^o \left(1 - \left(\frac{(S_o - 0.114e^{-1.556\cos\theta})}{(1 - 0.114e^{-1.556\cos\theta} - S_{wi})} \right) \right)^{ng} \quad (22)$$

Eqs. (21) & (22) are adjusted modified Corey relative permeability of oil and CO₂ based on the assumptions considered in section (7.4).

APPENDIX B-2: MODIFIED COREY RELATIVE PERMEABILITY MODEL ADJUSTMENT FOR SECTION 7.6

$$s_{or} = ae^{bcos\theta} \quad (1)$$

Applying initial wettability condition on Eq. (1) yields

$$0.430 = ae^{bcos(135)} \quad (2)$$

$$0.430 = ae^{-0.71b} \quad (3)$$

Thanking natural logarithm of Eq. (3) yields:

$$\ln(0.430) = \ln(a) - 0.71b \quad (4)$$

$$-0.844 = \ln(a) - 0.71b \quad (5)$$

Re-arranging Eq. (5) yields:

$$0.71b = \ln(a) + 0.844 \quad (6)$$

$$b = \frac{\ln(a)}{0.71} + 1.189 \quad (7)$$

Applying final wettability condition on Eq. (1) yields

$$0.389 = ae^{bcos(115)} \quad (8)$$

Substituting Eq. (7) into Eq. (8) yields:

$$0.389 = ae^{-0.422\left(\frac{\ln(a)}{0.71}+1.189\right)} \quad (9)$$

Thanking natural logarithm of Eq. (9) yields:

$$-0.944 = \ln(a) - 0.422\left(\frac{\ln(a)}{0.71} + 1.189\right) \quad (10)$$

$$-0.944 = \ln(a) - 0.595 \ln(a) - 0.502 \quad (11)$$

$$-0.443 = \ln(a)(1 - 0.595) \quad (12)$$

$$-0.443 = 0.405 \ln(a) \quad (13)$$

$$\ln(a) = -1.094 \quad (14)$$

$$a = 0.335 \quad (15)$$

$$b = \frac{\ln(a)}{0.71} + 1.189 \quad (16)$$

Substituting Eq. (15) into Eq. (16) yields:

$$b = \frac{-1.094}{0.71} + 1.189 \quad (17)$$

$$b = -0351 \quad (18)$$

Substituting Eqs. (15) & (18) into Eq. (1) yields:

$$s_{or} = 0.335e^{-0.351\cos\theta} \quad (19)$$

Substituting Eq. (19) into Eq. (4.26) yields:

$$S_{on} = \frac{(S_o - 0.335e^{-0.351\cos\theta})}{(1 - 0.335e^{-0.351\cos\theta} - S_{wi})} \quad (20)$$

Substituting Eq. (20) into Eqs. (4.27) & (4.28) yields:

$$k_{ro} = k_{ro}^o \left(\frac{(S_o - 0.335e^{-0.351\cos\theta})}{(1 - 0.335e^{-0.351\cos\theta} - S_{wi})} \right)^{no} \quad (21)$$

$$k_{rCO_2} = k_{rCO_2}^o \left(1 - \left(\frac{(S_o - 0.335e^{-0.351\cos\theta})}{(1 - 0.335e^{-0.351\cos\theta} - S_{wi})} \right) \right)^{ng} \quad (22)$$

Eqs. (21) & (22) are adjusted modified Corey relative permeability of oil and CO₂ based on the actual initial and operating conditions of the CO₂ core flooding experiment mentioned in section (7.6).

APPENDIX C: MATLAB PROGRAMMING CODES

Appendix C-1: Proposed Displacement Model

Appendix C-2: IMPES Displacement Model

Appendix C-3: BL Displacement Model

Appendix C-4: IMPES Displacement Model with Wettability Alteration Feature

Appendix C-5: IMPES Displacement Model with Wettability Alteration Feature and Gravity Effect

Appendix C-6: IMPES Displacement Model with Wettability Alteration Feature, Solubility and Gravity Effects

Appendix C-1: Proposed Displacement Model

```

%-----
%   ONE DIMENSION TWO INCOMPRESSIBLE PHASE SIMULATOR
%-----

clear all
close all

clc

%-----
%   INPUT DATA AND VARIABLES DEFINITIONS
%-----

poro=0.20;           % Porosity
Time=0.1;            % CO2 Injection Time (day)
N=60;                % Grid Cells Number
L=10;                % Core Length (ft)
dt=0.0001;          % Time Increment (day)
dx = L./N;           % Space Increment (ft)
viso=2.00;           % Oil Viscosity (cp)
visg=0.03;           % Gas Viscosity (cp)
dy=0.1;              % Width (ft)
dz=0.1;              % Height (ft)
A=dy*dz;             % Cross Sectional Area (ft^2)
k=300;               % Base Permeability (md)
Vp=(poro*dy*dz*dx); % Pore Volume (ft^3)
co=15.0e-6;          % Oil Compressibility (psi^-1)
cr=4.0e-6;           % Rock Compressibility (psi^-1)
cg=0.002;           % Gas Compressibility (psi^-1)
swi=0.1;             % Initial Water Saturation
so=0.9;              % Oil Saturation
kros=1.0;            % Oil Relative Permeability @ swi
sg=0;                % Gas Saturation
sori=0.25;           % Initial Residual oil saturation
sgi=0.0;             % initial gas saturation
no=4;                % Corey Exponent for Oil Phase
ng=2;                % Corey Exponent for Gas Phase
krgs=0.50;           % Gas Relative Permeability @ 1-sor
Bco=1.127e-3;        % Conversion Factor for Oil (to res. bbl)
Qi = 0.2;            % Gas Injection Rate (ft^3/day)
DU=Time/dt;          % Duration of CO2 injection
T=(k*dy*dz)/dx;     % Transmissibility (md.ft)
Cum=0;               % Cum oil production (ft^3)
p = repmat((500),1,N); % Initialization of pressure (psi)
Pwf=500;             % Flowing Bottom Hole Pressure (psi)
format long

%-----
%   RELATIVE PERMEABILITY CALCULATION
%-----

for j=1:N
    so(1,j)=0.90;

```

```

    sg(1,j)=0;
    son(1,j)=(so(1,j)-sori)/(1-sori-swi);
end

for s=1:DU

for j=1:N

    kro(s,j)=kros*(son(s,j))^no;
    krg(s,j)= krgs*(1-son(s,j))^ng;
    fg(s,j)= (krg(s,j)/visg)/((kro(s,j)/viso)+(krg(s,j)/visg));
    ct(s,j)=so(s,j)*co+sg(s,j)*cg+cr;

end

%-----
%   GAS PRESSURE CALCULATION (IMPLICIT SCHEME)
%-----

    j=1;

    TR(j)=Bco*(kro(s,j)/viso)+Bco*(krg(s,j)/visg);

    TRM1(j)=- (TR(j)*dt*T+Vp*ct(s,j));
    TRM2(j)=TR(j)*dt*T;
    TRM4(j)=- (dt*Qi/5.615)-Vp*ct(s,j)*p(s,j);

for j=2:N-1

    TR1(j)=Bco*(kro(s,j)/viso)+Bco*(krg(s,j)/visg);
    TR2(j)=Bco*(kro(s,j-1)/viso)+Bco*(krg(s,j-1)/visg);

    TRM3(j)=TR2(j)*dt*T;
    TRM1(j)=- (TR1(j)*dt*T+TR2(j)*dt*T+Vp*ct(s,j));
    TRM2(j)=TR1(j)*dt*T;
    TRM4(j)=-Vp*ct(s,j)*p(s,j);
end

    j=N;

    TR1(j)=Bco*(kro(s,j)/viso)+Bco*(krg(s,j)/visg);
    TR2(j)=Bco*(kro(s,j-1)/viso)+Bco*(krg(s,j-1)/visg);

    TRM3(j)=TR2(j)*dt*T;
    TRM1(j)=- (2*TR1(j)*dt*T+TR2(j)*dt*T+Vp*ct(s,j));
    TRM4(j)=-2*TR1(j)*dt*T*Pwf-Vp*ct(s,j)*p(s,j);

for i=1:N
    dd(i,i)=TRM1(i);
end

for i=2:N
    dd(i,i-1)=TRM3(i);
end

```

```

for i=1:N-1
    dd(i,i+1)=TRM2(i);
end

dd1=TRM4';
pp=inv(dd)*dd1;

p(s+1,:)=pp';

%-----
%   GAS SATURATION CALCULATION (EXPLICIT SCHEME)
%-----

j=1;

TM(s,j)=-
5.615*(0.001127*(kro(s,j)*k/viso)+0.001127*(krg(s,j)*k/visg));
sg(s+1,j)=sg(s,j)-(dt*TM(s,j)*fg(s,j)*(p(s+1,j+1)-
p(s+1,j))/(dx^2*poro))+...
((Qi*dt)/(poro*A*dx))-(sg(s,j)*cg*(p(s+1,j)-p(s,j)));
so(s+1,j)=1-sg(s+1,j)-swi;
son(s+1,j)=(so(s+1,j)-sori)/(1-sori-swi);

for j=2:N-1

    TM(s,j)=-
5.615*(0.001127*(kro(s,j)*k/viso)+0.001127*(krg(s,j)*k/visg));
    TM1(s,j-1)=-5.615*(0.001127*(kro(s,j-
1)*k/viso)+0.001127*(krg(s,j-1)*k/visg));
    sg(s+1,j)=sg(s,j)-(fg(s,j)*TM(s,j)*dt*(p(s+1,j-1)-
2*p(s+1,j)+p(s+1,j+1)))/...
(poro*dx^2)-(TM1(s,j-1)*dt*(p(s+1,j)-p(s+1,j-1))*(fg(s,j)-
fg(s,j-1)))/...
(poro*dx^2)-(fg(s,j-1)*dt*(p(s+1,j)-p(s+1,j-1))*(TM(s,j)-
TM1(s,j-1)))/...
(poro*dx^2)-(sg(s,j)*cg*(p(s+1,j)-p(s,j)));
    so(s+1,j)=1-sg(s+1,j)-swi;
    son(s+1,j)=(so(s+1,j)-sori)/(1-sori-swi);
end

j=N;

TM(s,j)=-
5.615*(0.001127*(kro(s,j)*k/viso)+0.001127*(krg(s,j)*k/visg));
TM1(s,j-1)=-5.615*(0.001127*(kro(s,j-
1)*k/viso)+0.001127*(krg(s,j-1)*k/visg));
sg(s+1,j)=sg(s,j)-(fg(s,j)*TM(s,j)*dt*(2*Pwf-2*p(s+1,j))/...
(poro*dx^2)+(fg(s,j-1)*TM1(s,j-1)*dt*(p(s+1,j)-p(s+1,j-1)))/...
(poro*dx^2)-(sg(s,j)*cg*(p(s+1,j)-p(s,j)));
so(s+1,j)=1-sg(s+1,j)-swi;
son(s+1,j)=(so(s+1,j)-sori)/(1-sori-swi);

Qo(s+1,N) = 5.615*Bco*k*kro(s,N)*A*(p(s+1,N)-
Pwf)/(viso*(dx/2));

```

```

    Qg(s+1,N) = 5.615*Bco*k*kr(s,N)*A*(p(s+1,N)-
Pwf)/(visg*(dx/2));
    Cum_inc = Qo(s+1,N)*dt;
    Cum(s+1) = Cum_inc+Cum(s);
    RF(s+1) = (Cum(s+1)*100)/(Vp*N*(1-swi));
    Vp_inj(s+1) = (Qi*dt*s)/(Vp*N);

end

x=[Vp_inj' RF']

%-----
% Plotting Section
%-----

j=1:N;
s=1:DU;
subplot(2,3,1), plot(sg(s,1), kro(s,1), '-g', sg(s,1), krg(s,1), '-
r', ...
    sg(s,1), fg(s,1), '-b'), title('kr & fg'), xlabel('Sg'), ylabel('kr
& fg'), grid on;
subplot(2,3,2), plot(Vp_inj(s), (Qg(s,N)), '-r', Vp_inj(s), (Qo(s,N)), '-
g'), ...
    title('Qo & Qg'), xlabel('CO2 PV Injected'), ylabel('Production
Rate (cu.ft/d)'), grid on;
subplot(2,3,3), plot(j, sg(end,:), '-r'), title('Displacement Front'),
xlabel('Number of Grid Cells'), ...
    ylabel('sg'), grid on;
subplot(2,3,5), plot(s*dt, p(s,1), '-r'), title('Pressure Distribution
for Cell #1'), xlabel('Time (Days)'), ...
    ylabel('Pressure'), grid on;
subplot(2,3,6), plot(j, p(end,:), '-k'), title('Pressure Distribution
for the Whole System'), xlabel('Grid Cells'), ...
    ylabel('Pressure'), grid on;

xlswrite('recovery.xls', x, 1, 'A2')

```

Appendix C-2: IMPES Displacement Model

```

%-----
%   ONE DIMENSION TWO INCOMPRESSIBLE PHASE SIMULATOR
%-----

clear all
close all

clc

%-----
%   INPUT DATA AND VARIABLES DEFINITIONS
%-----

poro=0.20;           % Porosity
Time=0.1;            % CO2 Injection Time (day)
N=60;                % Grid Cells Number
L=10;                % Core Length (ft)
dt=0.0001;          % Time Increment (day)
dx = L./N;           % Space Increment (ft)
viso=2.00;           % Oil Viscosity (cp)
visg=0.03;           % Gas Viscosity (cp)
dy=0.1;              % Width (ft)
dz=0.1;              % Height (ft)
A=dy*dz;             % Cross Sectional Area (ft^2)
k=300;               % Base Permeability (md)
Vp=(poro*dy*dz*dx); % Pore Volume (ft^3)
co=15.0e-6;          % Oil Compressibility (psi^-1)
cr=4.0e-6;           % Rock Compressibility (psi^-1)
cg=0.002;            % Gas Compressibility (psi^-1)
swi=0.1;             % Initial Water Saturation
so=0.9;              % Oil Saturation
kros=1.00;           % Oil Relative Permeability @ swi
sg=0;                % Gas Saturation
sori=0.25;           % Initial Residual oil saturation
sgi=0.0;             % initial gas saturation
no=4;                % Corey Exponent for Oil Phase
ng=2;                % Corey Exponent for Gas Phase
krgs=0.50;           % Gas Relative Permeability @ 1-sor
Bco=1.127e-3;        % conversion Factor for Oil (to res. bbl)
Qi = 0.2;            % Gas Injection Rate (ft^3/day)
DU=Time/dt;          % Duration of CO2 injection
T=(5.615*k*dy*dz)/dx; % Transmissibility (md.ft)
Cum=0;               % Cum oil production (ft^3)
p = repmat((500),1,N); % Initialization of pressure (psi)
Pwf=500;              % Flowing Bottom Hole Pressure (psi)
format long

%-----
%   RELATIVE PERMEABILITY CALCULATION
%-----

for j=1:N
    so(1,j)=0.9;

```



```

    sg(1,j)=0;
    son(1,j)=(so(1,j)-sori)/(1-sori-swi);
end

for s=1:DU

for j=1:N

    kro(s,j)=kros*(son(s,j))^no;
    krg(s,j)= krgs*(1-son(s,j))^ng;
    fg(s,j)= (krg(s,j)/visg)/((kro(s,j)/viso)+(krg(s,j)/visg));
    ct(s,j)=so(s,j)*co+sg(s,j)*cg+cr;

end

%-----
%   GAS PRESSURE CALCULATION (IMPLICIT SCHEME)
%-----

j=1;

TR(j)=Bco*(kro(s,j)/viso)+Bco*(krg(s,j)/visg);

TRM1(j)=- (TR(j)*dt*T+Vp*ct(s,j));
TRM2(j)=TR(j)*dt*T;
TRM4(j)=- (dt*Qi/5.615)-Vp*ct(s,j)*p(s,j);

for j=2:N-1

    TR1(j)=Bco*(kro(s,j)/viso)+Bco*(krg(s,j)/visg);
    TR2(j)=Bco*(kro(s,j-1)/viso)+Bco*(krg(s,j-1)/visg);

    TRM3(j)=TR2(j)*dt*T;
    TRM1(j)=- (TR1(j)*dt*T+TR2(j)*dt*T+Vp*ct(s,j));
    TRM2(j)=TR1(j)*dt*T;
    TRM4(j)=-Vp*ct(s,j)*p(s,j);
end

j=N;

TR1(j)=Bco*(kro(s,j)/viso)+Bco*(krg(s,j)/visg);
TR2(j)=Bco*(kro(s,j-1)/viso)+Bco*(krg(s,j-1)/visg);

TRM3(j)=TR2(j)*dt*T;
TRM1(j)=- (2*TR1(j)*dt*T+TR2(j)*dt*T+Vp*ct(s,j));
TRM4(j)=-2*TR1(j)*dt*T*Pwf-Vp*ct(s,j)*p(s,j);

for i=1:N
    dd(i,i)=TRM1(i);
end

```

```

for i=2:N
    dd(i,i-1)=TRM3(i);
end

for i=1:N-1
    dd(i,i+1)=TRM2(i);
end

dd1=TRM4';
pp=inv(dd)*dd1;

p(s+1,:)=pp';

%-----
%   GAS SATURATION CALCULATION (EXPLICIT SCHEME)
%-----

j=1;

so(s+1,j)=so(s,j)-so(s,j)*(co+cr)*(p(s+1,j)-
p(s,j))+((dt*T*Bco*(kro(s,j)/viso))*(p(s+1,j+1)-p(s+1,j)))/(Vp/5.615);
sg(s+1,j)=1-so(s+1,j)-swi;
son(s+1,j)=(so(s+1,j)-sori)/(1-sori-swi);
for j=2:N-1

    so(s+1,j)=so(s,j)-so(s,j)*(co+cr)*(p(s+1,j)-
p(s,j))+((dt*T*Bco*(kro(s,j)/viso))*(p(s+1,j+1)-p(s+1,j))...
- (dt*T*Bco*(kro(s,j-1)/viso))*(p(s+1,j)-p(s+1,j-
1)))/(Vp/5.615);
sg(s+1,j)=1-so(s+1,j)-swi;
son(s+1,j)=(so(s+1,j)-sori)/(1-sori-swi);
end

j=N;

so(s+1,j)=so(s,j)-so(s,j)*(co+cr)*(p(s+1,j)-p(s,j))+(...
- (dt*T*Bco*(kro(s,j-1)/viso))*(p(s+1,j)-p(s+1,j-
1)))+(dt*T*Bco*(kro(s,j)/viso)*(-2*p(s+1,j)+2*Pwf))/(Vp/5.615);
sg(s+1,j)=1-so(s+1,j)-swi;
son(s+1,j)=(so(s+1,j)-sori)/(1-sori-swi);

Qo(s+1,N) = 5.615*Bco*k*kro(s,N)*A*(p(s+1,N)-
Pwf)/(viso*(dx/2));
Qg(s+1,N) = 5.615*Bco*k*kr(s,N)*A*(p(s+1,N)-
Pwf)/(visg*(dx/2));
Cum_inc = 5.615*Qo(s+1,N)*dt;
Cum(s+1) = Cum_inc+Cum(s);
RF(s+1) = (Cum(s+1)*100)/(Vp*N*(1-swi));
Vp_inj(s+1) = (Qi*dt*s)/(Vp*N);
end

x=[Vp_inj' RF']

```

```

%-----
%   Plotting Section
%-----

j=1:N;
s=1:DU;
subplot (2,3,1), plot (sg(s,1), kro(s,1), '-g',sg(s,1),krg(s,1), '-
r',...
    sg(s,1),fg(s,1),'-b'),title('kr & fg'), xlabel ('Sg'), ylabel ('kr
& fg'), grid on;
subplot (2,3,2), plot (Vp_inj(s), (5.615*Qg(s,N)), '-
r',Vp_inj(s), (5.615*Qo(s,N)), '-g'),...
    title('Qo & Qg'), xlabel ('CO2 PV Injected'), ylabel ('Production
Rate (cu.ft/d)'), grid on;
subplot (2,3,3), plot (j,sg(end,:), '-r'),title('Displacment Front'),
xlabel ('Number of Grid Cells'),...
    ylabel ('Sg'), grid on;
subplot (2,3,5), plot (s*dt,p(s,1), '-r'), title('Pressure Distribution
for Cell #1'), xlabel ('Time (Days)'),...
    ylabel ('Pressure'), grid on;
subplot (2,3,6), plot (j,p(end,:), '-k'), title('Pressure Distribution
for the Whole System'), xlabel ('Grid Cells'),...
    ylabel ('Pressure'), grid on;

xlswrite('recovery.xls',x,1,'A2')

```

Appendix C-3: BL Displacement Model

```
%-----  
%   ONE DIMENSION TWO INCOMPRESSIBLE PHASE SIMULATOR  
%-----  
  
clear all  
close all  
  
clc  
  
%-----  
%   INPUT DATA AND VARIABLES DEFINITIONS  
%-----  
  
poro=0.20;           % Porosity  
Time=0.3;           % CO2 Injection Time (day)  
N=60;              % Grid Cells Number  
L=10;              % Core Length (ft)  
dt=0.0001;         % Time Increment (day)  
dx = L./N;         % Space Increment (ft)  
viso=2.00;         % Oil Viscosity (cp)  
visg=0.03;         % Gas Viscosity (cp)  
dy=0.1;           % Width (ft)  
dz=0.1;           % Height (ft)  
A=dy*dz;          % Cross Sectional Area  
k=300;            % Base Permeability (md)  
swi=0.1;          % Initial Water Saturation  
so=0.9;           % Oil Saturation  
kros=1.0;         % Oil Relative Permeability @ swi  
sg=0;            % Gas Saturation  
sori=0.25;        % Initial Residual oil saturation  
sgi=0.0;         % initial gas saturation  
no=4;            % Corey Exponent for Oil Phase  
ng=2;            % Corey Exponent for Gas Phase  
krgs=0.50;        % Gas Relative Permeability @ 1-sor  
Bco=1.127e-3;     % conversion Factor for Oil (to res. bbl)  
Qi = 0.2;         % Gas Injection Rate (ft^3/day)  
dta= poro.*A.*dx./(Qi*1); % dt < dta (for stability)  
alfa=Qi.*dt./(poro.*A.*dx); % alfa  
DU=Time/dt;       % Duration of CO2 injection  
Cum=0;           % Cum oil production (ft^3)  
Vp=(poro*dy*dz*dx); % Pore Volume (ft^3)  
format long  
  
%-----  
%   RELATIVE PERMEABILITY CALCULATION  
%-----  
  
for j=1:N  
    so(1,j)=0.9;  
    sg(1,j)=0;  
    son(1,j)=(so(1,j)-sori)/(1-sori-swi);  
end
```

```

for s=1:DU

for j=1:N

    kro(s,j)=kros*(son(s,j))^no;
    krg(s,j)= krgs*(1-son(s,j))^ng;
    fg(s,j)= (krg(s,j)/visg)/((kro(s,j)/viso)+(krg(s,j)/visg));

end

%-----
%   GAS SATURATION CALCULATION (EXPLICIT SCHEME)
%-----

j=1;
sg(s+1,j)=sg(s,j)-alfa.*(fg(s,j)-1);
so(s+1,j)=1-sg(s+1,j)-swi;
son(s+1,j)=(so(s+1,j)-sori)/(1-sori-swi);

for j=2:N
    sg(s+1,j)=sg(s,j)-alfa.*(fg(s,j)-fg(s,j-1));
    so(s+1,j)=1-sg(s+1,j)-swi;
    son(s+1,j)=(so(s+1,j)-sori)/(1-sori-swi);
end

    Qo(s+1,N) = (1-fg(s,N))*Qi;
    Qg(s+1,N) = (fg(s,N))*Qi;
    Cum_inc = Qo(s+1,N)*dt;
    Cum(s+1) = Cum_inc+Cum(s);
    RF(s+1) = (Cum(s+1)*100)/(Vp*N*(1-swi));
    Vp_inj(s+1) = (Qi*dt*s)/(Vp*N*(1-swi));
end

x=[Vp_inj' RF']

%-----
%   PLOTTING SECTION
%-----

j=1:N;
s=1:DU;
subplot (2,3,1), plot (sg(s,1), kro(s,1), '-g',sg(s,1),krg(s,1), '-r',...
    sg(s,1),fg(s,1),'-b'),title('kr & fg'), xlabel ('Sg'), ylabel ('kr & fg'), grid on;
subplot (2,3,2), plot (Vp_inj(s), (Qg(s,N)),'-r',Vp_inj(s), (Qo(s,N)),'-g'),...
    title('Qo & Qg'), xlabel ('CO2 PV Injected'), ylabel ('Production Rate (cu.ft/d)'), grid on;
subplot (2,3,3), plot (j,sg(end,:), '-r'),title('Displacment Front'),
xlabel ('Number of Grid Cells'),...
    ylabel ('sg'), grid on;

xlswrite('recovery.xls',x,1,'A2')

```

Appendix C-4: IMPES Displacement Model with Wettability Alteration Feature

```

%-----
%   ONE DIMENSION TWO INCOMPRESSIBLE PHASE SIMULATOR
%-----

clear all
close all

clc

%-----
%   INPUT DATA AND VARIABLES DEFINITIONS
%-----

poro=0.20;           % Porosity
Time=0.3;           % CO2 Injection Time (day)
N=60;              % Grid Cells Number
L=10;              % Core Length (ft)
dt=0.0001;         % Time Increment (day)
dx = L./N;         % Space Increment (ft)
viso=2.00;         % Oil Viscosity (cp)
visg=0.03;         % Gas Viscosity (cp)
dy=0.1;           % Width (ft)
dz=0.1;           % Height (ft)
A=dy*dz;          % Cross Sectional Area (ft^2)
k=300;            % Base Permeability (md)
Vp=(poro*dy*dz*dx); % Pore Volume (ft^3)
co=15.0e-6;       % Oil Compressibility (psi^-1)
cr=4.0e-6;        % Rock Compressibility (psi^-1)
cg=0.002;         % Gas Compressibility (psi^-1)
swi=0.1;          % Initial Water Saturation
so=0.9;           % Oil saturation
kros=1.00;        % Oil Relative Permeability @ swi
sg=0;             % Gas Saturation
sori=0.25;        % Initial Residual oil saturation
sgi=0.0;          % initial gas saturation
no=4;             % Corey Exponent for Oil Phase
ng=2;             % Corey Exponent for Gas Phase
krgs=0.50;        % Gas Relative Permeability @ 1-sor
Bco=1.127e-3;     % conversion Factor for Oil (to res. bbl)
Qi = 0.2;         % Gas Injection Rate (ft^3/day)
DU=Time/dt;       % Duration of CO2 injection
T=(5.615*k*dy*dz)/dx; % Transmissibility (md.ft)
Cum=0;           % Cum oil production (ft^3)
p = repmat((500),1,N); % Initialization of pressure (psi)
Pwf=500;         % Flowing Bottom Hole Pressure (psi)
sorf=0.15;       % Final Residual Oil Saturation
a=0.35;          % Coefficient of Contact Angle
d=-300;          % Coefficient of Contact Angle
cc=1.75;         % Coefficient of Contact Angle
%mm             Initial Contact Angle (Radian)
%ff             Changeable Contact Angle (Radian)
%hh             CO2 Exposure Time (Day)
%nt             Timer
format long

```

```

%-----
%   RELATIVE PERMEABILITY CALCULATION
%-----

for j=1:N
    so(1,j)=0.9;
    sg(1,j)=0;
    son(1,j)=(so(1,j)-sori)/(1-sori-swi);
    kro(1,j)=kros*(son(1,j))^no;
    krg(1,j)= krgs*(1-son(1,j))^ng;
    fg(1,j)= (krg(1,j)/visg)/((kro(1,j)/viso)+(krg(1,j)/visg));
    ct(1,j)=sg(1,j)*cg;
end

for s=1:DU
    for j=1:N
        mm(s,j)=2.10;
        nt(s,j)=0;
    end
end

for s=1:DU

    for j=1:N

        if sg(s,j)>0.001
            nt(s,j)=nt(s-1,j)+1;
            hh(s,j)=dt*nt(s,j);
            ff(s,j)=a*exp(d*hh(s,j))+cc;
            kro(s,j)=kros*((so(s,j)-(0.114*exp(-
1.556*cos(ff(s,j)))))/(1-(0.114*exp(-1.556*cos(ff(s,j))))-swi)).^no;
            krg(s,j)= krgs*(1-((so(s,j)-(0.114*exp(-
1.556*cos(ff(s,j)))))/(1-(0.114*exp(-1.556*cos(ff(s,j))))-swi))).^ng;
            fg(s,j)= (krg(s,j)/visg)/((kro(s,j)/viso)+(krg(s,j)/visg));
            ct(s,j)=sg(s,j)*cg;

        else

            kro(s,j)=kros*(son(s,j))^no;
            krg(s,j)= krgs*(1-son(s,j))^ng;
            fg(s,j)= (krg(s,j)/visg)/((kro(s,j)/viso)+(krg(s,j)/visg));
            ct(s,j)=sg(s,j)*cg;

        end
    end
end

%-----
%   GAS PRESSURE CALCULATION (IMPLICIT SCHEME)
%-----

j=1;

TR(j)=Bco*(kro(s,j)/viso)+Bco*(krg(s,j)/visg);

```

```

TRM1(j)=- (TR(j)*dt*T+Vp*ct(s,j));
TRM2(j)=TR(j)*dt*T;
TRM4(j)=- (dt*Qi/5.615)-Vp*ct(s,j)*p(s,j);

for j=2:N-1

    TR1(j)=Bco*(kro(s,j)/viso)+Bco*(krg(s,j)/visg);
    TR2(j)=Bco*(kro(s,j-1)/viso)+Bco*(krg(s,j-1)/visg);

    TRM3(j)=TR2(j)*dt*T;
    TRM1(j)=- (TR1(j)*dt*T+TR2(j)*dt*T+Vp*ct(s,j));
    TRM2(j)=TR1(j)*dt*T;
    TRM4(j)=-Vp*ct(s,j)*p(s,j);
end

j=N;

TR1(j)=Bco*(kro(s,j)/viso)+Bco*(krg(s,j)/visg);
TR2(j)=Bco*(kro(s,j-1)/viso)+Bco*(krg(s,j-1)/visg);

TRM3(j)=TR2(j)*dt*T;
TRM1(j)=- (2*TR1(j)*dt*T+TR2(j)*dt*T+Vp*ct(s,j));
TRM4(j)=-2*TR1(j)*dt*T*Pwf-Vp*ct(s,j)*p(s,j);

for i=1:N
    dd(i,i)=TRM1(i);
end

for i=2:N
    dd(i,i-1)=TRM3(i);
end

for i=1:N-1
    dd(i,i+1)=TRM2(i);
end

dd1=TRM4';
pp=inv(dd)*dd1;

p(s+1,:)=pp';

%-----
%   GAS SATURATION CALCULATION (EXPLICIT SCHEME)
%-----

j=1;

so(s+1,j)=so(s,j)-so(s,j)*(co+cr)*(p(s+1,j)-
p(s,j))+((dt*T*Bco*(kro(s,j)/viso))*(p(s+1,j+1)-p(s+1,j)))/(Vp/5.615);
sg(s+1,j)=1-so(s+1,j)-swi;

```



```

son(s+1,j)=(so(s+1,j)-sori)/(1-sori-swi);
for j=2:N-1

    so(s+1,j)=so(s,j)-so(s,j)*(co+cr)*(p(s+1,j)-
p(s,j))+((dt*T*Bco*(kro(s,j)/viso))*(p(s+1,j+1)-p(s+1,j))...
    -(dt*T*Bco*(kro(s,j-1)/viso))*(p(s+1,j)-p(s+1,j-
1)))/(Vp/5.615);
    sg(s+1,j)=1-so(s+1,j)-swi;
    son(s+1,j)=(so(s+1,j)-sori)/(1-sori-swi);
end

j=N;

so(s+1,j)=so(s,j)-so(s,j)*(co+cr)*(p(s+1,j)-p(s,j))+(...
    -(dt*T*Bco*(kro(s,j-1)/viso))*(p(s+1,j)-p(s+1,j-
1)))+(dt*T*Bco*(kro(s,j)/viso)*(-2*p(s+1,j)+2*Pwf))/(Vp/5.615);
sg(s+1,j)=1-so(s+1,j)-swi;
son(s+1,j)=(so(s+1,j)-sori)/(1-sori-swi);

Qo(s+1,N) = 5.615*Bco*k*kro(s,N)*A*(p(s+1,N)-
Pwf)/(viso*(dx/2));
Qg(s+1,N) = 5.615*Bco*k*kr(s,N)*A*(p(s+1,N)-
Pwf)/(visg*(dx/2));
Cum_inc = 5.615*Qo(s+1,N)*dt;
Cum(s+1) = Cum_inc+Cum(s);
RF(s+1) = (Cum(s+1)*100)/(Vp*N*(1-swi));
Vp_inj(s+1) = (Qi*dt*s)/(Vp*N);
end

x=[Vp_inj' RF']

%-----
% Plotting Section
%-----

j=1:N;
s=1:DU;
subplot(2,3,1), plot(sg(1:end-1,1), kro(:,1), '-g',sg(1:end-
1,1), krg(:,1), '-r',...
    sg(1:end-1,1), fg(:,1), '-b'), title('kr & fg for Cell#1'), xlabel
('Sg'), ylabel('kr & fg'), grid on;
subplot(2,3,2), plot(Vp_inj(s), (5.615*Qg(s,N)), '-
r', Vp_inj(s), (5.615*Qo(s,N)), '-g'), ...
    title('Qo & Qg'), xlabel('CO2 PV Injected'), ylabel('Production
Rate (cu.ft/d)'), grid on;
subplot(2,3,3), plot(j,sg(end,:), '-r'), title('Displacment Front'),
xlabel('Number of Grid Cells'), ...
    ylabel('sg'), grid on;
subplot(2,3,4), plot(hh(:,1), ff(:,1), '-k'), title('Wettability
Alteration for Cell#1'), xlabel('Exposure Time to CO2 (Days)')...
    , ylabel('Contact Angle(Radian)'), grid on;
subplot(2,3,5), plot(s*dt,p(1:end-1,1), '-r'), title('Pressure
Distribution for Cell #1'), xlabel('Time (Days)'), ...
    ylabel('Pressure'), grid on;

```

```
subplot (2,3,6), plot (j,p(end,:), '-k'), title('Pressure Distribution  
for the Whole System'), xlabel ('Grid Cells'), ...  
    ylabel ('Pressure'), grid on;  
  
xlswrite('recovery.xls',x,1,'A2')
```

Appendix C-5: IMPES Displacement Model with Wettability Alteration Feature and Gravity Effect

```

%-----
%   ONE DIMENSION TWO INCOMPRESSIBLE PHASE SIMULATOR
%-----

clear all
close all

clc

%-----
%   INPUT DATA AND VARIABLES DEFINITIONS
%-----

poro=0.28;           % Porosity
Time=1.300;         % CO2 Injection Time (day)
N=50;               % Grid Cells Number
L=0.38;             % Core Length (ft)
dt=0.0001;          % Time Increment (day)
dx = L./N;          % Space Increment (ft)
viso=6.70;          % Oil Viscosity (cp)
visg=0.02;          % Gas Viscosity (cp)
dy=0.112;           % Width (ft)
dz=0.112;           % Height (ft)
A=dy*dz;            % Cross Sectional Area (ft^2)
k=90;               % Base Permeability (md)
Vp=(poro*dy*dz*dx); % Pore Volume (ft^3)
co=15.0e-6;         % Oil Compressibility (psi^-1)
cr=4.0e-6;          % Rock Compressibility (psi^-1)
cg=0.002;           % Gas Compressibility (psi^-1)
swi=0.12;           % Initial Water Saturation
so=0.88;            % Oil Saturation
kros=1.00;          % Oil Relative Permeability @ swi
sg=0;               % Gas Saturation
sori=0.43;          % Initial Residual oil saturation
sgi=0.0;            % initial gas saturation
no=3;               % Corey Exponent for Oil Phase
ng=2;               % Corey Exponent for Gas Phase
krgs=0.30;          % Gas Relative Permeability @ 1-sor
Bco=1.127e-3;       % Conversion Factor for Oil (to res. bbl)
Qi = 0.005;         % Gas Injection Rate (ft^3/day)
DU=Time/dt;         % Duration of CO2 injection
T=(5.615*k*dy*dz)/dx; % Transmissibility (md.ft)
Cum=0;              % Cum oil production (ft^3)
p = repmat((500),1,N); % Initialization of pressure (psi)
Pwf=500;            % Flowing Bottom Hole Pressure (psi)
sorf=0.389;         % Final Residual Oil Saturation
a=0.35;             % Coefficient of Contact Angle
d=-350;             % Coefficient of Contact Angle
cc=2.01;            % Coefficient of Contact Angle
%mm                % Initial Contact Angle (Radian)
%ff                % Changeable Contact Angle (Radian)
%hh                % CO2 Exposure Time (Day)

```

```

%nt                               Timer
denso=52.44;                       % Oil Density (pound/ft^3)
densg=5.37;                         % Gas Density (pound/ft^3)
yy=4.4e-5;                          % Conversion Factor for Gravity Term
including g
format long

%-----
%   RELATIVE PERMEABILITY CALCULATION
%-----

for j=1:N
    so(1,j)=0.88;
    sg(1,j)=0;
    son(1,j)=(so(1,j)-sori)/(1-sori-swi);
    kro(1,j)=kros*(son(1,j))^no;
    krg(1,j)= krgs*(1-son(1,j))^ng;
    fg(1,j)= (krg(1,j)/visg)/((kro(1,j)/viso)+(krg(1,j)/visg));
    ct(1,j)=sg(1,j)*cg;
end

for s=1:DU
    for j=1:N
        mm(s,j)=2.36;
        nt(s,j)=0;
    end
end

for s=1:DU

    for j=1:N

        if sg(s,j)>0.001
            nt(s,j)=nt(s-1,j)+1;
            hh(s,j)=dt*nt(s,j);
            ff(s,j)=a*exp(d*hh(s,j))+cc;
            kro(s,j)=kros*((so(s,j)-(0.335*exp(-
0.351*cos(ff(s,j)))))/(1-(0.335*exp(-0.351*cos(ff(s,j))))-swi)).^no;
            krg(s,j)= krgs*(1-((so(s,j)-(0.335*exp(-
0.351*cos(ff(s,j)))))/(1-(0.335*exp(-0.351*cos(ff(s,j))))-swi))).^ng;
            fg(s,j)= (krg(s,j)/visg)/((kro(s,j)/viso)+(krg(s,j)/visg));
            ct(s,j)=sg(s,j)*cg;

        else

            kro(s,j)=kros*(son(s,j))^no;
            krg(s,j)= krgs*(1-son(s,j))^ng;
            fg(s,j)= (krg(s,j)/visg)/((kro(s,j)/viso)+(krg(s,j)/visg));
            ct(s,j)=sg(s,j)*cg;

        end
    end
end

```

```

%-----
%   GAS PRESSURE CALCULATION (IMPLICIT SCHEME)
%-----
    j=1;

    TR(j)=Bco*(kro(s,j)/viso)+Bco*(krg(s,j)/visg);

    TRM1(j)=- (TR(j)*dt*T+Vp*ct(s,j));
    TRM2(j)=TR(j)*dt*T;
    TRM4(j)=- (dt*Qi/5.615)-
Vp*ct(s,j)*p(s,j)+(dt*A*yy*((krg(s,j)*k/visg)*densg)+((kro(s,j)*k/viso
)*denso))/5.615...
    - (dt*A*yy*((k/visg)*densg))/5.615;

    for j=2:N-1

        TR1(j)=Bco*(kro(s,j)/viso)+Bco*(krg(s,j)/visg);
        TR2(j)=Bco*(kro(s,j-1)/viso)+Bco*(krg(s,j-1)/visg);

        TRM3(j)=TR2(j)*dt*T;
        TRM1(j)=- (TR1(j)*dt*T+TR2(j)*dt*T+Vp*ct(s,j));
        TRM2(j)=TR1(j)*dt*T;
        TRM4(j)=-
Vp*ct(s,j)*p(s,j)+(dt*A*yy*((krg(s,j)*k/visg)*densg)+((kro(s,j)*k/viso
)*denso))/5.615...
        - (dt*A*yy*((krg(s,j-1)*k/visg)*densg)+((kro(s,j-
1)*k/viso)*denso))/5.615;
        end

        j=N;

        TR1(j)=Bco*(kro(s,j)/viso)+Bco*(krg(s,j)/visg);
        TR2(j)=Bco*(kro(s,j-1)/viso)+Bco*(krg(s,j-1)/visg);

        TRM3(j)=TR2(j)*dt*T;
        TRM1(j)=- (2*TR1(j)*dt*T+TR2(j)*dt*T+Vp*ct(s,j));
        TRM4(j)=-2*TR1(j)*dt*T*Pwf-
Vp*ct(s,j)*p(s,j)+(dt*A*yy*((krg(s,j)*k/visg)*densg)+((kro(s,j)*k/viso
)*denso))/5.615...
        - (dt*A*yy*((krg(s,j-1)*k/visg)*densg)+((kro(s,j-
1)*k/viso)*denso))/5.615;

        for i=1:N
            dd(i,i)=TRM1(i);
        end

        for i=2:N
            dd(i,i-1)=TRM3(i);
        end

        for i=1:N-1
            dd(i,i+1)=TRM2(i);
        end

```

```

ddl=TRM4';
pp=inv(dd)*ddl;

p(s+1,:)=pp';

%-----
%   GAS SATURATION CALCULATION (EXPLICIT SCHEME)
%-----

j=1;

so(s+1,j)=so(s,j)-so(s,j)*(co+cr)*(p(s+1,j)-
p(s,j))+((dt*T*Bco*(kro(s,j)/viso))* (p(s+1,j+1)-p(s+1,j)))/(Vp/5.615);
sg(s+1,j)=1-so(s+1,j)-swi;
son(s+1,j)=(so(s+1,j)-sori)/(1-sori-swi);
for j=2:N-1

    so(s+1,j)=so(s,j)-so(s,j)*(co+cr)*(p(s+1,j)-
p(s,j))+((dt*T*Bco*(kro(s,j)/viso))* (p(s+1,j+1)-p(s+1,j))...
    -(dt*T*Bco*(kro(s,j-1)/viso))* (p(s+1,j)-p(s+1,j-
1)))/(Vp/5.615);
    sg(s+1,j)=1-so(s+1,j)-swi;
    son(s+1,j)=(so(s+1,j)-sori)/(1-sori-swi);
end

j=N;

so(s+1,j)=so(s,j)-so(s,j)*(co+cr)*(p(s+1,j)-p(s,j))+(...
    -(dt*T*Bco*(kro(s,j-1)/viso))* (p(s+1,j)-p(s+1,j-
1)))+(dt*T*Bco*(kro(s,j)/viso))* (-2*p(s+1,j)+2*Pwf))/(Vp/5.615);
sg(s+1,j)=1-so(s+1,j)-swi;
son(s+1,j)=(so(s+1,j)-sori)/(1-sori-swi);

Qo(s+1,N) = 5.615*Bco*k*kro(s,N)*A*(p(s+1,N)-
Pwf)/(viso*(dx/2));
Qg(s+1,N) = 5.615*Bco*k*kr(s,N)*A*(p(s+1,N)-
Pwf)/(visg*(dx/2));
Cum_inc = 5.615*Qo(s+1,N)*dt;
Cum(s+1) = Cum_inc+Cum(s);
RF(s+1) = (Cum(s+1)*100)/(Vp*N*(1-swi));
Vp_inj(s+1) = (Qi*dt*s)/(Vp*N);
end

x=[Vp_inj' RF']

%-----
%   Plotting Section
%-----

j=1:N;
s=1:DU;

```

```

subplot (2,3,1), plot (sg(1:end-1,1), kro(:,1), '-g',sg(1:end-
1,1),krg(:,1), '-r',...
    sg(1:end-1,1),fg(:,1),'-b'),title('kr & fg for Cell#1'), xlabel
('Sg'), ylabel ('kr & fg'), grid on;
subplot (2,3,2), plot (Vp_inj(s), (5.615*Qg(s,N)),'-
r',Vp_inj(s), (5.615*Qo(s,N)),'-g'),...
    title('Qo & Qg'), xlabel ('CO2 PV Injected'), ylabel ('Production
Rate (cu.ft/d)'), grid on;
subplot (2,3,3), plot (j,sg(end,:), '-r'),title('Displacment Front'),
xlabel ('Number of Grid Cells'),...
    ylabel ('sg'), grid on;
subplot (2,3,4), plot (hh(:,1),ff(:,1),'-k'),title('Wettability
Alteration for Cell#1'), xlabel ('Exposure Time to CO2 (Days)')...
    , ylabel ('Contact Angle(Radian)'), grid on;
subplot (2,3,5), plot (s*dt,p(1:end-1,1),'-r'), title('Pressure
Distribution for Cell #1'), xlabel ('Time (Days)'),...
    ylabel ('Pressure'), grid on;
subplot (2,3,6), plot (j,p(end,:), '-k'), title('Pressure Distribution
for the Whole System'), xlabel ('Grid Cells'),...
    ylabel ('Pressure'), grid on;

xlswrite('recovery.xls',x,1,'A2')

```

Appendix C-6: IMPES Displacement Model with Wettability Alteration Feature, Solubility and Gravity Effects

```

%-----
%   ONE DIMENSION TWO INCOMPRESSIBLE PHASE SIMULATOR
%-----

clear all
close all

clc

%-----
%   INPUT DATA AND VARIABLES DEFINITIONS
%-----

poro=0.28;           % Porosity
Time=1.300;          % CO2 Injection Time (day)
N=50;                % Grid Cells Number
L=0.38;              % Core Length (ft)
dt=0.0001;           % Time Increment (day)
dx = L./N;           % Space Increment (ft)
viso=6.70;           % Oil Viscosity (cp)
visg=0.02;           % Gas Viscosity (cp)
dy=0.112;            % Width (ft)
dz=0.112;            % Height (ft)
A=dy*dz;             % Cross Sectional Area (ft^2)
k=90;                % Base Permeability (md)
Vp=(poro*dy*dz*dx); % Pore Volume (ft^3)
co=15.0e-6;          % Oil Compressibility (psi^-1)
cr=4.0e-6;           % Rock Compressibility (psi^-1)
cg=0.002;            % Gas Compressibility (psi^-1)
swi=0.12;            % Initial Water Saturation
so=0.88;             % Oil Saturation
kros=1.00;           % Oil Relative Permeability @ swi
sg=0;                % Gas Saturation
sori=0.43;           % Initial Residual oil saturation
sgi=0.0;             % initial gas saturation
no=3;                % Corey Exponent for Oil Phase
ng=2;                % Corey Exponent for Gas Phase
krgs=0.30;           % Gas Relative Permeability @ 1-sor
Bco=1.127e-3;        % Conversion Factor for Oil (to res. bbl)
Qi = 0.005;          % Gas Injection Rate (ft^3/day)
DU=Time/dt;          % Duration of CO2 injection
T=(5.615*k*dy*dz)/dx; % Transmissibility (md.ft)
Cum=0;               % Cum oil production (ft^3)
p = repmat((500),1,N); % Initialization of pressure (psi)
Pwf=500;              % Flowing Bottom Hole Pressure (psi)
sorf=0.389;          % Final Residual Oil Saturation
a=0.35;              % Coefficient of Contact Angle
d=-350;              % Coefficient of Contact Angle
cc=2.01;             % Coefficient of Contact Angle
%mm                  % Initial Contact Angle (Radian)
%ff                  % Changeable Contact Angle (Radian)
%hh                  % CO2 Exposure Time (Day)

```



```

%nt                               Timer
%check                             Checking solubility parameter
denso=52.44;                       % Oil Density (pound/ft^3)
densg=5.37;                        % Gas Density (pound/ft^3)
yy=4.4e-5;                         % Conversion Factor for Gravity Term
including g
format long

%-----
%  RELATIVE PERMEABILITY CALCULATION
%-----

for j=1:N
    so(1,j)=0.88;
    sg(1,j)=0;
    son(1,j)=(so(1,j)-sori)/(1-sori-swi);
    kro(1,j)=kros*(son(1,j))^no;
    krg(1,j)= krgs*(1-son(1,j))^ng;
    fg(1,j)= (krg(1,j)/visg)/((kro(1,j)/viso)+(krg(1,j)/visg));
    ct(1,j)=sg(1,j)*cg;

end

for s=1:DU

    for j=1:N
        mm(s,j) = 2.36;
        nt(s,j) = 0;
        check(s,j)= 0;
    end

end

for s=1:DU

    for j=1:N

        if sg(s,j)>0.05
            viso=2.1;

            if check(s,j) == 0;
                so(s,j)=so(s,j)+0.04;
                sg(s,j)=sg(s,j)-0.04;
                check(s:end,j)=1;
            end

            nt(s,j)=nt(s-1,j)+1;
            hh(s,j)=dt*nt(s,j);
            ff(s,j)=a*exp(d*hh(s,j))+cc;
            kro(s,j)=kros*((so(s,j)-(0.335*exp(-
0.351*cos(ff(s,j)))))/(1-(0.335*exp(-0.351*cos(ff(s,j)))))-swi)).^no;

```

```

        krg(s,j)= krgs*(1-((so(s,j)-(0.335*exp(-
0.351*cos(ff(s,j)))))/(1-(0.335*exp(-0.351*cos(ff(s,j))))-swi))).^ng;
        fg(s,j)= (krg(s,j)/visg)/((kro(s,j)/viso)+(krg(s,j)/visg));
        ct(s,j)=(1-so(s,j)-swi)*cg;

else

kro(s,j)=kros*(son(s,j))^no;
krg(s,j)= krgs*(1-son(s,j))^ng;
fg(s,j)= (krg(s,j)/visg)/((kro(s,j)/viso)+(krg(s,j)/visg));
ct(s,j)=(1-so(s,j)-swi)*cg;

end
end

%-----
% GAS PRESSURE CALCULATION (IMPLICIT SCHEME)
%-----

j=1;

TR(j)=Bco*(kro(s,j)/viso)+Bco*(krg(s,j)/visg);

TRM1(j)=- (TR(j)*dt*T+Vp*ct(s,j));
TRM2(j)=TR(j)*dt*T;
TRM4(j)=- (dt*Qi/5.615)-
Vp*ct(s,j)*p(s,j)+(dt*A*yy*((krg(s,j)*k/visg)*densg)+((kro(s,j)*k/viso
)*denso))/5.615...
- (dt*A*yy*((k/visg)*densg))/5.615;

for j=2:N-1

TR1(j)=Bco*(kro(s,j)/viso)+Bco*(krg(s,j)/visg);
TR2(j)=Bco*(kro(s,j-1)/viso)+Bco*(krg(s,j-1)/visg);

TRM3(j)=TR2(j)*dt*T;
TRM1(j)=- (TR1(j)*dt*T+TR2(j)*dt*T+Vp*ct(s,j));
TRM2(j)=TR1(j)*dt*T;
TRM4(j)=-
Vp*ct(s,j)*p(s,j)+(dt*A*yy*((krg(s,j)*k/visg)*densg)+((kro(s,j)*k/viso
)*denso))/5.615...
- (dt*A*yy*((krg(s,j-1)*k/visg)*densg)+((kro(s,j-
1)*k/viso)*denso))/5.615;
end

j=N;

TR1(j)=Bco*(kro(s,j)/viso)+Bco*(krg(s,j)/visg);
TR2(j)=Bco*(kro(s,j-1)/viso)+Bco*(krg(s,j-1)/visg);

TRM3(j)=TR2(j)*dt*T;
TRM1(j)=- (2*TR1(j)*dt*T+TR2(j)*dt*T+Vp*ct(s,j));
TRM4(j)=-2*TR1(j)*dt*T*Pwf-
Vp*ct(s,j)*p(s,j)+(dt*A*yy*((krg(s,j)*k/visg)*densg)+((kro(s,j)*k/viso
)*denso))/5.615...

```

```

        -(dt*A*yy*((krg(s,j-1)*k/visg)*densg)+((kro(s,j-
1)*k/viso)*denso))/5.615;

    for i=1:N
        dd(i,i)=TRM1(i);
    end

    for i=2:N
        dd(i,i-1)=TRM3(i);
    end

    for i=1:N-1
        dd(i,i+1)=TRM2(i);
    end

dd1=TRM4';
pp=inv(dd)*dd1;

p(s+1,:)=pp';

%-----
%   GAS SATURATION CALCULATION (EXPLICIT SCHEME)
%-----

j=1;

so(s+1,j)=so(s,j)-so(s,j)*(co+cr)*(p(s+1,j)-
p(s,j))+((dt*T*Bco*(kro(s,j)/viso))*(p(s+1,j+1)-p(s+1,j)))/(Vp/5.615);
sg(s+1,j)=1-so(s+1,j)-swi;
%   stot(s+1,j)=
son(s+1,j)=(so(s+1,j)-sori)/(1-sori-swi);
for j=2:N-1

        so(s+1,j)=so(s,j)-so(s,j)*(co+cr)*(p(s+1,j)-
p(s,j))+((dt*T*Bco*(kro(s,j)/viso))*(p(s+1,j+1)-p(s+1,j))...
        -(dt*T*Bco*(kro(s,j-1)/viso))*(p(s+1,j)-p(s+1,j-
1)))/(Vp/5.615);
        sg(s+1,j)=1-so(s+1,j)-swi;
        son(s+1,j)=(so(s+1,j)-sori)/(1-sori-swi);
    end

j=N;

so(s+1,j)=so(s,j)-so(s,j)*(co+cr)*(p(s+1,j)-p(s,j))+(...
        -(dt*T*Bco*(kro(s,j-1)/viso))*(p(s+1,j)-p(s+1,j-
1)))+(dt*T*Bco*(kro(s,j)/viso)*(-2*p(s+1,j)+2*Pwf))/(Vp/5.615);
sg(s+1,j)=1-so(s+1,j)-swi;
son(s+1,j)=(so(s+1,j)-sori)/(1-sori-swi);

Qo(s+1,N) = 5.615*Bco*k*kro(s,N)*A*(p(s+1,N)-
Pwf)/(viso*(dx/2));

```

```

    Qg(s+1,N) = 5.615*Bco*k*kr(s,N)*A*(p(s+1,N)-
Pwf)/(visg*(dx/2));
    Cum_inc = 5.615*Qo(s+1,N)*dt/1.04;
    Cum(s+1) = Cum_inc+Cum(s);
    RF(s+1) = (Cum(s+1)*100)/(Vp*N*(1-swi));
    Vp_inj(s+1) = (Qi*dt*s)/(Vp*N);
end

x=[Vp_inj' RF']

%-----
% Plotting Section
%-----

j=1:N;
s=1:DU;
subplot(2,3,1), plot(sg(1:end-1,1), kro(:,1), '-g', sg(1:end-
1,1), krg(:,1), '-r', ...
    sg(1:end-1,1), fg(:,1), '-b'), title('kr & fg for Cell#1'), xlabel
('Sg'), ylabel('kr & fg'), grid on;
subplot(2,3,2), plot(Vp_inj(s), (5.615*Qg(s,N)), '-
r', Vp_inj(s), (5.615*Qo(s,N)), '-g'), ...
    title('Qo & Qg'), xlabel('CO2 PV Injected'), ylabel('Production
Rate (cu.ft/d)'), grid on;
subplot(2,3,3), plot(j, sg(end,:), '-r'), title('Displacment Front'),
xlabel('Number of Grid Cells'), ...
    ylabel('sg'), grid on;
subplot(2,3,4), plot(hh(:,1), ff(:,1), '-k'), title('Wettability
Alteration for Cell#1'), xlabel('Exposure Time to CO2 (Days)')...
    , ylabel('Contact Angle(Radian)'), grid on;
subplot(2,3,5), plot(s*dt, p(1:end-1,1), '-r'), title('Pressure
Distribution for Cell #1'), xlabel('Time (Days)'), ...
    ylabel('Pressure'), grid on;
subplot(2,3,6), plot(j, p(end,:), '-k'), title('Pressure Distribution
for the Whole System'), xlabel('Grid Cells'), ...
    ylabel('Pressure'), grid on;

xlswrite('recovery.xls', x, 1, 'A2')

```

References

- [1] Donaldson, Erle and Alam, Waqi, 2008. Wettability. Gulf Publishing Company, Houston, Texas.
- [2] Cole, Frank W., 1969. Reservoir Engineering Manual. Second Edition, Gulf Publishing Company, Houston, Texas.
- [3] Amyx, J., Bass, D. and Whiting, R., 1960. Petroleum Reservoir Engineering Book. McGraw-Hill Book Company, Inc., New York.
- [4] Alotaibi, M., Nasralla, R. and Nasr-El-Din, H., 2010. Wettability Challenges in Carbonate Reservoirs. Paper SPE 129972, presented at the SPE Improved Oil Recovery Symposium, Tulsa, Oklahoma, USA, April 24-28.
- [5] Morgan, W. and Pirson, S., 1964 .The Effect of Fractional Wettability on the Archie Saturation Exponent. The University of Texas, Austin.
- [6] Anderson, William G., 1986. Wettability Literature Survey – Part 1: Rock/Oil/Brine Interactions and the Effects of Core Handling on Wettability. Journal of Petroleum Technology, October 1986.
- [7] Lewis, Michael, Sharma, M. and Dunlap, H., 1988. Wettability and Stress Effects on Saturation and Cementation Exponents. SPWLA 29th Annual Logging Symposium, June 5-8.
- [8] Sharma, Mukul, Garrouch, A. and Dunlap, H., 1991 . Effects of Wettability, Pore Geometry, and Stress on Electrical Conduction in Fluid-Saturated Rocks. The University of Texas, Austin, September-October.
- [9] Okasha T. M., Funk J. and Al-Rashidi HN: “Fifty Years of Wettability Measurements in the Arab-D Carbonate Reservoir,” paper SPE 105114, presented at the 15th SPE Middle East Oil & Gas Show and Conference, Bahrain, March 11–14, 2007.
- [10] Civan, Faruk, 2004. Temperature Dependence of Wettability Related Properties Correlated by the Arrhenius Equation. Petrophysics, Volume 45, No. 4, pp 350-362.
- [11] Blunt, Martin, 1997. Pore Level Modeling of the Effects of Wettability. SPE Journal, December, Volume 2, No. 4.

- [12] Kovscek, A., Radke, C. and Wong, H., 1993. A Pore-Level Scenario for the Development of Mixed Wettability in Oil Reservoirs. *AIChE Journal*, 39(6), pp 1072-1085.
- [13] Bona, N., Radaelli, F., Orteni, A., De Poli, A., Peduzzi, C. and Giorgioni, M., 2001. Use of an Integrated Approach for Estimating Petrophysical Properties in a Complex Fractured Reservoir: A Case History. paper SPE 71741, presented at the SPE Annual Technical Conference and Exhibition, New Orleans, Louisiana, September 30 - October 3.
- [14] Lake, Larry, 1989. *Enhanced Oil Recovery*. Prentice Hall, Englewood Cliffs, New Jersey 07632.
- [15] Awan, A.R., Teigland, R. and Kleppe, J., 2006. EOR Survey in the North Sea. paper SPE 99546, presented at the SPE IOR Symposium, Tulsa, OK, April 22-26.
- [16] Manrique, E., Muci, V.E. and Gurfinkel, M.E., 2007. EOR Field Experiences in Carbonate Reservoirs in the US. *SPEREE*, December.
- [17] Manrique, E., Thomas, C., Ravikiran, R., Izadi, M., Lantz, M., Romero, J. and Alvarado, V., 2010. EOR: Current Status and Opportunities. paper SPE 130113, presented at the IOR Symposium, Tulsa, OK, April 26-28.
- [18] Schulte, W., 2005. Challenges and Strategy for Increased Oil Recovery. paper IPTC 10146, presented at the IPTC, Doha, Qatar, November 21-23.
- [19] Thomas, S., 2008. EOR – An Overview. *Oil and Gas Science and Technology, Rev. IFP*, Vol 63, #1.
- [20] Wilkinson, J.R., Teletzke, G.F. and King, K.C., 2006. Opportunities and Challenges for EOR in the Middle East. paper SPE 101679, presented at the Abu Dhabi IPTC, Abu Dhabi, U.A.E., November 5-8.
- [21] *Oil & Gas Journal*, April, 2010.
- [22] Kokal, Sunil and Al-Kaabi, Abdulaziz, 2010. *Enhanced Oil Recovery: Challenges & Opportunities*. World Petroleum Council, Official Publication.
- [23] Vukalovich, M. P. and Altunin, V.V.: *Thermophysical Properties of Carbon Dioxide*, Collet's Ltd., London (1968) 243-263, 351.
- [24] Dyer, S. B. and Farouq Ali, S. M., "Linear model studies of the immiscible CO₂ WAG process for heavy oil recovery", paper published in *SPE Reservoir Engineering*, 107–111, May 1994.

- [25] Jarrell, P., Fox, C., Stein, Michael, S. and Stev, 2002. Practical Aspects of CO₂ Flooding. Henry H. Doherty Series, SPE Monograph, Volume 22 Richardson, Texas.
- [26] Johnson, R.E. and Dettre, R.H., 1993. Wetting of Low Energy Surfaces. In: J. C. Berg (Ed.), Wettability. Surfactant Science Series, Volume 49. Marcel Dekker Inc., New York.
- [27] Office of Science, Office of Fossil Energy, February 1999. Working Paper on Carbon Sequestration Science and Technology. U. S. DOE, Washington, DC.
- [28] Stalkup, Fred, 1984. Miscible Displacement. Henry H. Doherty Series, SPE Monograph Volume 8, New York.
- [29] Yuan, H., Johns, R., Egwuenu, A. and Dindoruk, B., 2005. Improved MMP Correlations for CO₂ Floods Using Analytical Gasflooding Theory. SPE Reservoir Evaluation & Engineering, October.
- [30] Dyer, S. B. and Farouq Ali, S. M., "The Potential of the Immiscible Carbon Dioxide Flooding Process for the Recovery of Heavy Oil", paper preprint No. 27, for the Third Technical Meeting of the South Saskatchewan Section, the Petroleum Society of CIM, Regina, September 25-27, 1989.
- [31] Briggs, J. P. and Puttagunta, V. R., "The Effect of Carbon Dioxide on the Viscosity of Lloydminster Aberfeldy Oil at Reservoir Temperature", Alberta Research Council Report, Edmonton Alberta, January 1984.
- [32] Holm, L. W., "Carbon Dioxide Solvent Flooding for Increased Oil Recovery", Trans., AIME, 1959, 216, 225-231.
- [33] Crawford, H. R., G. H. Neill, B. J. Lucy, and P. B. Crawford, "Carbon dioxide- A Multipurpose Additive for Effective Well Stimulation," Journal of Petroleum Technology, 15 (March 1963), 237-242.
- [34] Tumasyan, A. B., V. G. Panteleev, and G. P. Meinster, "The effect of Carbon Dioxide Gas on the Physical Properties of Crude Oil and Water," Nauk.-Tekh. Sb Ser. Neftepromyslovoe Delo #2, 20-30, 1969.
- [35] Parkinson, W. J. and N. De Nevers, "Partial Molal Volume of Carbon Dioxide in Water Solutions," Industrial and Engineering Chemistry Fundamentals, 8 (November 1969), 709-713.

- [36] Rojas, G. and Farouq Ali, S. M., “Dynamics of Supercritical C/Brine Floods for Heavy Oil Recovery”, paper SPE 13598 presented at the 1985 California Regional Meeting, Bakersfield, CA, March 27-29.
- [37] Laidler, K. J. and Meiser, J. H., “Physical Chemistry”, Benjamin/Cummings Publishing Company, Inc., Ontario, 1982.
- [38] Ashgari, K. and Torabi, F., “Laboratory Experimental Results of Huff ‘n’ Puff CO₂ Flooding in a Fractured Core System”, SPE paper 110577 presented at the SPE Annual Technical Conference and Exhibition, Anaheim, CA, 11–14 November 2007.
- [39] Bailey, N.A., Fishlock, T.P., Puckett, D.A., “Experimental studies of oil recovery by gas displacement”, proceeding of 5th European Symposium on Improved Oil Recovery, Budapest, April 1989.
- [40] Brush, R., Davitt, J., Aimar, O., Arguellos, J., and Whiteside, J., “Immiscible CO₂ Flooding for Increased Oil Recovery and Reduced Emissions”, SPE paper 59328 presented at the SPE/DOE Improved Recovery Symposium, Tulsa, OK, 3–5 April, 2000.
- [41] Chung, F.T.H., Jones, R.A., Burchfield, T.E., “Recovery of viscous oil under high pressure by CO₂ displacement: a laboratory study”, SPE Paper 17588 presented at the SPE International Meeting on Petroleum Engineering, Tiajin, China, 1988.
- [42] Mangalsingh, D. and Jagai, T., “A Laboratory Investigation of the Carbon Dioxide Immiscible Process”, SPE paper 36134 presented at the 4th Latin American and Caribbean Petroleum Engineering Conference, Port-of-Spain, Trinidad & Tobago, 23–25 April 1996.
- [43] Sigmund, P., Kerr, W. and MacPherson, R., “A Laboratory and Computer Model Evaluation of Immiscible CO₂ Flooding in a Low-Temperature Reservoir”, SPE paper 12703 presented at the SPE/DOE 4th EOR Symposium, Tulsa, OK, April 15–18, 1984.
- [44] Zekri, A., Almehaideb, R. and Shedid, S., “Displacement Efficiency of Supercritical CO₂ Flooding in Tight Carbonate Rocks Under Immiscible and Miscible Conditions”, SPE paper 98911 presented at the SPE EUROPEC/EAGE Annual Conference and Exhibition, Vienna, Austria, 12–15 June 2006.
- [45] Grogan A., Pinczewski, V., Ruskauff, G. and Orr, F., “Diffusion of CO₂ at Reservoir Conditions: Models and Measurements”, SPE paper published in SPE Reservoir Engineering, February 1988.

- [46] McManamey, W. and Wollen, J., "The Diffusivity of Carbon Dioxide in Some Organic Liquids at 25 °C and 50 °C, AICHE J., (May 1973), 667–669.
- [47] Zhu. T.: "Displacement of A Heavy Oil By Carbon Dioxide and Nitrogen in a Scaled Model", M.Sc. Thesis, The University of Alberta (March 1986).
- [48] Nordbotten, J. and Dahle, H., "Impact of Capillary Forces on Large-Scale Migration of CO₂", paper presented at the International Conference on Water Resources, Barcelona, 2010.
- [49] Savioli, G. and Santos, J., "Modeling of CO₂ Storage in Aquifers", paper published under License by IOP Publishing Ltd in Journal of Physics: Conference Series 296, 2011.
- [50] Negara, A., El-Amin, M. and Sun, S., "Simulation of CO₂ Plume in Porous Media: Consideration of Capillarity and Buoyancy Effects," paper published at International Journal of Numerical Analysis and Modeling, Series B, Volume 2, Number 4, Pages 315–337, 2001.
- [51] Beecher, C. E. and Parkhurst, I. P., "Effect of Dissolved Gas upon the Viscosity and Surface Tension of Crude Oils", Petroleum Development and Technology in 1926, Pet. Div. AIME, 51-69.
- [52] Strausz, O. P., "Some Recent Advances in the Chemistry of Oil Sand Bitumen", presented at the UNITAR First International Conference on the Future of Heavy Crude and Tar Sand, McGraw-Hill Inc., Edmonton, AB, 1979, 187-194.
- [53] Fuhr, B. J., Klein, L.L., Komishke, B. D., Reichert, C., and Ridley, R. K., "Effects of Diluents and Carbon Dioxide on Asphaltene Flocculation in Heavy Oil Solutions", paper preprint No. 75, for the Fourth UNITAR/UNDP Conference on Heavy Crude and Tar Sands, 1985.
- [54] Koederitz, L. F., Harvey A. H. and Honarpour M. : Introduction to Petroleum Reservoir Analysis, Gulf Publishing Company, Houston, Texas, (1989).
- [55] Shelton, L. L. and Schneider, F. N., 1975. The Effects of Water Injection on Miscible Flooding Methods Using Hydrocarbons and Carbon Dioxide. SPEJ (June) 217.
- [56] Stalkup, F.I., 1970. Displacement of Oil by Solvent at High Water Saturation. SPEJ (December) 337.
- [57] Tiffin, D. and Yellig, W. F., 1983. Effects of Mobile Water on Multiple-Contact Miscible Gas Displacement. SPEJ (June) 447.

- [58] Mathis, R. L., 1984. Effect of CO₂ Flooding on Dolomite Reservoir Rock, Denver Unit, Wasson (san Andres) Field, TX. paper SPE 13132, presented at the Annual Technical Conference and Exhibition, Houston, Texas, September 16-19.
- [59] Jackson, D., Andrews, G. and Claridge, E., 1985. Optimum WAG Ratio vs. Rock Wettability in CO₂ Flooding,” SPE 14303 paper presented at the Annual Technical Conference and Exhibition, Las Vegas, NV, September 22-25.
- [60] Irani, C. A., Solomon, C. Jr.,1986. Slim-Tube Investigation of CO₂ Foams. paper SPE/DOE 14962, presented at the SPE/DOW 5th Symposium on Enhance Oil Recovery, Tulsa, OK, April 20-23.
- [61] Lescure, B. M. and Claridge, E., 1986. CO₂ Foam Flooding Performance vs. Rock Wettability. Paper SPE15445, presented at the Annual Technical Conference and Exhibition, New Orleans, LA, October 5-8.
- [62] Potter G. F., 1987. The effects of CO₂ Flooding on Wettability of West Texas Dolomitic Formations. Paper SPE 16716, presented at the Annual Technical Conference and Exhibition, Dallas, TX, September 27-30.
- [63] Yeh, S. W. et al., 1992. Miscible-Gasflood-Induced Wettability Alterations: Experimental Observations and Oil Recovery Implications. SPE Formation Evaluation, June.
- [64] Zekri, A. and Natuh, A. A., 1992. Laboratory Study of the Effects of Miscible WAG Process on Tertiary Oil Recovery. paper SPE 24481, presented at the Abu Dhabi Petroleum Conference, Abu Dhabi.
- [65] Attanucci, V., Aslesen, K., Hejl, K. and Wright, C., 1993. WAG Process Optimization in the Rangeley CO₂ Miscible Flood. Paper SPE 26622, presented at the Annual Technical Conference and Exhibition, Houston, Texas, October 3-6.
- [66] Vives, M., Chang, Y., Mohanty, K., 1999. Effect of Wettability on Adverse-Mobility Immiscible Floods,” SPE Journal, September.
- [67] Wylie, Philip and Mohanty, Kishore, 1999. Effect of Wettability on Oil Recovery by Near-Miscible Gas Injection. SPE Reservoir Evaluation & Engineering, December, Volume 2, No.6.
- [68] Chalbaud, C., Lombard, M., Martin, F., Robin, M., Bertin, H. and Egermann, P., 2007. Two Phase Flow Properties of Brine-CO₂ Systems in Carbonate Core: Influence of Wettability on Pc and Kr. paper SPE 111420, presented at the SPE/EAGE Reservoir Characterization and Simulation Conference, Abu Dhabi, UAE, October 28-31.

- [69] Zekri, A., Shedid, S. and Almehaideb, R., 2007. Possible Alteration of Tight Limestone Rocks Properties and the Effect of Water Shielding on the Performance of Supercritical CO₂ Flooding for Carbonate Formation. paper SPE 104630, presented at the SPE Middle East Oil & Gas Show and Conference, Bahrain, March 11-147.
- [70] Egermann, P., Bazin, B. and Visika, O., 2010. An integrated Approach to Assess the Petrophysical Properties of Rocks Altered by Rock-Fluid Interactions (CO₂ Injection). *Petrophysics*, Volume 51, No. 1, (February), pp 32-40
- [71] Fjelde, Ingebret and Asen, Siv Marie, 2010. Wettability Alteration during Water Flooding and Carbon Dioxide Flooding of Reservoir Chalk Rocks. paper SPE 130992, presented at SPE EUROPEC/EAGE Annual Conference and Exhibition, Barcelona, Spain, June 14-17.
- [72] Yang, Y., van Dijke, M. and Yao, J., 2010. Efficiency of Gas Injection Scenarios for Intermediate Wettability: Pore Network Modeling. paper presented at the International Symposium of the Society of Core Analysts, Halifax, Nova Scotia, Canada, October 4-7.
- [73] van Dijke, M.I.J. and K.S. Sorbie, 2002. Pore-Scale Network Model for Three-Phase Flow in Mixed-Wet Porous Media. *Physical Review E*, 66(4), pp 046302.
- [74] van Dijke, M.I.J. and K.S. Sorbie. The Relation Between Interfacial Tensions and Wettability in Three Phase Systems: Consequences for Pore Occupancy and Relative Permeability,” Department of Petroleum Engineering, Herriot-Watt University, Edinburgh, Scotland, UK.
- [75] Tehrani, D., Danesh, A., Sohrabi, M. and Henderson, G., 2001. Improved Oil Recovery from Oil-Wet and Mixed-Wet Reservoirs by Gas Flooding, Alternately with Water. presented to IEA Annual Workshop & Symposium, Vienna, September.
- [76] Bartell, F.E. and Osterhof, H.J., 1927. Determination of the Wettability of a Solid by a Liquid, *Ind. Eng. Chem.* 19 (11): 1277-1280.
- [77] Zhou, D. and Blunt, M., 1997. Effect of Spreading Coefficient on the Distribution of Light Non-aqueous Phase Liquid in the Subsurface. *J. Contam. Hydrol*, 25: 1-19.
- [78] Delshad, Mojdeh, Najafabadi, N., Anderson, G., Pope, Gary, Sepehrnoori, K., 2006. Modeling Wettability Alteration by Surfactants in Naturally Fractured Reservoir. paper SPE 100081, presented at the SPE/DOE Symposium on Improved Oil Recovery, Tulsa, April 22-26.

- [79] Farhadinia, M. and Delshad M., 2010. Modeling and Assessment of Wettability Alteration Processes in Fractured Carbonates using Dual Porosity and Discrete Fracture Approaches. paper SPE 129749, presented at the 2010 SPE Improved Oil Recovery Symposium, Tulsa, Oklahoma, USA, April 24-28.
- [80] Ju., B., Qin, J. and Chen, X., 2010. Modeling Formation Damage and Wettability Alteration Induced by Asphaltene Precipitation and Their Effects on Percolation Performances during Oil Production. paper SPE 129803, presented at the CPS/SPE International Oil & Gas Conference and Exhibition, Beijing, China, June 8-10.
- [81] Hossain, M., Mousavizadegan, H. and Islam, R., 2008. Effects of Thermal Alterations of Formation Permeability and Porosity. *Petroleum Science and Technology*, 26: 1282 – 1302.
- [82] Hossain, M., Mousavizadegan, H. and Islam, R., 2008. A New Porous Media Diffusivity Equation with the Inclusion of Rock and Fluid Memories. manuscript SPE 114287, submitted to the SPE for distribution and possible in an SPE Journal.
- [83] Willhite, Paul, “Waterflooding”, Third Printing 1986, Richardson, TX.
- [84] Odeh, A. and Babu, D., “Comparison of Solutions of the Nonlinear and Linearized Diffusion Equations”, *SPE Reservoir Engineering*, November 1988.
- [85] Temeng, K. and Horne, R., “The Effect of High-Pressure Gradients on Gas Flow”, SPE 18269 paper presented at the 63rd Annual Technical Conference and Exhibition, Houston, TX, October 2-5, 1988.
- [86] Corey, A. T.: "The Interrelation between Gas and Oil Relative Permeabilities", *Producers Monthly*, Nov. (1954), 38-41.
- [87] Lorenz, P. B. Donaldson, E.C. and Thomas, R.D., “Use of Centrifugal Measurements of Wettability to Predict Oil Recovery,” report 7873, USBM, Bartlesville Energy Technology Center (1974).
- [88] Grogan, A. T., Pinczewski, W. V., Ruskhauff, G. J., and Orr, F. M. Jr., “Diffusion of Carbon Dioxide at Reservoir Conditions: Models and Measurements”, paper SPE/DOE 14897 presented at the 1986 SPE/DOE Fifth Symposium on Enhanced Oil Recovery, Tulsa OK April 1986).
- [89] Dake, L., “The Practice of Reservoir Engineering”, Revised Edition 2001, *Developments in Petroleum Science*.

- [90] Ertekin, T., Abou-Kassem, J and King, G., “Basic Applied Reservoir Simulation”, Henry Doherty Memorial Fund of AIME, 2001.
- [91] Aziz, Khalid and Settari, Antonin, “Petroleum Reservoir Simulation”, Blitzprint
- [92] Craft, B. and Hawkins, M., “Applied Petroleum Reservoir Engineering”, Hall PTR, 1991.
- [93] Crank, J., “The Mathematics of Diffusion”, Oxford Clarendon Press, 1967.
- [94] Davies, G. A., Ponter, A. B., and Craine, K.: “The Diffusion of Carbon Dioxide in Organic Liquids”, Cdn. J. Chem. Eng. (Dec. 1976) 372-376.
- [95] Eide, Lars, 2009. Carbon Dioxide Capture for Storage in Deep Geologic Formations – Results from the CO₂ Capture Project. CPL Scientific Publishing Services Ltd trading as CPL Press, UK.
- [96] Morrow, N. R. and Mungan, N., “Wettability and Capillarity in Porous Media.” Report RR-7, Petroleum Recovery Research Inst., Calgary (Jan. 1971)
- [97] Schneider, F. N. and Owens, W. W., 1976. Relative Permeability Studies of Gas-Water Flow Following Solvent Injection in Carbonate Rocks. SPEJ, February, pp 23-30.
- [98] Unlamiser S., Al-Saleh, S. Al-Khudair W., Al-Faqeer S., and Balobaid Y. Gas-Oil Relative Permeability, Shu’aiba Reservoir. Saudi Aramco Internal Report. Sep. 2000.

Vitae

Name : Saad Menahi Al-Mutairi

Nationality : Saudi

Date of Birth : 6/17/1977

Email : saad.mutairi@gmail.com

Address : Dammam

Academic Background : **PhD (Petroleum Engineering), December 2013**
King Fahd University of Petroleum and Minerals
Dhahran, Saudi Arabia

MS (Petroleum Engineering), June 2008
King Fahd University of Petroleum and Minerals
Dhahran, Saudi Arabia

BS (Petroleum Engineering), June 2000
King Fahd University of Petroleum and Minerals
Dhahran, Saudi Arabia |